

การออกแบบและการสังเคราะห์อนุภาคระดับนาโนเมตรของซีลีเนียมเพื่อแก้ปัญหาการดื้อยาหลาย
ชนิดของเซลล์มะเร็ง



นางสาวอุฬาริกา ลือสกุล

บทคัดย่อและแฟ้มข้อมูลฉบับเต็มของวิทยานิพนธ์ตั้งแต่ปีการศึกษา 2554 ที่ให้บริการในคลังปัญญาจุฬาฯ (CUIR)
เป็นแฟ้มข้อมูลของนิสิตเจ้าของวิทยานิพนธ์ ที่ส่งผ่านทางบัณฑิตวิทยาลัย

The abstract and full text of theses from the academic year 2011 in Chulalongkorn University Intellectual Repository (CUIR)
are the thesis authors' files submitted through the University Graduate School.

วิทยานิพนธ์นี้เป็นส่วนหนึ่งของการศึกษาตามหลักสูตรปริญญาวิทยาศาสตรดุษฎีบัณฑิต

สาขาวิชาเคมี ภาควิชาเคมี

คณะวิทยาศาสตร์ จุฬาลงกรณ์มหาวิทยาลัย

ปีการศึกษา 2560

ลิขสิทธิ์ของจุฬาลงกรณ์มหาวิทยาลัย

DESIGN AND SYNTHESIS OF SELENIUM NANOPARTICLES TO OVERCOME MULTIPLE
DRUG RESISTANCE OF CANCER CELLS



A Dissertation Submitted in Partial Fulfillment of the Requirements
for the Degree of Doctor of Philosophy Program in Chemistry

Department of Chemistry

Faculty of Science

Chulalongkorn University

Academic Year 2017

Copyright of Chulalongkorn University

อุฬาริกา ลือสกุล : การออกแบบและการสังเคราะห์อนุภาคระดับนาโนเมตรของซีลีเนียม เพื่อแก้ปัญหาการดื้อยาหลายชนิดของเซลล์มะเร็ง (DESIGN AND SYNTHESIS OF SELENIUM NANOPARTICLES TO OVERCOME MULTIPLE DRUG RESISTANCE OF CANCER CELLS) อ.ที่ปรึกษาวิทยานิพนธ์หลัก: ศ. ดร.นงนุช เหมืองสิน, หน้า.

งานวิจัยนี้มีจุดประสงค์เพื่อสังเคราะห์อนุภาคซีลีเนียมระดับนาโนเมตรที่ทำให้เสถียรด้วยไคโตซานสำหรับนำส่งสารต้านมะเร็งเพื่อแก้ปัญหาการดื้อยาของเซลล์มะเร็ง โดยหนึ่งในปัจจัยของการดื้อยาที่สำคัญคือ การทำงานของโปรตีนที่หลักยาออกจากเซลล์มะเร็งทำให้มีปริมาณยาไม่เพียงพอในการฆ่าเซลล์มะเร็ง ดังนั้นเพื่อเพิ่มความสามารถการนำส่งยาเข้าสู่เซลล์และลดปัญหาการดื้อยา ระบบนำส่งยาดด้วยอนุภาคซีลีเนียมถูกดัดแปลงพื้นผิวประกอบด้วยส่วนประกอบสำคัญ 3 ส่วนคือ (i) ประจุบวกเพื่อเพิ่มความสามารถในการละลายน้ำและเพิ่มความสามารถในการเข้าสู่เซลล์ (ii) แกลลิกแอซิด ซึ่งเป็นไฮโดรโฟบิกโมเลกุลเพื่อเพิ่มความเข้ากันได้กับเซลล์ และ (iii) โพลีลิกแอซิด ซึ่งเป็นลิแกนด์เป้าหมายเพื่อเพิ่มความจำเพาะกับเซลล์มะเร็งและเพิ่มความสามารถในการเข้าสู่เซลล์ จากการศึกษาความเป็นพิษต่อเซลล์มะเร็งรังไข่ที่เกิดการดื้อยา NCI/ADR-RES ด้วยเทคนิค MTT พบว่า ระบบนำส่งยาต้านมะเร็ง Doxorubicin (DOX) ด้วยอนุภาคซีลีเนียมระดับนาโน DOX-SeNPs@TMC-FA สามารถเพิ่มประสิทธิภาพในการฆ่าเซลล์มะเร็งดื้อยาของ DOX ได้ประมาณ 10 เท่าเมื่อเปรียบเทียบกับ free DOX ที่ไม่ได้กักเก็บในอนุภาคนาโน โดยโพลีลิกแอซิดที่อยู่บนพื้นผิวของอนุภาคช่วยเพิ่มความจำเพาะกับเซลล์มะเร็ง ลดความเป็นพิษต่อเซลล์ปกติ WI-38 และที่สำคัญช่วยเพิ่มการเข้าสู่เซลล์โดยผ่านกระบวนการ folate receptor-mediated endocytosis นอกจากนี้ระบบนำส่งยาดด้วยอนุภาคซีลีเนียมระดับนาโนเมตรยังสามารถควบคุมการปลดปล่อยยาได้ที่ pH ต่างกัน จากการศึกษาการปลดปล่อยยาพบว่า ที่ pH 5.3 สามารถปลดปล่อยยาได้ 54.1% ในเวลา 2 ชั่วโมงและ 95.5% ในเวลา 6 ชั่วโมง ในขณะที่ pH 7.4 สามารถปลดปล่อยยาได้ 12.3% ในเวลา 2 ชั่วโมงและ 42.2% ในเวลา 6 ชั่วโมง และจากการศึกษากลไกการฆ่าเซลล์มะเร็งพบว่า สามารถฆ่าเซลล์มะเร็งโดยผ่านกลไกการ apoptosis ที่เกี่ยวข้องกับโปรตีน caspase-3 และ PARP ดังนั้นระบบนำส่งยาดด้วยอนุภาคซีลีเนียมระดับนาโนเมตรนี้มีแนวโน้มที่จะพัฒนาเป็นแนวทางการรักษามะเร็งต่อไปในอนาคต

ภาควิชา เคมี

ลายมือชื่อนิสิต

สาขาวิชา เคมี

ลายมือชื่อ อ.ที่ปรึกษาหลัก

ปีการศึกษา 2560

5772863123 : MAJOR CHEMISTRY

KEYWORDS: SELENIUM NANOPARTICLES / CHITOSAN / RESISTANT CANCER CELLS / PH-SENSITIVE / DOXORUBICIN

URARIKA LUESAKUL: DESIGN AND SYNTHESIS OF SELENIUM NANOPARTICLES TO OVERCOME MULTIPLE DRUG RESISTANCE OF CANCER CELLS. ADVISOR: PROF. DR.NONGNUJ MUANGSIN, Ph.D., pp.

The objective of this research is to synthesize selenium nanoparticles (SeNPs) stabilized by chitosan as a drug carrier for delivery doxorubicin to overcome drug-resistant in cancer cells. One important mechanism of multidrug resistance (MDR) includes decreased drug influx and increased drug efflux, leading to insufficient drug concentration to kill cancer cells. Therefore, to overcome MDR by increasing cellular uptake, the surface of SeNP was functionalized to provide 3 structural features: (i) a positive charge to improve their solubility, (ii) gallic acid, a hydrophobic molecule to enhance biocompatibility and (iii) folic acid, a targeting molecule to target cancer cells and enhance cellular uptake. The cytotoxicity of the DOX-SeNPs@TMC-FA was evaluated and found to enhance the activity of DOX by approximately 10-fold, resulting in decreased IC_{50} values compared to free DOX, while it showed less toxic in normal cells (WI-38). SeNPs@TMC-FA were taken up by cells, with cellular uptake increased further by folate receptor-mediated endocytosis, to overcome multidrug resistance. In addition, the DOX release profiles showed a pH dependence, which exhibited a faster release of DOX at pH 5.3 than at pH 7.4. The cumulative release amount of DOX at pH 5.3 was 54.1% within 2 h and 95.5% at 6 h, whereas the release rate at pH 7.4 was 12.3% in 2 h and 42.2% for 6 h. Mechanistic studies suggested that DOX-SeNPs@TMC-FA induced cell death through the apoptosis pathway by involvement of caspase-3 and PARP proteins. Hence, the results demonstrated that SeNPs@TMC-FA, has potential to develop as targeted carrier for overcoming drug resistance cells.

Department: Chemistry

Student's Signature

Field of Study: Chemistry

Advisor's Signature

Academic Year: 2017

ACKNOWLEDGEMENTS

I would like to thank my thesis advisor, Professor Dr. Nongnuj Muangsin, for her support, advice and encouragement to give me the good opportunity during this project. I am also grateful to Professor Dr. Neamati Nouri for their valuable advice and kindness during this project at University of Michigan, USA.

I would like to extend to Associate Professor Dr. Vudhichai Parasuk as the chairman, Professor Dr. Thawatchai Tuntulani, Associate Professor Dr. Nuanphun Chantarasiri and Dr. Thitiphan Chimsook for their kindness and suggestion throughout my research.

Moreover, I also would like to thank Khun Songchan Puthong for cytotoxicity experiments. I am strongly grateful for my financial support from the Department of Chemistry and funding from the Thailand Research Fund through the Royal Golden Jubilee Ph.D. Program (Grant No. PHD/0053/2557).

Finally, I am very appreciative of my family and my friends for their assistance and encouragement throughout my study period.

CONTENTS

	Page
THAI ABSTRACT	iv
ENGLISH ABSTRACT	v
ACKNOWLEDGEMENTS	vi
CONTENTS	vii
LIST OF TABLES	xi
LIST OF FIGURES	xii
LIST OF ABBREVIATIONS AND SYMBOLS.....	xv
CHAPTER 1 Introduction.....	1
1.1 Introduction.....	1
1.2 Scope of Research	3
1.3 Objectives of this research.....	5
CHAPTER 2 Background and Literature review.....	6
2.1 Multidrug Resistance.....	6
2.2 Nanoparticles	8
2.2.1 Classification of nanoparticles.....	9
2.2.2 Property of nanoparticles	9
2.2.3 Preparation of nanoparticles	11
2.2.3.1 Chemical method.....	12
2.2.3.2 Physical methods	12
2.2.3.3 Self-assembly method	13
2.2.4 Cellular uptake and exocytosis of nanoparticles.....	14
2.3 Selenium nanoparticles (SeNPs).....	16

	Page
2.3.1 Synthetic strategies.....	16
2.3.2 Surface functionalization of SeNPs for cancer treatment	18
2.4 Stimuli-responsive nanocarriers.....	23
CHAPTER III Experiments	25
3.1 Analytical Instrument	25
3.1.1 Nuclear magnetic resonance spectroscopy (NMR).....	25
3.1.2 Fourier transform infrared spectrometry (FT-IR).....	25
3.1.3 Scanning electron microscopy (SEM).....	25
3.1.4 Transmission electron microscopy (TEM)	26
3.2 Materials.....	26
3.3 Methods	27
Part I: Design and synthesis of chitosan and its derivatives used as stabilizer for preparation of SeNPs	28
3.3.1 Modification of chitosan and its derivatives.....	28
3.3.1.1 Synthesis of N,N,N-trimethylammonium chitosan (TMC)	29
3.3.1.2 Synthesis of folic acid-gallic acid-N,N,N-trimethylammonium chitosan (FA-GA-TMC).....	29
3.3.2 Calculation of degree of quaternization (%DQ) and degree of substitution (%DS).....	30
3.3.3 Determination of gallic acid content TMC-GA-FA	30
Part II: Preparation, surface functionalization, characterization and preliminary cytotoxic study of selenium nanocarriers using modified chitosan as a stabilizer.....	31
3.3.4 Preparation and functionalization of selenium nanocarriers.....	31

	Page
3.3.5 Fabrication of DOX-loaded SeNPs@TMC-FA.....	32
3.3.6 Cytotoxicity study	33
3.3.7 Colony formation assay.....	34
3.3.8 Cellular uptake study.....	34
3.3.9 Intracellular localization of DOX-SeNPs@TMC-FA.....	35
3.3.10 pH-responsive drug release.....	35
3.3.11 Combination assay	36
3.3.12 Western blotting.....	36
CHAPTER IV Results and Discussion.....	37
Part I: Modification of chitosan used as stabilizer.....	37
4.1 Synthesis and characterization of chitosan and its derivatives (CS, TMC, TMC-FA, TMC-GA-FA).....	38
4.1.1 ¹ H-NMR.....	39
4.1.2 FT-IR.....	41
Part II: Preparation, functionalization, characterization and preliminary cytotoxic study of selenium nanocarriers using modified chitosan as a stabilizer.....	43
4.2 Preparation and functionalization of selenium nanocarriers using modified chitosan as a stabilizer.....	43
4.3 Characterization of selenium nanocarriers using modified chitosan as a stabilizer.....	45
4.3.1 SEM.....	45
4.3.2 TEM and EDX	47
Proposed mechanism of cubic-like SeNPs	48
4.3.3 UV/VIS.....	50

	Page
4.3.4 DLS.....	51
4.3.5 Zetasizer Analysis.....	52
4.4 Preliminary cytotoxic study of selenium nanocarriers using modified chitosan as a stabilizer.....	53
4.4.1 The effect of functionalized molecules on the surface of SeNPs	53
4.4.2 The effect of folic acid content in SeNPs@TMC-FA on their cytotoxic activity.....	54
Part III Fabrication of doxorubicin drug-loaded SeNPs and evaluation of their biological activity	57
4.5 Preparation and Characterization of DOX-SeNPs@TMC-FA.....	57
4.6 Cytotoxic activities against sensitive (OVCAR8) and resistant (NCI/ADR-RES) ovarian cancer cells.....	61
4.6.1 MTT assay	61
4.6.2 Colony assay.....	63
4.7 Cellular uptake	64
4.8 Intracellular localization of DOX-SeNPs@TMC-FA	66
4.9 Release profile of DOX-SeNPs@TMC-FA.....	67
4.10 Cell morphology of NCI/ADR-RES after treatment with DOX-SeNPs@TMC- FA	69
4.11 Mechanism of action of DOX-SeNPs@TMC-FA.....	70
4.11.1 Combination assay	70
4.11.2 Western blotting	72
CHAPTER V Conclusion.....	73
REFERENCES	74

VITA.....87



จุฬาลงกรณ์มหาวิทยาลัย
CHULALONGKORN UNIVERSITY

LIST OF TABLES

Table 1 Examples of the modification of SeNPs for cancer treatment applications as therapeutic agent, drug carriers and for overcoming MDR	22
Table 2 Characterization of SeNPs stabilized with all types of stabilizers	52
Table 3 Characterization of SeNPs@TMC-FA at different concentrations.....	56
Table 4 Cytotoxicity of DOX-SeNPs@TMC-FA, SeNPs@TMC-FA and DOX	62



LIST OF FIGURES

Figure 1 Scope of this research	4
Figure 2 Cellular factors responsible for the multidrug resistance [23]	6
Figure 3 A model of the internalization process for free drugs and drugs in nanocarriers in normal tumor cells and MDR tumor cells [26]	7
Figure 4 Illustration of the enhanced permeation and retention (EPR) effect of macromolecular structures as drug delivery systems in malignant tissue [28]	8
Figure 5 Classification of nanoparticles: inorganic and organic NPs	9
Figure 6 A summary of important factors influencing property of nanoparticles for cancer treatment [41]	11
Figure 7 The possible mechanism for the formation of controlled assembly chains of Au, Ag, or PtNPs based on the electrostatic interaction [15]	13
Figure 8 Chemical structure of thiolated chitosan and illustration of chitosan- directed gold nanoparticles assembly into differently shaped nanoparticles [46]	14
Figure 9 Endocytosis and exocytosis patterns of nanoparticles [47]	15
Figure 10 SeNPs with various morphologies, such as (A) nanoribbons, (B) nanoplates, (C) flower-like structure, (D) nanospheres, (E) nanorods, and (F) nanotubes, have been synthesized by numerous synthetic strategies	17
Figure 11 The levels of mRNA expression for the FOLR1 gene on a logarithmic scale in various cancer cell types	18
Figure 12 (A) The proposed structure of FA-SeNPs (B) The TEM image and (C) the cell viability of resistant-HepG2 compared with sensitive-HepG2 and normal cells, and the schematic of selective cellular uptake via endocytosis[19]	19
Figure 13 (A) Formation of the arginine stabilized-selenium nanoparticles conjugate with Ru(II) complex (Ru@L/D-SeNPs) delivery systems. (B) Mechanism of	

drug resistance and the inducement of apoptosis in cis-platinum resistance cancer cells [20].....	20
Figure 14 SeNPs was designed for systemic dual-delivering siRNA and cisplatin [24]..	21
Figure 15 Schematic diagram of the dynamic response progress of intelligent nanoparticles. (A) pH-responsive nanoparticles, (B) Redox-responsive nanoparticles, (C) Light-triggered nanoparticles [56].	24
Figure 16 Experiment procedure	27
Figure 17 Schematic representation of the Synthesis of TMC, and TMC-GA-FA	28
Figure 18 Preparation of SeNPs using modified chitosan as a stabilizer	31
Figure 19 Preparation and proposed structure of DOX-SeNPs@TMC-FA.....	32
Figure 20 Molecular structure of modified chitosan (TMC-GA-FA)	38
Figure 21 Synthesis of TMC and TMC-GA-FA.....	38
Figure 22 ¹ H-NMR of chitosan and its derivatives.....	40
Figure 23 FTIR spectra of chitosan and its derivatives.....	42
Figure 24 SEM images of (A) SeNPs@Vc, (B) SeNPs@CS, (C) SeNPs@TMC, (D) SeNPs@FA-TMC, and (E) SeNPs@FA-GA-TMC.....	47
Figure 25 (A) TEM image and (B) EDX spectrum of SeNPs@FA-GA-TMC.....	48
Figure 26 Scheme of the proposed mechanism for the formation.....	50
Figure 27 UV/VIS spectrum of SeNPs stabilized with different types of stabilizer.....	51
Figure 28 Growth inhibition by SeNPs with different types of stabilizers at a concentration of 3 μ M against resistant NCI/ADR-RES cancer and WI-38 normal cells	54
Figure 29 UV/VIS of SeNPs at different concentrations of TMC-FA.....	55
Figure 30 Preparation and proposed structure of DOX-SeNPs@TMC-FA.....	57

Figure 31 Characterization of DOX-SeNPs@TMC-FA: (A) TEM image of DOX-SeNPs@TMC-FA dispersed in PBS (pH 7.4) and in (B) acidic PBS solution, pH 5.3, and the inset shows an enlarged image.....	58
Figure 32 EDX analysis of DOX-SeNPs@TMC-FA.....	59
Figure 33 Characterization of DOX-SeNPs@TMC-FA: (A) size distribution from DLS analysis and (B) zeta potential of DOX-SeNPs@TMC-FA.....	60
Figure 34 IR spectra of DOX, SeNPs@TMC-FA and DOX-loaded SeNPs@TMC-FA.....	60
Figure 35 Colony formation assay of DOX, SeNPs@TMC-FA and DOX-SeNPs@TMC-FA.....	64
Figure 36 Quantitative analysis of cellular uptake efficacy of coumarin-6-loaded SeNPs at concentrations of 1 μ M for 24, 48 and 72 h in NCI/ADR-RES cells.....	66
Figure 37 Intracellular localization of SeNPs in NCI/ADR-RES cells labeled with Hoechst (nucleus) and treated with SeNPs at 37°C for 6 h and visualized by fluorescence microscopy.....	67
Figure 38 In vitro release profiles of DOX-SeNPs@TMC-FA in PBS solution at pH 7.4 and in acetic acid solution at pH 5.3.....	69
Figure 39 Morphology of NCI/ADR-RES cells treated with DOX-SeNPs@TMC-FA at 37°C for different periods of time and visualized under a fluorescence microscope .	70
Figure 40 Cell viability of DOX-SeNPs@TMC-FA after pretreatment with Z-VAD (40 μ M), NAC (3 mM), DFO (10 μ M), Necrostatin (40 μ M) and Necro (10 μ M) in NCI/ADR-RES cells.....	71
Figure 41 Effects of DOX-SeNPs@TMC-FA on the expression levels of apoptosis-associated proteins, PARP and Caspase-3, was analyzed by Western blotting. NCI/ADR-RES cells were treated with DOX-SeNPs@TMC-FA at different concentrations (0.5 and 1.0 μ M) for 24 h.....	72

LIST OF ABBREVIATIONS AND SYMBOLS

NMR	Nuclear magnetic resonance spectroscopy
UV/VIS	Ultraviolet-visible spectroscopy
FT-IR	Fourier Transform Infrared spectroscopy
SEM	Scanning electron microscopy
TEM	Transmission electron microscopy
CH ₃ I	Methyl iodide
NMP	<i>N</i> -methylpyrrolidone
EDC	1-ethyl-3-(3-dimethylaminopropyl)carbodiimide
NHS	<i>N</i> -hydroxysuccinimide
GA	gallic acid
FA	folic acid
DOX	doxorubicin
CS	chitosan
TMC	<i>N,N,N</i> -trimethylammonium chitosan
TMC-FA	folic acid- <i>N,N,N</i> -trimethylammonium chitosan
TMC-GA	gallic acid- <i>N,N,N</i> -trimethylammonium chitosan
TMC-GA-FA	folic acid-gallic acid- <i>N,N,N</i> -trimethylammonium chitosan
SeNPs	selenium nanoparticles
SeNPs@Vc	selenium nanoparticles stabilized with ascorbic acid
SeNPs@CS	selenium nanoparticles stabilized with chitosan
SeNPs@TMC	selenium nanoparticles stabilized with <i>N,N,N</i> -trimethylammonium chitosan
SeNPs@TMC-FA	selenium nanoparticles stabilized with folic acid- <i>N,N,N</i> -trimethylammonium chitosan
SeNPs@TMC-GA-FA	selenium nanoparticles stabilized with folic acid-gallic acid- <i>N,N,N</i> -trimethylammonium chitosan
DOX-SeNPs@TMC-FA	doxorubicin-loaded selenium nanoparticles stabilized with folic acid- <i>N,N,N</i> -trimethylammonium chitosan

Z-VAD-FMK	N-Benzyloxycarbonyl-Val-Ala-Asp(O-Me) fluoromethyl ketone;),
NAC	n-acety-cysteine
DFO	deferoxamine
Necro	necrostatin
%DQ	degree of quaternization
%DS	degree of substitution
δ	chemical shift
μL	microliter
μM	micromolar
μmol	micromole
aq	aqueous
g	gram
h	hour
MeOH	methanol
mg	milligram
MHz	megahertz
min	minute
μL	microliter
mL	milliliter
mM	millimolar
mmol	millimole
$^{\circ}\text{C}$	celcius degress
PBS	phosphate buffered saline
ppm	part per million
PVDF	polyvinylidene-fluoride
SDS-PAGE	sodium dodecyl sulfate-polyacrylamide gel electrophoresis
OVCAR8	sensitive ovarian cancer cells
NCI/ADR-RES	resistant ovarian cancer cells
WI-38	normal cells
MTT	3-(4,5-dimethylthiazol-2-yl)-2,5-diphenyltetrazolium bromide

CHAPTER 1

Introduction

1.1 Introduction

Cancer is one of the major causes of death worldwide and projected to continue rising [1]. Currently, doxorubicin (DOX)-based combination chemotherapy is the main therapeutic strategy for various types of carcinomas, but it fails to treat cancers with multidrug resistance or MDR. The most well-documented mechanism of MDR involves drug efflux mediated by ATP-binding cassette (ABC) transporters, typically P-glycoprotein (P-gp) [2]. P-gp is over-expressed in many human cancers and increases the efflux of intracellular anticancer drugs, leading to low intracellular drug accumulation and down-regulation of the chemotherapy efficacy [3, 4]. Therefore, overcoming the increased drug efflux is a great challenge for cancer treatments. One of the current strategies for overcoming MDR is using an inhibitor of the drug efflux pump to circumvent the efflux by P-gp. Various small molecules, including natural products, pharmaceutical inert excipients and formulations including cyclosporine A, verapamil and PSC833, have been identified as P-gp inhibitors, but failed in clinical trials due to their poor specificity and high toxicity [5].

Nanoparticles enable unique approaches for cancer treatment. Over the last two decades, a large number of nanoparticle delivery systems have been developed for cancer therapy [6]. Basically, the property of nanoparticles depends on numerous important factors, including their shape, size, surface charge and surface functional groups [7-9]. Therefore, appropriate NPs need to be designed rationally according to specific application. These nanoparticles also have been designed to overcome the drug resistance of cancer cells by bypassing the P-gp-mediated drug efflux pumps through (i) enhanced biodistribution and cell internalization, (ii) inhibition of drug efflux, (iii) combinational treatments (e.g., siRNA and radiation), or (iv) nanoparticle-mediated

endocytosis, as well as increasing intracellular drug accumulation through stimuli-responsive drug release [10-12].

Among those strategies, stimuli-responsive drug release based on pH variation, which is expected to stabilize the drug in the natural environment, has received more attention and rapidly achieves drug release once the pH of the microenvironment reaches the trigger point, resulting in increased intracellular drug accumulation to overcome resistance. Furthermore, in the case of cancer therapy, tumor cells have lower pH values than normal cells because of anaerobic glucose metabolism. The pH difference between normal and cancer cells can also be used for targeted drug delivery to reduce side effects in normal cells; therefore, the pH-triggered approach is one of the most efficient strategies for a drug delivery system. Hence, several groups have worked to develop pH-sensitive nanoparticles to overcome multidrug resistance.

Chitosan (CS) is known for pH-dependent swelling and is a controlled drug release polymer, providing selective drug release in acidic intracellular vesicles such as endosomes and lysosomes in targeted tumor cells [13]. It has been reported that CS provides pH-responsive drug release because its amino groups are protonated at acidic pH. In addition, chitosan is also widely used as a stabilizer for various nanoparticles because of its nontoxicity, high biodegradability and good biocompatibility [14-16]. As a result, various studies have shown that chitosan-based nanocarriers can overcome MDR in cancer cells.

Selenium nanoparticles (SeNPs) have received considerable attention as both potential cancer therapeutic agents and drug carriers due to their biocompatibility, low toxicity, and excellent chemopreventative effects [17, 18]. To our knowledge, there are few previous reports on the design and development of SeNPs to overcome MDR. For instance, the first report demonstrated a nanoparticle-mediated endocytosis strategy using folate (FA)-conjugated SeNPs as a cancer-targeted nanodrug delivery

system, which can bypass the P-gp-mediated drug efflux pumps through FA receptor-mediated endocytosis to overcome the MDR in resistant-HepG2 cancer cells [19]. Other studies have designed combinational treatments of genes (siRNA) and/or drugs, including a Ru(II) complex and cisplatin using SeNPs as nanocarriers, which achieved efficacy in vitro and overcame MDR [4, 18, 20]. Taken together, we hypothesized that selenium nanodrug delivery system combining receptor-mediated endocytosis with pH-responsive drug release for bypassing the P-gp-mediated drug efflux pumps, increasing cellular uptake and drug intracellular accumulation would be able to overcome MDR.

1.2 Scope of Research

In this study, to overcome drug resistance effectively, we have designed a selenium nanodrug delivery system stabilized with targeting molecule, folic acid modified-chitosan that would be able to bypass P-gp efflux and enhance cellular uptake by resistant cells via receptor-mediated endocytosis, while pH-dependent property of chitosan outer coating of SeNPs could control drug release and increase intracellular drug accumulation, as shown in Figure 1.

Firstly, chitosan was modified to provide three structural features: (i) the positive charge from the $-N^+(CH_3)_3$ of the quaternized chitosan (TMC) increases the electrostatic interaction with cell membrane and increase cellular uptake; (ii) hydrophobic components, gallic acid (TMC-GA) to enhance biocompatibility and (iii) targeting molecule, folic acid (TMC-FA-GA) to specifically target the folate receptor overexpressed on cancer cells and also increase cellular uptake via folate-receptor mediated endocytosis [21]. As a result, we obtained 4 different types of stabilizing agents, including TMC, TMC-GA, TMC-FA, and TMC-GA-FA.

Secondly, each modified chitosan was then used as a stabilizer for fabrication of SeNPs as nanocarriers to investigate effect of functional molecule decorating SeNPs

surface on their activity and to explore suitable selenium nanocarriers for resistant cancer cells.

Finally, among various SeNPs, appropriate SeNPs were further used as nanocarrier for the delivery of anticancer drug, doxorubicin (DOX) to resistant cancer cells and evaluated their biological activity, including cytotoxicity, cellular uptake, intracellular localization, drug release, and protein expression.

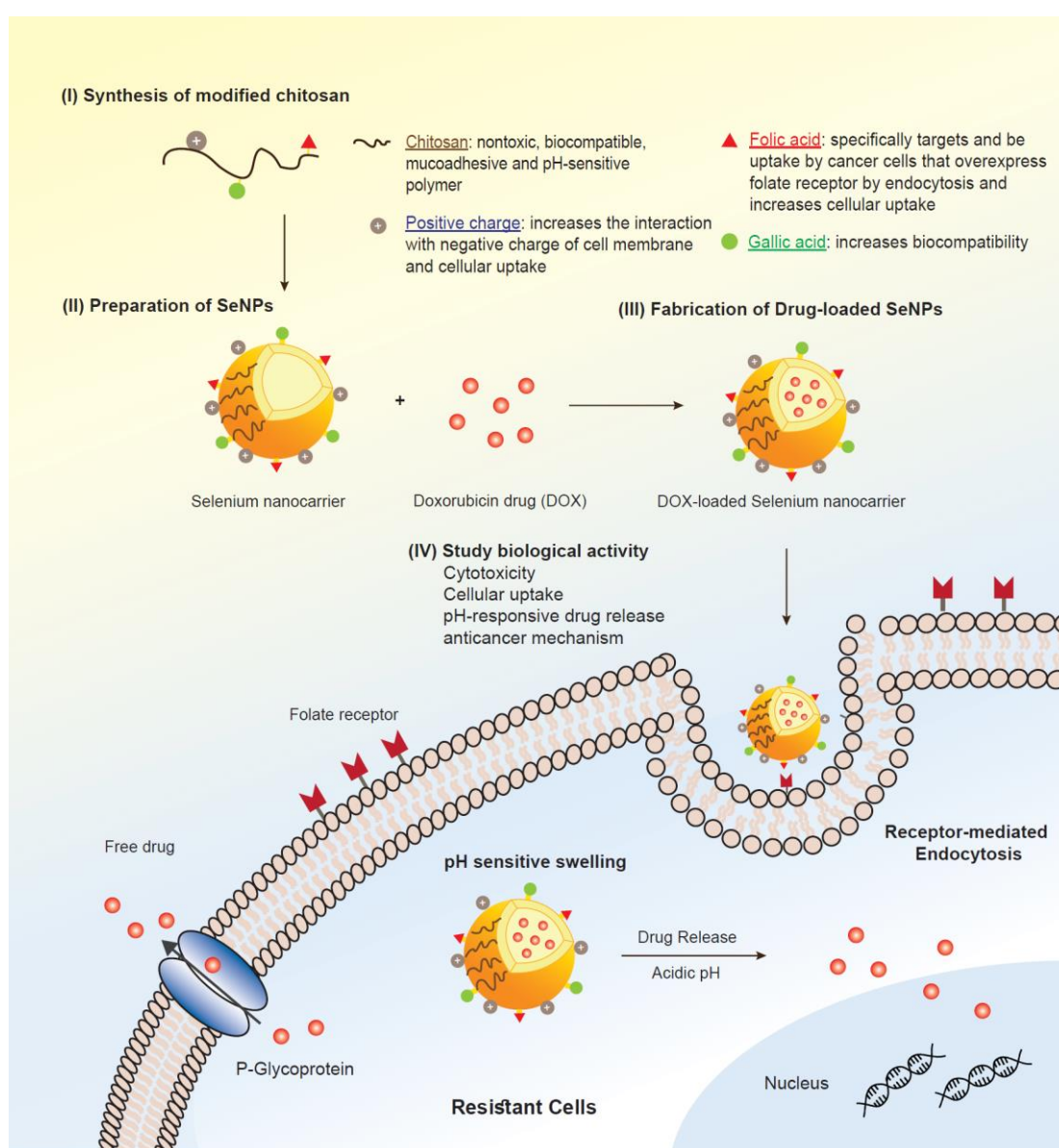


Figure 1 Scope of this research

1.3 Objectives of this research

1. To design, synthesize and characterize chitosan and its derivatives as a stabilizing agent for the preparation of SeNPs
2. To prepare, functionalize and characterize selenium nanoparticles as nanocarriers for delivery anticancer drug
3. To evaluate bioactivities of drug-loaded SeNPs against sensitive and resistant cancer cells, including cytotoxicity, cellular uptake, intercellular localization, pH-responsive drug release and anticancer mechanism for overcoming MDR



CHAPTER 2

Background and Literature review

2.1 Multidrug Resistance

Cancer is one of the major causes of death worldwide and projected to continue rising [1]. Although many researchers have devoted to the development of the effective ways for anticancer treatment, it is still limited by two major challenges [22]. First, chemotherapeutic agents enter into both cancer and normal cells, resulting in undesirable side effects. Second, the occurrence of multidrug resistance (MDR) leads to chemotherapeutic failure. The mechanisms of MDR include decreased drug influx, increased drug efflux, increased drug metabolism, increased DNA repair, lack of apoptotic machinery and increased antiapoptotic machineries as shown in Figure 2. Among them, P-glycoprotein (P-gp) has been regarded as the major mechanism that can pump drug outside the cells, lead to low intracellular drug accumulation [23]. Currently, various small molecules, including natural products, pharmaceutical inert excipients and formulations including cyclosporine A, verapamil and PSC833, have been identified as P-gp inhibitors, but failed in clinical trials due to their poor specificity and high toxicity.

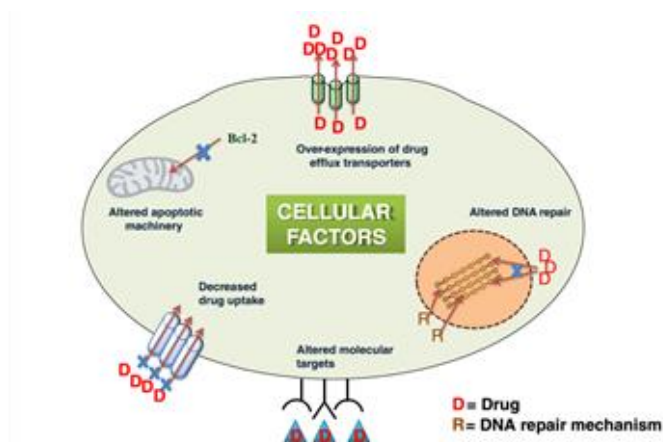


Figure 2 Cellular factors responsible for the multidrug resistance [23]

One important strategy for overcoming MDR is the use of nanoparticles to transport drug or codelivery of both drug and P-gp inhibitor to targeted site [17, 24]. Nanoparticles can efficiently bypass the drug efflux pump, circulate within blood vessel and penetrate into tumor cells by enhanced permeability and retention (EPR) effect [25]. Figure 3 demonstrated a model of the internalization process for free drugs and drugs in nanocarriers in normal tumor cells and MDR tumor cells. In normal tumor cells, most of drug reach their target site (A), while in MDR tumor cells, free drugs were pumped outside by transporters, resulting in very little drug reaches its target site (B). Furthermore, (C) and (D) showed that drugs encased in nanocarriers are internalized by endocytosis process that cannot be sensed by transporters on the MDR membrane. Therefore, nanoparticles could be potential candidate to overcome MDR [26].

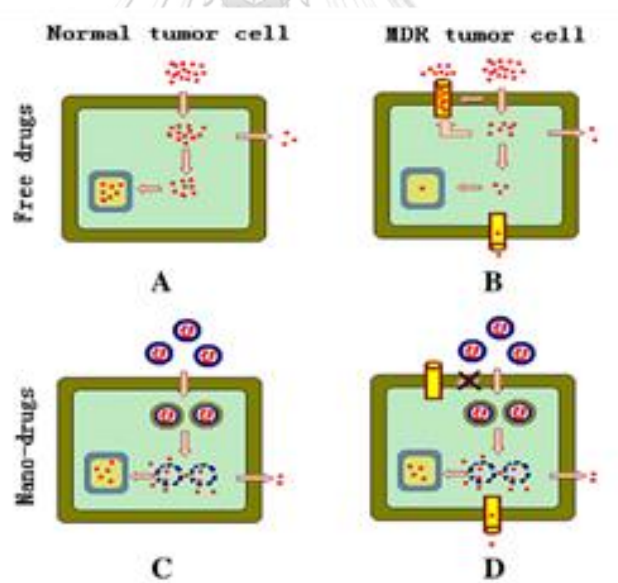


Figure 3 A model of the internalization process for free drugs and drugs in nanocarriers in normal tumor cells and MDR tumor cells [26]

2.2 Nanoparticles

Nanotechnology has unlocked new opportunities to overcome MDR through the controlled and targeted drug delivery especially for transportation drug across the targeted sites because of their unique properties. Nanoparticle-based drug delivery for cancer treatment primarily relies on the enhanced permeability and retention effect (EPR). The EPR is based on the nanometer size range of the nanoparticles and unique features of blood vessels that facilitates transport of macromolecules into tumor tissues. According to Figure 4, the leaky vascular structure in tumors allows extravasation of nanoparticles, and long-term retention of nanoparticles is attributed to the lack of lymphatic drainage [27].

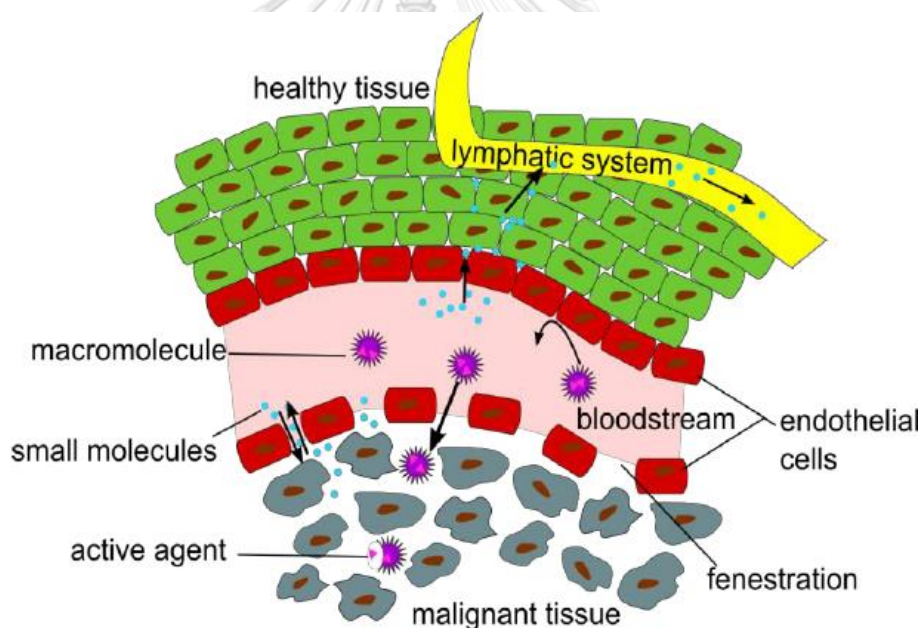


Figure 4 Illustration of the enhanced permeation and retention (EPR) effect of macromolecular structures as drug delivery systems in malignant tissue [28]

2.2.1 Classification of nanoparticles

In general, nanoparticles (NPs) can be classified as organic/polymeric (e.g. liposomes, dendrimers, micelles, and ferritin) and inorganic (e.g. gold nanoparticles, quantum dots, iron oxide and lanthanide ions) NPs, as shown in Figure 5. Comparison between organic and inorganic NPs, organic NPs provide more flexibility in terms of chemistry and structure for fabrication, while inorganic NPs have interesting physical properties such as specific optical or magnetic features [29-32].

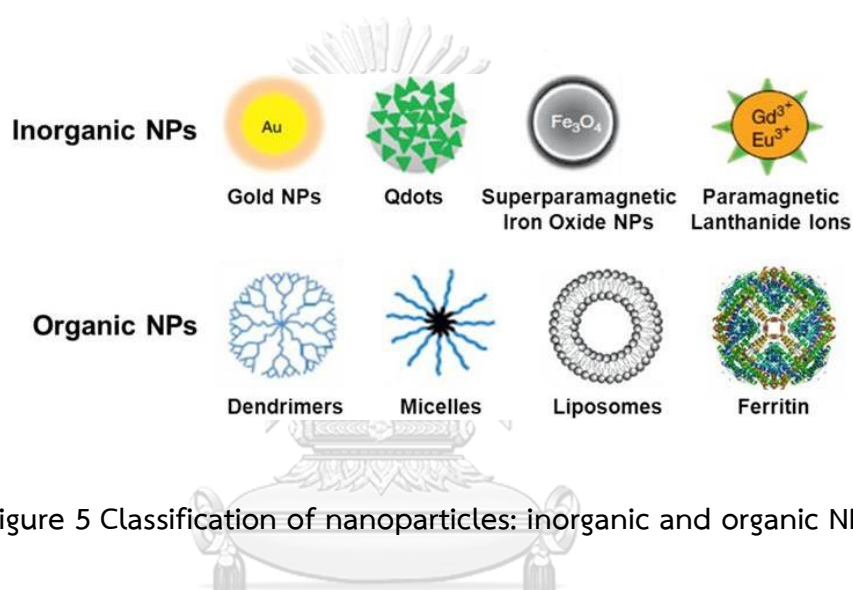


Figure 5 Classification of nanoparticles: inorganic and organic NPs

2.2.2 Property of nanoparticles

There are several important factors influencing the properties of NPs, especially in medical application such as composition, size, charge, shape and surface functionalization.

The size of NPs is a fundamental characteristic property that determines the passive targeting and biodistribution within tumors [33]. Several studies have shown NPs within the size range of 5-750 nm had selective penetration into tumor and showed extremely low accumulation in the healthy tissue. This phenomenon is due to the enhanced permeability and retention (EPR) effect of NPs as mentioned before [34]. The Surface charge is also an important factor determining the transport of NPs through the barrier. For example, positive surface charge of SeNPs enhances selective

cellular uptake of skin malignant cells, while against brain cancer, neutral and low concentrations of anionic NPs can be utilized safely as colloidal drug carriers to brain. In contrast, high concentration anionic NPs (zeta potential between -15 to -60 mV) and cationic NPs (zeta potential between 15 to 45 mV) cause immediate toxicity to barrier integrity [35, 36]. Therefore, the surface charges of NPs should be considered for toxicity and distribution profiles, as well as cell types.

In addition, specifically-designed nanoparticles with surface functionalization can provide the selective or specific site, non-toxicity, enhanced cellular uptake, as well as improved payload capacity for effective delivery. Using different strategies, nanoparticles have been functionalized with a variety of ligands such as small molecules, surfactants, dendrimers, polymers, and biomolecules. For examples, ligands are: i) capable of mediating protein adsorption (e.g. polysorbate) [37]; ii) capable of increasing charge and hydrophobicity (e.g. amphiphilic peptides) [29, 38]; iii) able to improve blood circulation (e.g. polyethylene glycol) [39] and iv) able to target directly with receptor on cell membrane such as peptides (e.g. RGD, NGR and pep-1 peptides), proteins (transferrin) and antibodies (e.g. nicotinic acetylcholine receptor, EGFR, IL13R α 2, and LRP1 antibodies) [40]. In addition, small molecules and polymeric ligands offer the capability to incorporate therapeutic drugs or bio-macromolecules by covalent or non-covalent conjugation.

Overall, several parameters can influence the property of NPs to transport the drug across cell membrane. Therefore, it is important to note that appropriate nanoparticles system need to be designed and modulated to meet the objectives of the proposed function.

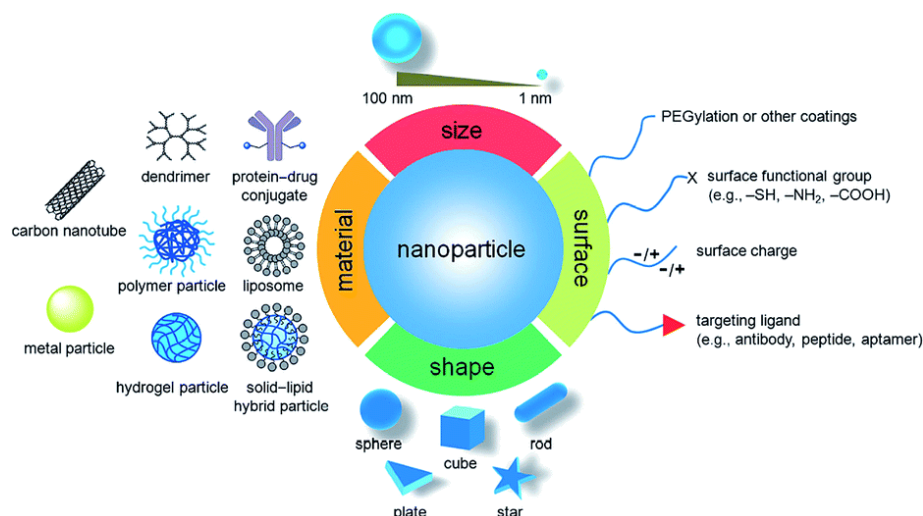


Figure 6 A summary of important factors influencing property of nanoparticles for cancer treatment [41]

2.2.3 Preparation of nanoparticles

Nanoparticles find applications in a wide variety of fields, especially biomedical application. Numerous methods have been developed to obtain material with nanometer scale. The ideal for preparation of nanoparticles should possess ability to control the size and shape of the particles with monodisperse that are related to their property. Nanoparticles can be synthesized from various materials by several physical and chemical methods. For NPs, physical methods often rely on a “top-down” approach by subdividing some bulk (precursor) material into smaller units. In contrast, chemical procedures are mainly “bottom-up” approaches that start with a chemical reaction delivering the metal atoms, followed or accompanied by controlled aggregation of atoms into particles [42].

2.2.3.1 Chemical method

Chemical method is the most frequently applied method for fabrication of nanoparticles because of the potential to synthesize large quantity of nanoparticles with good control of size, shape, morphology, composition, and surface chemistry at a reasonable low production cost [43]. Essentially, a precursor of metal such as an inorganic salt or an organometallic complex is reduced to generate neutral metal atoms by reducing agents such as sodium citrate, ascorbic acid, sodium borohydride, and polyol compounds. In the absence of stabilizers, the atoms quickly agglomerate and precipitate as “metal black” with larger size. It is important to use stabilizer to stabilize nanoparticles growth, prevent the aggregation through the steric effect and possible to control the size and shape of the particles with monodisperse that are related to their property. Besides the appropriate choice of the stabilizer, the metal precursor, the reducing agent, and the solvent are also important.

2.2.3.2 Physical methods

Physical methods such as solvated metal atoms, laser ablation, electrochemical synthesis, plasma method, photochemical method, generally require a specific apparatus (laser, solvated metal atom dispersion (SMAD) reactor, source of γ -rays, etc. The advantage of physical methods is no chemical reducing agent is involved, as laser ablation and metal vapor deposition methods do not require reduction, while metal cations are reduced by electric current in case of the electrochemical synthesis [43].

2.2.3.3 Self-assembly method

The self-assembly of nanoparticles into high-order and stable structures has become an attractive strategy to control size and shape of nanoparticles. Self-assembly is typically driven by simple interactions such as electrostatic interaction, hydrophobic interaction, hydrogen bonding, and van der Waals forces [44]. During the assembly process, biomacromolecules with well-defined monomer units are usually introduced to direct and control the assembly of particles to obtain the desired structure [14, 15, 45]. In many cases, polymers were modified with functional ligands, providing an effective template for controlling the size and shape of nanoparticles through the assembly process [16, 46], as well as its biological activity.

For example, according to Figure 7 chitosan was modified with an anionic ligand, o-carboxymethyl, or a cationic N-trimethylamino group. Through the controlling effect of the negative and positive charges of chitosan, gold nanoparticles were assembled into different structures [15].

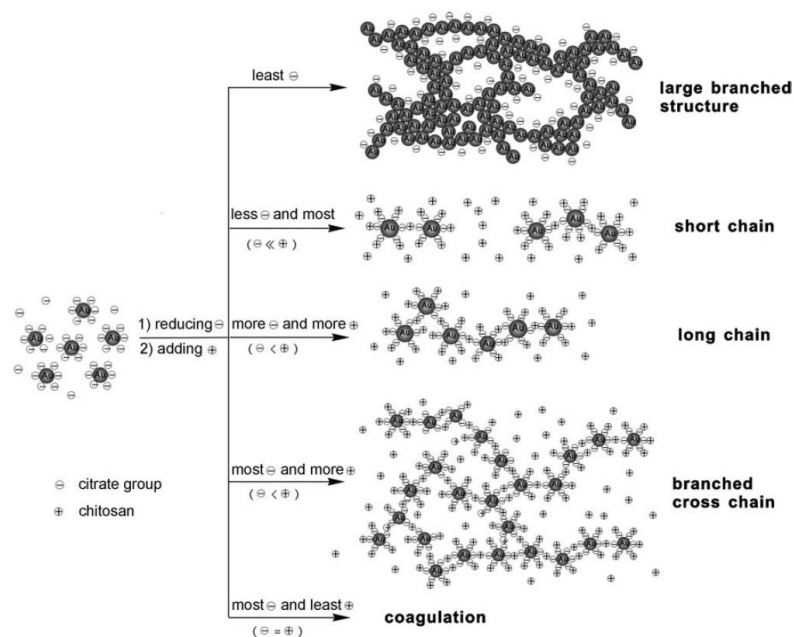


Figure 7 The possible mechanism for the formation of controlled assembly chains of Au, Ag, or PtNPs based on the electrostatic interaction [15]

Ding et al. (2009) [46] reported thiolate-functionalized chitosan as a soft template for the fabrication of gold nanochains, nanoneedles and nanoflowers. The –SH group of chitosan interacts extensively with gold nanoparticles belonging to different assemblies.

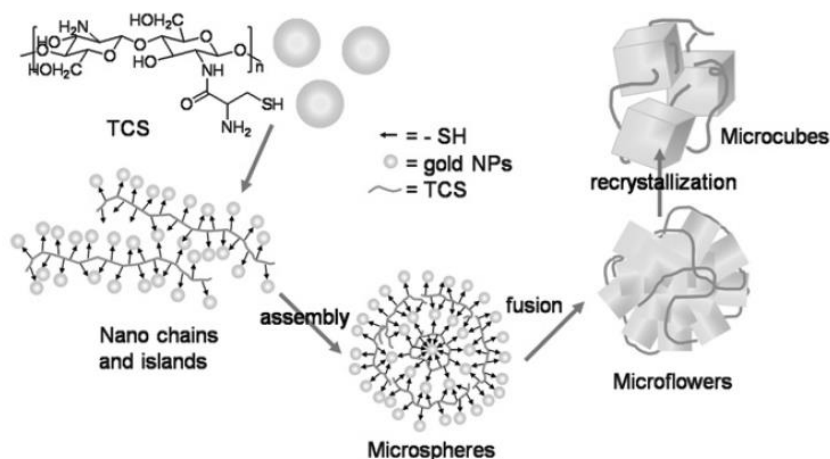


Figure 8 Chemical structure of thiolated chitosan and illustration of chitosan-directed gold nanoparticles assembly into differently shaped nanoparticles [46]

2.2.4 Cellular uptake and exocytosis of nanoparticles

Nanoparticles enter into the cells via 4 pathways: phagocytosis, endocytosis, macropinocytosis and pinnocytosis, and exit via 3 pathways: non-vesicle related secretion, exocytosis, and vesicle related secretion as described in Figure 9. The phagocytosis involves the ingestion of large particles by large vesicles called phagosomes (diameter 250 nm), while the pinnocytosis involves the ingestion of fluids and solutes through small pinocytotic vesicles (diameter from a few up to hundreds of nm), except for macropinocytosis that involves formation of vesicles bigger than 1 μm up to 5 μm [47, 48]. In addition, the best-characterized form of endocytosis is receptor-mediated endocytosis, which provides a mechanism for the selective uptake of specific nanoparticles that bind to specific cell surface receptors. There are 5 main steps involved in endocytic pathway as followed: (1) binding of targeting ligand-

conjugated NPs to cell-surface receptor. (2) Membrane invagination results in an endosome. (3) membrane degradation results in a late endosome and (4) lysosome (5) lysosomes fuse with membrane, called exocytosis. It is also believed that the endocytosis efficiency of nanoparticles depends on the physicochemical properties, such as size, shape, and surface chemistry, as well as cell type.

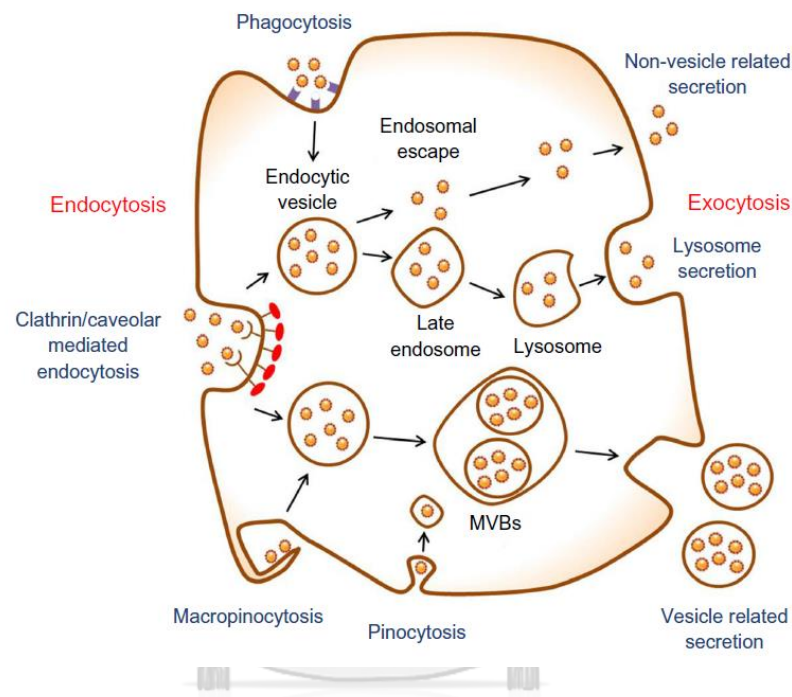


Figure 9 Endocytosis and exocytosis patterns of nanoparticles [47]

2.3 Selenium nanoparticles (SeNPs)

2.3.1 Synthetic strategies

Selenium nanoparticles (SeNPs) have attracted considerable attention in biomedical applications because of their unique physical and chemical properties, which differ from the properties of the corresponding bulk materials). SeNPs exhibit potential as therapeutic agents and drug carriers, as well as excellent bioavailability and low toxicity [20, 25, 49, 50]. The preparation method needs to control the factors influencing the properties of nanoparticles such as size, shape, surface charge and composition. In the past decade, SeNPs with various morphologies, such as nanowires, nanoribbons, nanoplates, nanotubes, and nanospheres, have been synthesized by numerous synthetic strategies, as shown in Figure 10 [51-53]. For example, Cao et al. used a direct physical vapor deposition process to produce selenium nanoribbons [51]. Yin et al. reported the ethylenediamine-assisted growth of selenium nanoplates via a hydrothermal process [53]. Selenium spherical particles were prepared by reducing selenous acid with hydroquinone in the presence of a dispersing agent. In addition, Chen et al. described a controllable approach to synthesize selenium nanospheres and nanorods by using L-cysteine as both a reductant and soft template, accompanied by ultrasonication [54]. To our knowledge, among the various shapes of SeNPs, only spherical particles have been focused for investigating their biological activity.

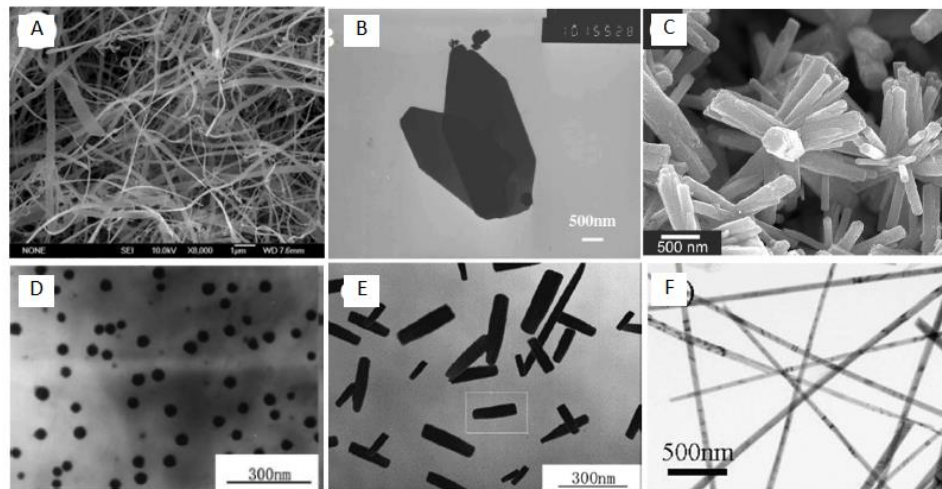
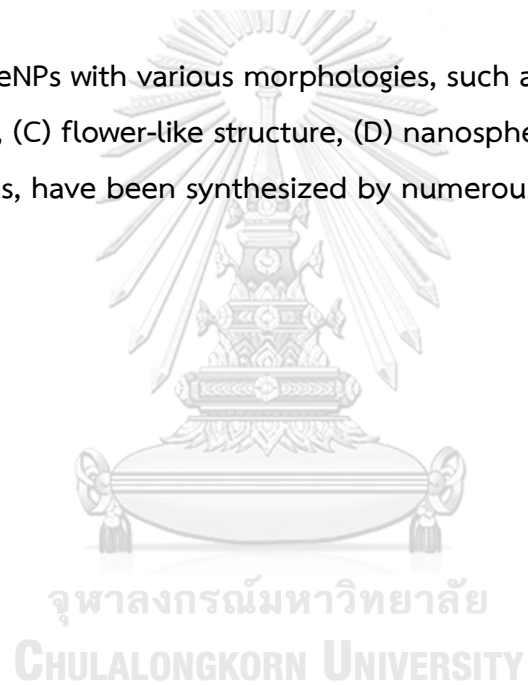


Figure 10 SeNPs with various morphologies, such as (A) nanoribbons, (B) nanoplates, (C) flower-like structure, (D) nanospheres, (E) nanorods, and (F) nanotubes, have been synthesized by numerous synthetic strategies



2.3.2 Surface functionalization of SeNPs for cancer treatment

As mentioned before, surface functional group is one of the important factors influencing the properties of nanoparticles. With respect to anticancer efficacy, previous studies have developed the activity of SeNPs through their surface functionalization as summarized in Table 1. For examples, modification with positive surface charge, targeting molecules such as folic acid and transferrin in order to enhanced selective cellular uptake and efficacy. For example, previous study evaluated FOLR1 gene expression levels in cancer models. A summary of gene expression data (generated from the Cancer Cell Line Encyclopaedia) showing the levels of mRNA expression for the FOLR1 gene on a logarithmic scale in various cancer cell types as shown in Figure 11.

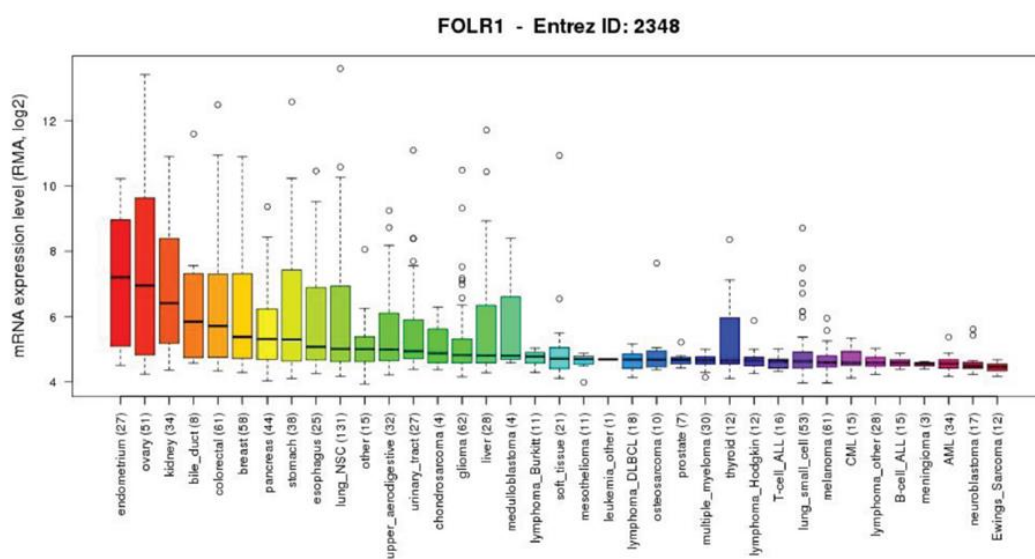


Figure 11 The levels of mRNA expression for the FOLR1 gene on a logarithmic scale in various cancer cell types

However, in case of overcoming MRD, there are few previous reports on the design and development of SeNPs to overcome MDR. For instance, according to Figure 12 the first report demonstrated a nanoparticle-mediated endocytosis strategy using folate (FA)-conjugated SeNPs as a cancer-targeted nanodrug delivery system, which can bypass the P-gp-mediated drug efflux pumps through FA receptor-mediated endocytosis, leading to overcome the MDR in R-HepG2 cells [19].

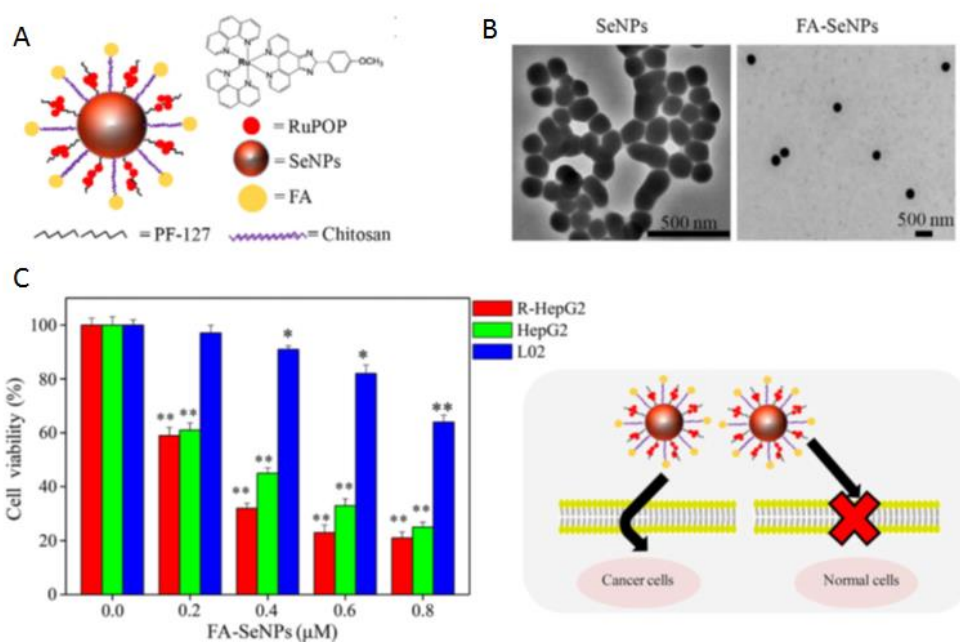


Figure 12 (A) The proposed structure of FA-SeNPs (B) The TEM image and (C) the cell viability of resistant-HepG2 compared with sensitive-HepG2 and normal cells, and the schematic of selective cellular uptake via endocytosis[19]

Other studies have designed combinational treatments of drugs, including a Ru(II) complex and cisplatin using SeNPs as nanocarriers. SeNPs were modified with arginine, an amphiphilic molecule bearing a hydrophilic head and hydrophobic tailing to increase biocompatibility with cell membrane. Cisplatin-resistant A549R cells treated with SeNPs demonstrated significant downregulation of P-glycoprotein (P-gp) expression, resulting in unprecedented enhanced cytotoxicity through the induction of apoptosis and finally overcame MDR [20].

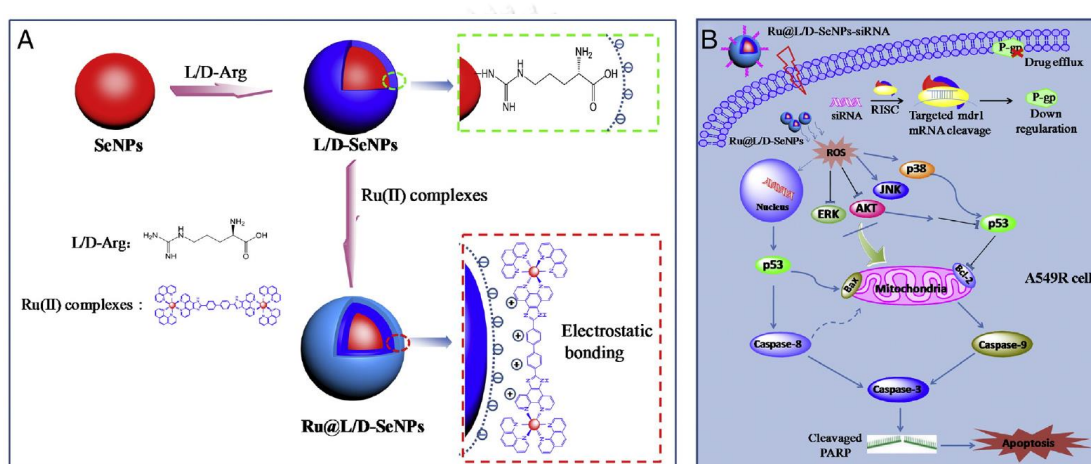


Figure 13 (A) Formation of the arginine stabilized-selenium nanoparticles conjugate with Ru(II) complex (Ru@L/D-SeNPs) delivery systems. (B) Mechanism of drug resistance and the induction of apoptosis in cis-platinum resistance cancer cells [20]

In addition, Zheng et al. have designed multifunctional polyamidoamine-modified selenium nanoparticles as nanocarriers for dual-delivering siRNA and cisplatin to A549/DDP cells) to downregulate the expression of P-gp and induce cell apoptosis, leading to overcome MDR [24].

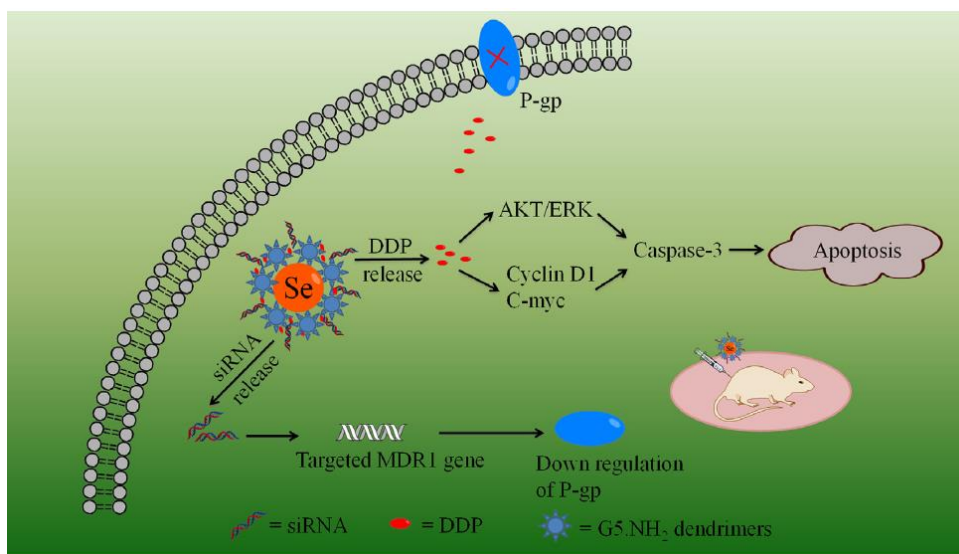


Figure 14 SeNPs was designed for systemic dual-delivering siRNA and cisplatin

[24]

Table 1 Examples of the modification of SeNPs for cancer treatment applications as therapeutic agent, drug carriers and for overcoming MDR

Ref	Size (nm)	Surface group	surface charge	Therapeutic agent	Advantages
SeNPs as therapeutic agent					
Yu et al (2012)	120	chitosan coated (NH ₂)	(+)	NR*	Positive surface charge enhanced selective cellular uptake and anticancer efficacy of SeNPs
Pi et al (2013)	70	Folic acid (FA) (COOH)	(-)	NR	FA-protected SeNPs induced apoptosis and enhanced internalize through endocytosis
SeNPs as drug carriers					
Liu et al (2012)	70	5-Fluorouracil (OH-)	(-)	5-Fluorouracil	SeNPs as a carrier of 5FU achieved anticancer synergism
Shirazi et al (2014)	110-150	Cyclic peptide - tryptophan - arginine - cysteine (COOH, NH ₂ , SH)	(+)	Irinotecan Gemcitabine Doxorubicin Paclitaxel etc.	SeNPs as drug transporter Improving the cellular uptake of drugs
Huang et al (2013)	130	Transferrin (COOH, NH ₂)	(-)	Doxorubicin	Transferrin targeted SeNPs showed selective cellular uptake and induction of apoptosis of cancer
Yu et al (2014)	200	Folate-chitosan Snowflake	(+)	Curcumin	Folate conjugated SeNPs as a transformable drug carrier enhanced chemotherapeutic effects
SeNPs for overcoming MDR					
Zheng et al (2015)	50-100	Polyamidoamine (NH ₂)	(+)	Dual delivery siRNA and cisplatin	SeNPs served as dual-delivery of siRNA and cisplatin for overcoming multidrug resistance
Chen et al (2015)	100	Arginine (COOH, NH ₂)	(-)	Dual delivery siRNA and Ruthenium complex	SeNPs served as dual-delivery of siRNA and cisplatin for overcoming multidrug resistance
Lui et al (2015)	250	Folic acid	(+)	Ruthenium complex	SeNPs overcoming the MDR I R- HepG2 cells through inhibition of ABC family protein expression

*NR = not report

2.4 Stimuli-responsive nanocarriers

One of the major problem of MDR is insufficient drug concentration and also tumor cells in low concentration of drug could result in acquired resistance. To overcome these problems, enhance drug accumulation and rapid drug release is crucial to provide optimum drug concentration and destroy tumor cells before they acquire the capability to efflux drug. Stimuli-responsive nanomedicine have been developed to trigger drug release for enhancing their activity in cancer treatment. There are different stimuli, such as physical stimuli (electrical, electrochemical, temperature, light, ultrasonic, and magnetic), chemical stimuli (ionic, redox, and pH), and biological stimuli (glucose, enzymes, and inflammation) [55]. Among those strategies, stimuli-responsive drug release based on pH variation, which is expected to stabilize the drug in the natural environment, has received more attention and rapidly achieves drug release once the pH of the microenvironment reaches the trigger point, resulting in increased intracellular drug accumulation to overcome resistance. Furthermore, in the case of cancer therapy, tumor cells have lower pH values than normal cells because of anaerobic glucose metabolism. The pH difference between normal and cancer cells can also be used for targeted drug delivery to reduce side effects in normal cells; therefore, the pH-triggered approach is one of the most efficient strategies for a drug delivery system. Hence, several groups have worked to develop pH-sensitive nanoparticles to overcome multidrug resistance.

Figure 15 showed (A) an example of pH-responsive nanoparticles loaded with small molecule inhibitors. In the acidic endosomal environment, cargo was triggered and release drug to inhibit P-gp function. Redox-responsive nanoparticles, as shown in Figure 15B was triggered and release siRNA and drug under GSH rich condition via disulfide bond cleavage. In addition, light-triggered nanoparticles with photosensitizer could increase the temperature in tumor sites via photothermal therapy (PTT) or generate reactive oxygen species (ROS), leading to endosomal disruption and abundant drug release as shown in Figure 15C [56].

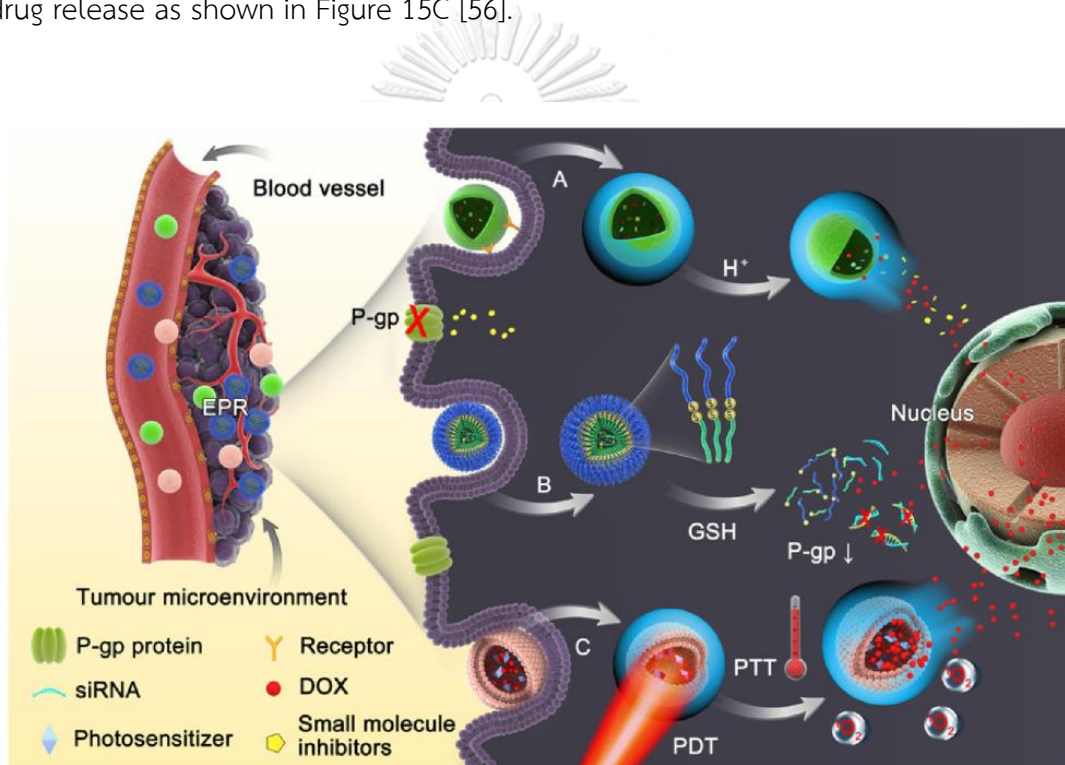


Figure 15 Schematic diagram of the dynamic response progress of intelligent nanoparticles. (A) pH-responsive nanoparticles, (B) Redox-responsive nanoparticles, (C) Light-triggered nanoparticles [56].

CHAPTER III

Experiments

3.1 Analytical Instrument

3.1.1 Nuclear magnetic resonance spectroscopy (NMR)

The ^1H NMR spectra at 400 MHz were recorded on Varian Mercury spectrometer. The ^{13}C NMR spectra at 400 MHz were recorded on Bruker model ACF200 spectrometer. All chemical shifts were reported in part per million (ppm) using the residual proton or carbon signal in deuterated solvents as internal reference. The coupling constant (J) were reported in Hertz (Hz) and the ^1H and ^{13}C -NMR data were processed with the MestReNova software.

3.1.2 Fourier transform infrared spectrometry (FT-IR)

Fourier transform infrared spectra were recorded on Nicolet FT-IR Impact 410 Spectrophotometer. The solid samples were prepared by pressing sample with KBr. IR spectra were recorded between 400 cm^{-1} to 4000 cm^{-1} in Transmittance mode.

3.1.3 Scanning electron microscopy (SEM)

SEM samples were mounted onto an aluminum stub using double-sided carbon adhesive tape and coated with gold-palladium. Scanning was performed under high vacuum and at ambient temperature using a beam voltage of 15 kV.

3.1.4 Transmission electron microscopy (TEM)

TEM samples were prepared by dropping an aqueous solution onto copper grids. The micrographs were obtained on a transmission electron microscope (JEM-1400) operated at 120 kV and equipped with an energy-dispersive X-ray spectrometer.

3.1.5 Zetasizer

The size distribution of the SeNPs was evaluated with a particle size analyzer (Zetasizer nano series, Malvern instrument). The SeNPs were prepared in distilled water at a concentration of 1 mM. The sample size calculation was based on the dynamic light scattering (DLS) method as a software protocol. The scattered light was collected at an angle of 90° through fiber optics and converted to an electrical signal by an avalanche photodiode (APDS). The zeta potential of the SeNPs was determined using the particle sizer. The analysis was performed at a scattering angle of 90°.

3.2 Materials

Chitosan with an average molecular weight, Mw, of 500 kDa was provided by Seafresh Chitosan (Lab.) Co. Ltd., Thailand. The degree of deacetylation of the chitosan was determined to be 81% by ¹H NMR. Methyl iodide (CH₃I), N-methylpyrrolidone (NMP), 1-ethyl-3-(3-dimethylaminopropyl)carbodiimide (EDC), N-hydroxysuccinimide (NHS), gallic acid (GA), folic acid (FA), sodium selenite, ascorbic acid and doxorubicin (DOX), were purchased from Sigma-Aldrich Co., USA. All organic solvents used in this research were analytical grade, purchased from Aldrich, Fluka, or Merck Co., Lt. Cellulose dialysis tubing (Membrane Filtration Products, Inc., USA) with a molecular weight cutoff of 12-14 kDa was used to purify all modified chitosan samples.

3.3 Methods

The experiment is divided into 3 parts as shown in Figure 16:

Part I: Design and synthesis of chitosan and its derivatives used as stabilizer for preparation of SeNPs

Part II: Preparation, surface functionalization and preliminary cytotoxic study of selenium nanocarriers using modified chitosan as a stabilizer

Part III: Fabrication of doxorubicin drug-loaded SeNPs and evaluation of its biological activity

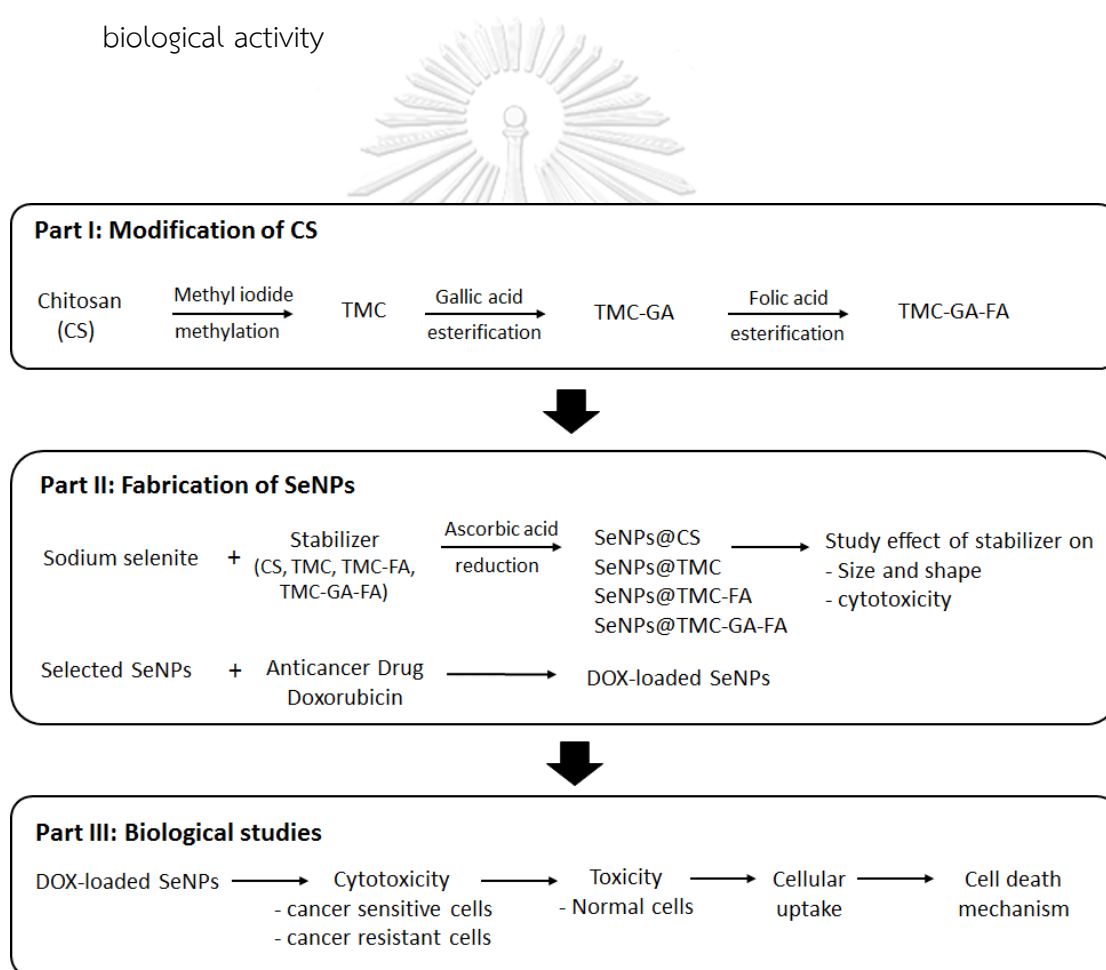


Figure 16 Experiment procedure

Part I: Design and synthesis of chitosan and its derivatives used as stabilizer for preparation of SeNPs

3.3.1 Modification of chitosan and its derivatives

Chitosan was modified to provide three structural features: (i) the positive charge from the $-N^+(CH_3)_3$ of the quaternized chitosan increases the electrostatic interaction with cell membrane; TMC (ii) hydrophobic component, gallic acid to enhance biocompatibility; TMC-GC (iii) targeting molecule, folic acid to specifically target the folate receptor, which is overexpressed on cancer cells; TMC-GA-FA, as shown in Figure 17.

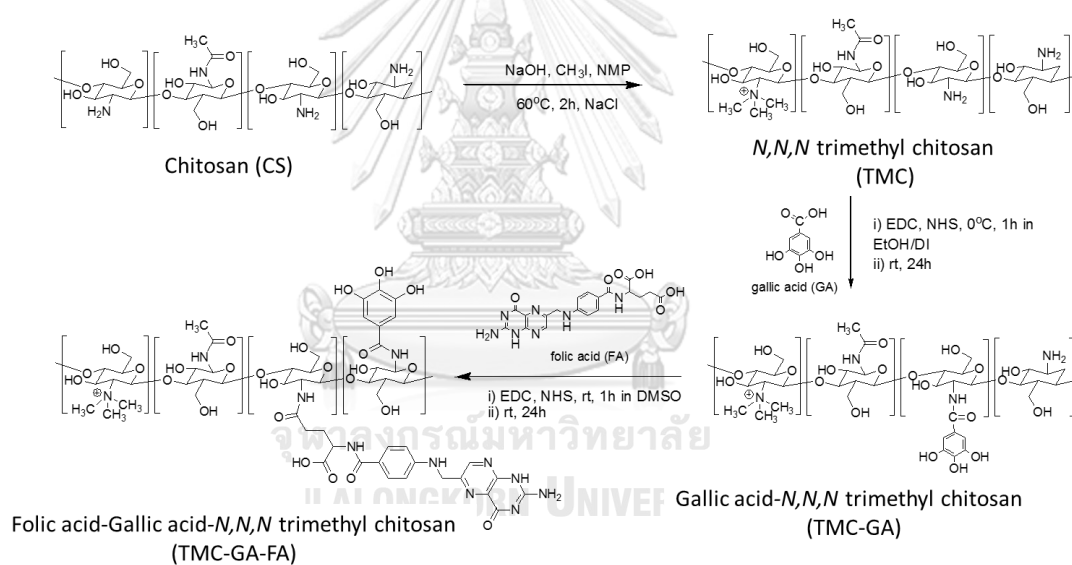


Figure 17 Schematic representation of the Synthesis of TMC, and TMC-GA-FA

3.3.1.1 Synthesis of *N,N,N*-trimethylammonium chitosan (TMC)

Chitosan powder (2 g) was dissolved in 200 mL of 1% (v/v) acetic acid solution at room temperature overnight until completely dissolved. Then, 10 mL of 15% (w/v) NaOH and 60 mL of 1:1 (v/v) of iodomethane:NMP were added. The reaction mixture was stirred at 60°C for 2 h and then precipitated in ethanol. The precipitate was subjected to dialysis in NaCl to exchange iodide for chloride ions and then for 2 days in DI water to remove the residual NMP and acetic acid. The precipitate was then washed with acetone and collected by centrifugation to obtain the product.

3.3.1.2 Synthesis of folic acid-gallic acid-*N,N,N*-trimethylammonium chitosan (FA-GA-TMC)

Gallic acid (0.600 g, 3.5 mmol), EDC (0.670 g, 3.5 mmol) and NHS (0.402 g, 3.5 mmol) were mixed in 10 mL of 50% (v/v) ethanol and stirred in an ice bath for 1 h to obtain activated gallic acid. Then, the activated gallic acid was added to 100 mL of 1% (w/v) TMC in 1% (v/v) acetic acid solution and stirred at room temperature overnight. To eliminate unbound gallic acid, the solution was precipitated in acetone and dialyzed against DI water for 3 days to obtain *N,N,N*-trimethylammonium chitosan conjugated with gallic acid (TMC-GA).

The mixture of folic acid (0.605 g, 1.4 mmol), EDC (0.260 g, 1.4 mmol) and NHS (0.156 g, 1.4 mmol) in DMSO (10 mL) was stirred for 1 h under dark conditions to obtain activated folic acid. Then, the activated folic acid was added to 400 mL of 0.5% (w/v) TMC-GA in acetate buffer (pH 4.7) and stirred at room temperature overnight. The solution was precipitated in acetone, dialyzed against phosphate buffer (pH 7.4) for 3 days to remove unreacted folic acid and then in water for 3 days to obtain *N,N,N*-trimethylammonium chitosan conjugated with gallic acid and folic acid (TMC-GA-FA).

3.3.2 Calculation of degree of quaternization (%DQ) and degree of substitution (%DS)

Degree of quaternization and substitution of gallic acid (GA) and folic acid (FA) was evaluated by ^1H NMR spectroscopy using Eq. (1) for the %DQ and Eq. (2) and (3) for the %DS of GA and FA, respectively, as previously reported [57].

$$\%DQ = \left[\frac{I_{(CH_3)_3}}{I_{(H_3-H_6)}} \times \frac{5}{9} \right] \times 100\% \quad (1)$$

$$\%DS_{GA} = \left[\frac{I_{(H7)}}{I_{(H_3-H_6)}} \times \frac{5}{2} \right] \times 100\% \quad (2)$$

$$\%DS_{FA} = \left[\frac{I_{(H8)}}{I_{(H_3-H_6)}} \times \frac{5}{1} \right] \times 100\% \quad (3)$$

Here, $I_{(CH_3)_3}$ is the integral of the trimethyl amino groups' protons of TMC (2.83 ppm), $I_{(H7)}$ is the integral of the proton of the gallic acid benzene ring (6.75 ppm), $I_{(H8)}$ is the integral of the proton of the benzene ring of folic acid (8.54 ppm) and $I_{(H_3-H_6)}$ is the integral of the H3-H6 protons of chitosan.

3.3.3 Determination of gallic acid content TMC-GA-FA

The gallic acid content was determined according to the Folin-Ciocalteu procedure [58]. Folin-Ciocalteu's phenol reagent reacts with phenolic compounds to form chromogens that can be detected spectrophotometrically. Typically, a total of 20 μL of modified chitosan solution was placed in a 96-well plate. A total of 100 μL of Folin-Ciocalteu reagent (diluted 1:10 with DI water) and 80 μL of 1 M sodium carbonate were added. The mixtures were shaken and allowed to stand at room temperature for 30 min. The absorbance was measured at 765 nm using a microtiter plate (BioTek PowerWave XS2). Gallic acid solution in the range 10–130 ppm was used to construct a calibration curve. The total gallic acid content of TMC-GA-FA was expressed as mg of gallic acid equivalents (GAE) per g of TMC-GA-FA.

Part II: Preparation, surface functionalization, characterization and preliminary cytotoxic study of selenium nanocarriers using modified chitosan as a stabilizer

3.3.4 Preparation and functionalization of selenium nanocarriers

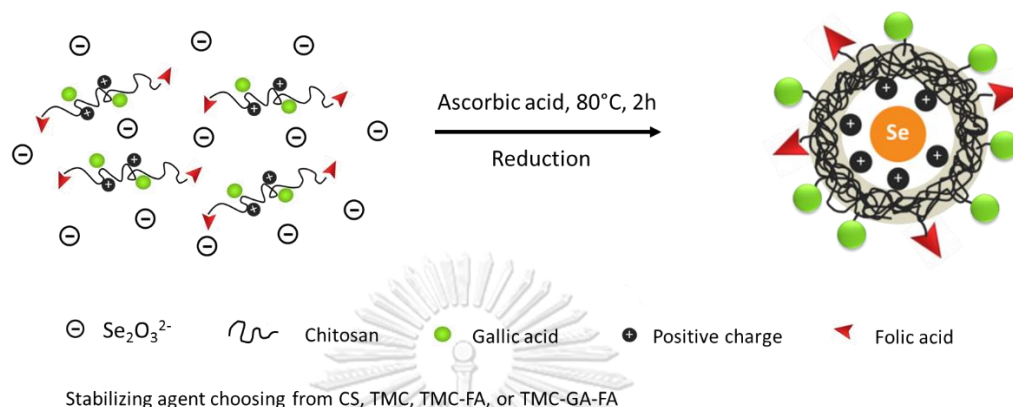


Figure 18 Preparation of SeNPs using modified chitosan as a stabilizer

In this work, we studied the effect of different stabilizing agents, including ascorbic acid, CS and modified chitosans (TMC, TMC-FA, and FA-GA-TMC) at final concentration of 0.3 mg/mL, and further evaluated the effect of various final concentrations of TMC-FA (0.3, 0.6 and 0.9 mg/mL) to demonstrate the role of folic acid on the activity of SeNPs.

Before the experiment, a stock solution of 5 mM sodium selenite (Na_2SeO_3), 0.5% (w/v) CS and its derivatives in 0.5% acetic acid, and 20 mM ascorbic acid were prepared. SeNPs were synthesized by the reduction of sodium selenite by ascorbic acid. In a typical procedure, chitosan or modified chitosans was mixed with 200 μL of Na_2SeO_3 . Then, 200 μL of ascorbic acid was added dropwise into the mixture, which was reconstituted to a final volume of 1 mL with DI water. The mixed solution was heated at 80°C for 2 h, and the color changed from colorless to orange in 5 min. The solution of SeNPs was centrifuged at 12,000 rpm for 10 min to remove unreacted reagents, and the resulting pellet was resuspended in water. The concentration of Se was determined by ICP-AES analysis, while size and shape of SeNPs were characterized

by SEM and TEM. The size distribution and surface charge of the SeNPs was evaluated with a particle size analyzer.

Part III: Fabrication of doxorubicin drug-loaded SeNPs and evaluation of their biological activity
Preparation of the doxorubicin drug-loaded SeNPs (DOX-SeNPs@TMC-FA)

3.3.5 Fabrication of DOX-loaded SeNPs@TMC-FA

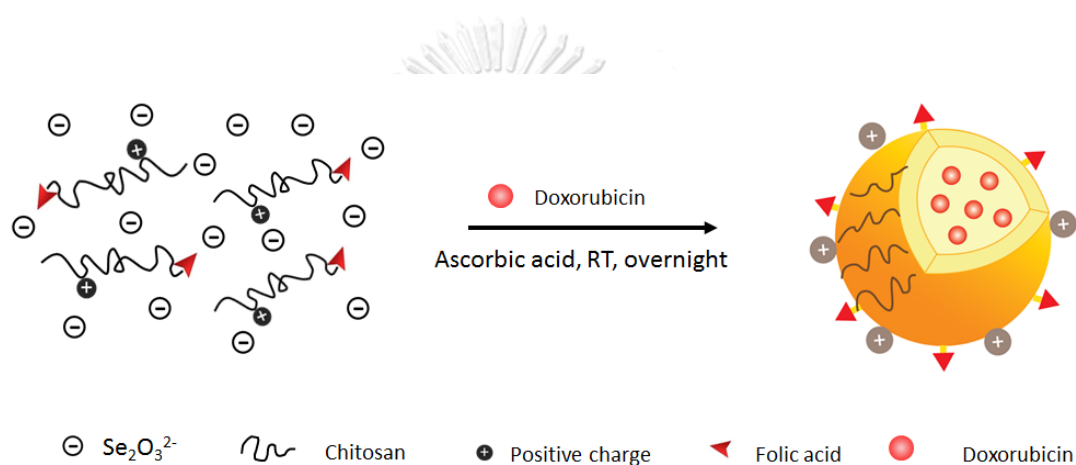


Figure 19 Preparation and proposed structure of DOX-SeNPs@TMC-FA

The solution of selected stabilizer, TMC-FA was mixed with 30 μL of 10 mM DOX solutions and 200 μL of 5 mM sodium selenite to obtain the final concentration of TMC-FA equal to 0.6 mg/mL. The concentration ratio of SeNPs and DOX was maintained at 1:0.3. 200 μL of 20 mM ascorbic acid was added dropwise to the above solution which was reconstituted to a final volume of 1 mL with DI water. The mixture was stirred overnight at room temperature in the dark to obtain DOX-SeNPs@TMC-FA. The solution of DOX-SeNPs@TMC-FA was centrifuged at 12,000 rpm for 10 min to remove unreacted reagents, and the resulting pellet was resuspended in water. The concentration of Se was determined by ICP-AES analysis. In addition, the DOX amount was quantified by fluorescence spectroscopy. The binding of DOX to the SeNPs@TMC-

FA was predominantly through electrostatic interactions between the positively charged ammonium of TMC-FA and the negatively charged hydroxyl group of DOX. To calculate the loading efficiency, the following equation was used (Nasrolahi Shirazi et al., 2014):

$$\text{Loading efficiency (wt/wt, \%)} = (\text{DOX in feed} - \text{Free DOX}) / \text{DOX in feed} \times 100$$

Biological studies

Cell Culture

Ovarian cancer cells sensitive (OVCAR8) and resistant (NCI/ADR-RES) to doxorubicin were cultured in RPMI1640 medium, which was supplemented with 10% fetal bovine serum, in a humidified atmosphere containing 5% CO₂ at 37°C

3.3.6 Cytotoxicity study

The evaluation of cytotoxicity was based on the reduction of 3-(4,5-dimethylthiazol-2-yl)-2,5-diphenyltetrazolium bromide (MTT) dye by viable cells to generate purple formazan products, which were measured spectrophotometrically at 570 nm. Two hundred microliters of cancer cells were seeded into 96-well plates at 5,000 cells/well and incubated at 37°C. After 24 h, the cells were treated with various concentrations of compounds for 3 days. Then, 20 µL of MTT solution (3 mg/mL) was added, and the cells were incubated again for 3 h. After the medium was removed and the formazan crystals were solubilized in 150 µL of DMSO, the absorbance was measured at 570 nm. The cytotoxicity activity was measured as %cell viability. The IC₅₀ values were calculated using the software GraphPad Prism 5 (GraphPad Software, Inc.), using a nonlinear regression of “log(inhibitor) versus response”: $Y = \text{Bottom} + (\text{Top} - \text{Bottom}) / (1 + 10^{-(X - \text{LogIC}_{50})})$.

3.3.7 Colony formation assay

Cells were placed in a 96-well plate at 300 cells/well. After treatment, cells were stored in culture until colonies were observed in control wells. Colonies were then fixed and stained with 0.05% crystal violet solution (2% formaldehyde, 40% methanol in DI water), washed with water to remove excess stain and imaged with an Odyssey Imaging Systems (LI-COR Biosciences, Lincoln, NE).

3.3.8 Cellular uptake study

To evaluate the role of folic acid, cellular uptake of DOX-SeNPs@TMC and DOX-SeNPs@TMC-FA in NCI/ADR-RES cells was quantified by a fluorescence microplate reader. Briefly, NCI/ADR-RES cells were seeded in 96-well plates at a density of 5,000 cells/well and allowed to attach for 24 h. The medium in the wells was replaced with coumarin-6-loaded SeNPs at a concentration of 1 μ M, and the cells were incubated for various periods of time (24, 48 and 72 h) at 37°C in a CO₂ incubator. At the end of the incubation, the medium was removed from the wells and the cells were rinsed three times with cold PBS to remove the nanoparticles outside the cells. After that, 100 mL of 0.1% Triton X-100 in 0.1 N NaOH solution was added to lyse the cells. A fluorescence microplate reader with excitation and emission wavelengths set at 430 and 485 nm, respectively, was used to measure the fluorescence intensity from the coumarin-6-loaded nanoparticles inside the wells. The cellular uptake efficacy was expressed as the percentage of the fluorescence of the test wells over that of the positive control wells [59].

3.3.9 Intracellular localization of DOX-SeNPs@TMC-FA

The intracellular localization of DOX-SeNPs@TMC-FA in NCI/ADR-RES cells was traced with Hoechst nuclei staining dye. Briefly, the cells, cultured in 96-well plates at a density of 5,000 cells/well, were incubated with coumarin-6-loaded SeNPs@TMC-FA at a concentration of 1 μM for 6 h. After washing with PBS twice, the cells were stained with Hoechst (1:2000 in PBS) for nuclear staining, for 20 min at 37°C. At the end of incubation, the cells were rinsed with PBS twice and observed under a fluorescence microscope.

3.3.10 pH-responsive drug release

Two samples of 10 mg of DOX-SeNPs@TMC-FA were suspended in 10 mL of PBS solution at pH 7.4, which represents the pH of the bloodstream and normal tissue, and pH 5.3, which represents the average acidity of intracellular endosomes and lysosomes (pH range = 4.5–6.5), with constant shaking (500 rpm) in the dark at 37°C. At specific intervals, a certain volume of buffer was removed from the tubes. The DOX concentration was detected in the collected buffer with a fluorescence microplate reader, with excitation and emission wavelengths at 485 nm and 590 nm, respectively (Yu et al., 2014).

3.3.11 Combination assay

Two hundred microliters of cancer cells were seeded into 96-well plates at 5,000 cells/well and incubated at 37°C. After 24 h, the cells were pretreated with N-Benzyloxycarbonyl-Val-Ala-Asp(O-Me) fluoromethyl ketone, Z-VAD-FMK (40 μ M); n-acety-cysteine, NAC (3 mM); deferoxamine, DFO (10 μ M) and necrostatin, Necro (10 μ M). After 2 h, SeNPs were added at concentration of 3 μ M. After 72 h, 20 μ L of MTT solution (3 mg/ml) was added, and the cells were incubated again for 3 h. After removal of the media and solubilization of the formazan crystals in 150 μ L of DMSO, the absorbance was measured at 570 nm.

3.3.12 Western blotting

Cells (5×10^5) were cultured in 6-well plates and treated with SeNPs at designated concentrations. After treatment, cells were lysed with cell lysis buffer on ice at 4°C, sonicated for 3 min, centrifuged (12,000 rpm, 10 min, 4°C) and then, the supernatant was collected. Protein concentrations of the supernatants were evaluated with a BCA assay. Proteins were resolved in 10% SDS/PAGE and were electrotransferred to Immun-Blot PVDF membranes (Bio-Rad). After blocking with 5% milk in TBST (Tris-buffered saline with 0.1% Tween 20), membranes were probed with primary antibodies (anti-PARP, anti-caspase 3 and anti-GAPDH) at 1:1000 dilutions, overnight at 4°C. Membranes were then washed with TBST (5 min \times 3), incubated with Dylight 800-conjugated secondary antibodies at 1:7500 dilutions in 5% milk for 1 h at room temperature, and washed with TBST (5 min \times 3). The fluorescence signal was then scanned by the Odyssey Imaging Systems (LI-COR Biosciences).

CHAPTER IV

Results and Discussion

Selenium nanoparticles (SeNPs) have attracted considerable attention in biomedical applications because of their unique physical and chemical properties, which differ from the properties of the corresponding bulk materials. SeNPs exhibited potential as therapeutic agents and drug carriers, as well as excellent bioavailability and low toxicity. It is noted that numerous important factors affect the properties of nanoparticles, including their shape, size, surface charge and surface functional groups. Therefore, SeNPs have been developed due to its application. In this study, to overcome drug resistance effectively, we have designed a selenium nanodrug delivery system through the combination between (i) folate-mediated endocytosis for bypassing the P-gp-mediated drug efflux pumps, increasing cellular uptake, and reducing toxicity against normal cells, and (ii) pH-responsive swelling property of chitosan for triggering and increasing drug accumulation at tumor site.

Part I: Modification of chitosan used as stabilizer

Basically, the surface of nanoparticles was functionalized through modification of the molecular structure of stabilizer. Therefore, chitosan was modified to provide three structural features, as shown in Figure 20:

- (i) the positive charge from the $-N^+(CH_3)_3$ of the quaternized chitosan increases the electrostatic interaction with cell membrane and improves its water solubility (pKa value = 6.5) [60];
- (ii) hydrophobic component, gallic acid to enhance biocompatibility
- (iii) targeting molecule, folic acid to specifically target the folate receptor, which is overexpressed on cancer cells [21].

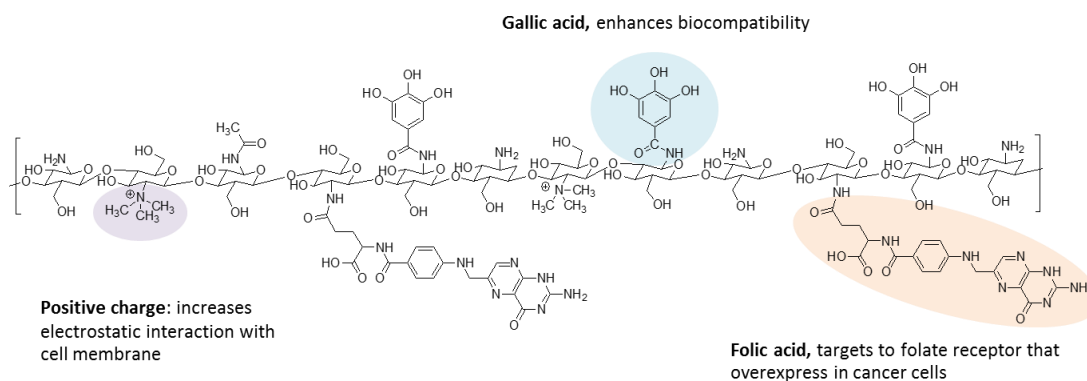


Figure 20 Molecular structure of modified chitosan (TMC-GA-FA)

4.1 Synthesis and characterization of chitosan and its derivatives (CS, TMC, TMC-FA, TMC-GA-FA)

To understand the synthesis of TMC-GA-FA, chitosan was modified by quaternization using methyl iodide (CH₃I) as a quaternizing agent, which reacted with both the primary amine and hydroxyl groups. Gallic acid and folic acid were then attached via coupling of the carboxylic acid groups of both gallic acid and folic acid to the primary amine groups of chitosan using EDC and NHS as coupling agents, resulting in FA-GA-TMC (Figure 21). The modified chitosan samples were characterized using ¹H NMR and FTIR, as shown in Figure 22 and 23, respectively.

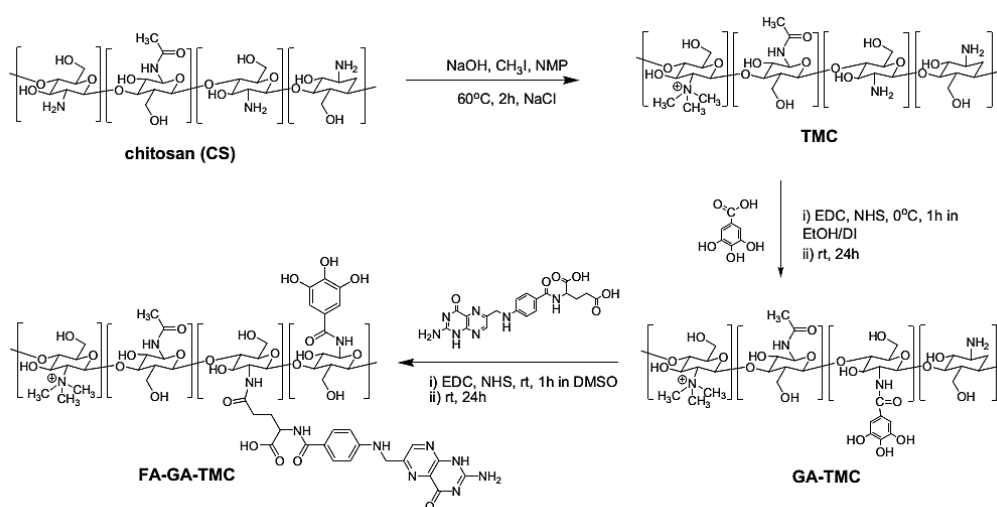
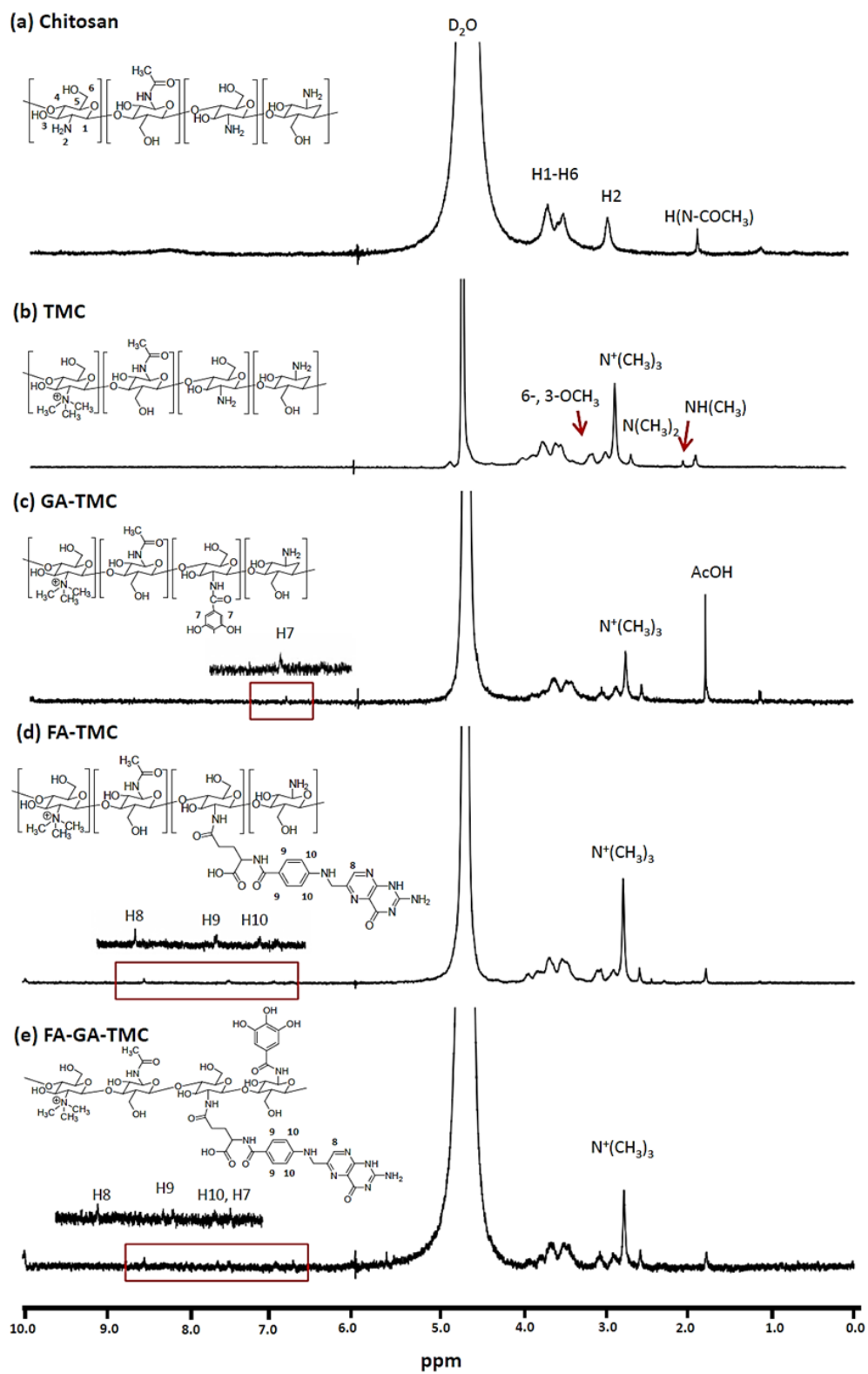


Figure 21 Synthesis of TMC and TMC-GA-FA

4.1.1 $^1\text{H-NMR}$

The ^1H NMR spectrum of chitosan (Figure 22A) showed the signals of the H3-H6 protons at approximately 3.85-3.40 ppm, corresponding to the pyranose ring; the H2 proton at 2.99 ppm, corresponding to the acetyl; and the proton of the *N*-acetylglucosamine unit at 1.88 ppm. After quaternization, the ^1H NMR spectrum of TMC exhibited new peaks at 3.22-3.00 ppm because of the O-methylation and other peaks at 2.83, 2.64 and 2.00 ppm related to N-methylation of chitosan, as shown in Figure 22B. Compared with the spectrum of TMC, the ^1H NMR spectrum of TMC-GA-FA showed new peaks of the aromatic proton of gallic acid with a chemical shift of 6.75 ppm and folic acid at 8.54, 7.53 and 6.96 ppm, which contributed to H8, H9 and H10, respectively, as shown in Figure 22E. In addition, ^1H NMR analysis indicated the degree of quaternization (DQ) of TMC to be 23.1% and the degree of substitution of GA and FA on TMC to be 6.0% and 5.3%, respectively.

Figure 22 ¹H-NMR of chitosan and its derivatives

4.1.2 FT-IR

FTIR spectra of unmodified chitosan and modified chitosan are shown in Figure 23. The FTIR spectrum of chitosan showed a broad absorption peak at 3424 cm^{-1} , which corresponds to O-H and N-H stretching. The characteristic peaks at 1640 cm^{-1} and 1593 cm^{-1} are assigned to C=O stretching of amide I and N-H bending of amide II, respectively. In addition, the broad absorption in the $1220\text{-}900\text{ cm}^{-1}$ region is related to the polysaccharide skeleton, including the symmetric stretching of glycosidic bonds (C-O-C) and the skeletal vibration of C-O stretching. The spectrum of TMC showed a new peak at 1470 cm^{-1} , which is attributed to C-H asymmetric stretching of methyl groups. After the conjugation of gallic acid and folic acid, new peaks were observed at 1603 cm^{-1} and 1513 cm^{-1} and were assigned to the characteristic peaks of folic acid. Moreover, spectrum of TMC-GA-FA showed a peak at 1566 cm^{-1} , which is attributed to the deformation of N-H bonds in the amino group, whereas the C=O of the ester bond between gallic acid or folic acid (-COOH) and chitosan (-NH₂) possibly overlapped with the amide I and amide II peaks of chitosan. These results indicate that the gallic acid and folic acid were successfully conjugated onto the chitosan backbone to obtain TMC-GA-FA.

In summary, we obtained 4 different types of stabilizers (CS, TMC, TMC-FA and TMC-GA-FA) and all of them were then subjected to use as a stabilizing agent for the preparation of SeNPs

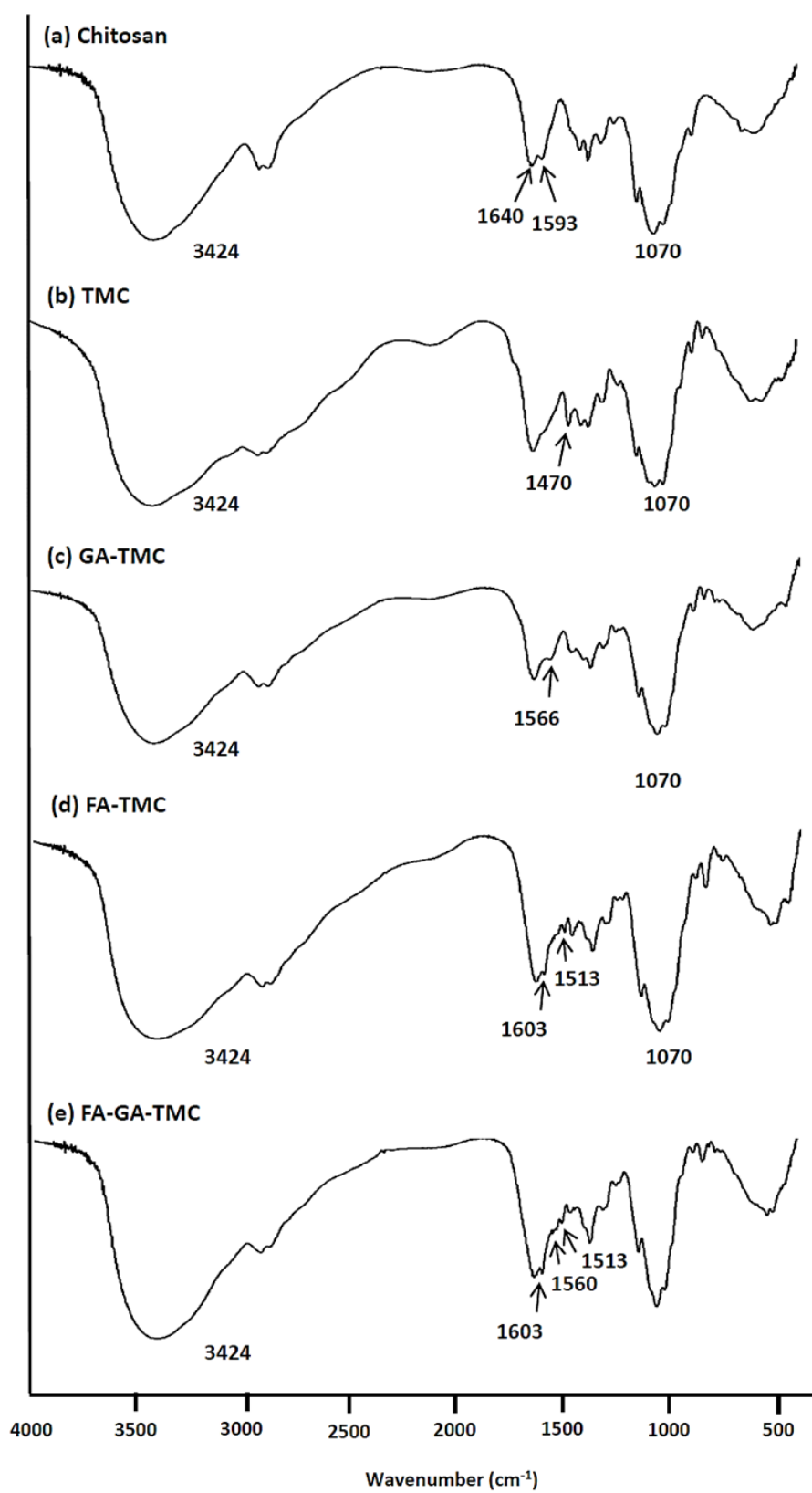
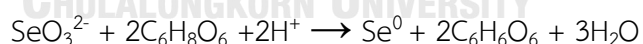


Figure 23 FTIR spectra of chitosan and its derivatives

Part II: Preparation, functionalization, characterization and preliminary cytotoxic study of selenium nanocarriers using modified chitosan as a stabilizer

4.2 Preparation and functionalization of selenium nanocarriers using modified chitosan as a stabilizer

The idea for preparation of nanoparticles should be possess ability to control the size and shape of the particles with monodisperse that are related to their property. One important factor has been reported to affect the final structure of nanoparticles is synthesis conditions, including the pH, solvent, temperature, and the concentration of stabilizer. Apart from synthesis conditions, one key in controlling the size and shape of nanoparticles is the design of the molecular structure of a stabilizer that can direct particles to organize or assemblies, and final structures. Hence, to study of how SeNPs' size and shape change when modifying stabilizer, we fabricated SeNPs in the presence of each types of stabilizer, including, CS, TMC, TMC-FA, and TMC-GA-FA and compared the resulting SeNPs with those prepared in the absence of stabilizer as illustrated in Figure 24. Typically, SeNPs were generally prepared by the reduction of selenite with ascorbic acid in the presence of each of those stabilizers, which can be described by the following reaction: [61]



Ascorbic acid used as reducing agent could efficiently reduce Se^{+4} ions in Na_2SeO_3 to neutral Se^0 (SeNPs), while a stabilizing agent surround nanoparticles surface in order to prevent the aggregation achieving through both electrostatic and steric stabilization. The formation of SeNPs was evident from change in color from colorless to bright orange, which is a characteristic color of SeNPs. In contrast, in the absence of a stabilizer, ascorbic acid, which served a dual role as reductant and stabilizer, was added to the colorless SeO_3^{2-} solution. After a few minutes, the color of the solution changed to orange because of the formation of SeNPs and then rapidly changed from

orange to a pale-pink color within 30 min because of aggregation to the larger particles. The observed change in color of the SeNPs is consistent with the results of a previous study in which the color of SeNPs was reported to change from red to pink with increasing particle size [62].

In addition, in this work, the influence of pH on the preparation of SeNPs was not considered. Because chitosan is not soluble in aqueous or alkali solutions ($pK_a=6.5$) [63], we dissolved chitosan and its derivatives in 0.5% acetic acid. Thus, pH of solution was kept constant and the obtained SeNPs suspension has a final pH value of around 5. Among the experimental parameters, reaction temperature has been considered of great importance [64]. Previous studies reported that the fabrication of SeNPs at room temperature requires an extended reaction time to complete the reaction, whereas higher temperatures (90°C) may accelerate nanoparticle aggregation [65]. In order to investigate the influence of temperature in the preparation of SeNPs, the solution temperature was heated from room temperature to 40, 60 and 80°C . For the same heating duration (2 hours), the color of solution becomes more intense at higher heating temperature. These may due to a low temperature could slow down the formation and growth reaction, which results in incomplete reduction. At temperature over 80°C , the solution is not clear and becomes slightly turbid (data not shown), indicating the aggregation of nanoparticles. Therefore, 80°C was chosen as the optimal temperature for the preparation of SeNPs

4.3 Characterization of selenium nanocarriers using modified chitosan as a stabilizer

The size, shape and surface charge of SeNPs stabilized with different types of stabilizers including CS, TMC, TMC-FA and TMC-GA-FA was characterized using SEM, TEM, UV/VIS, DLS and zetasizer, compared SeNPs without stabilizer.

4.3.1 SEM

In the absence of a template, SEM images of SeNPs@Vc revealed the aggregation of SeNPs to form the large particles shown in Figure 24A. These results indicate that the reduction and stabilization of SeNPs with ascorbic acid resulted in unstable particles, which formed rapidly, grew and aggregated into larger particles because of a lack of adequate protection on the surface of the nanoparticles [66]. In order to avoid the aggregation, stabilization need to be achieved.

In the presence of chitosan, an orange-colored solution is observed because of the formation of spherical SeNPs, consistent with previous studies [67, 68]. The SeNPs@CS were clearly spherical in shape, with an average size of 198 nm, as shown in Figure 24B. Figure 24C shows an SEM image of SeNPs stabilized by TMC (cationic chitosan). In comparison with the chitosan structure, TMC provided positive charges, with a degree of TMC quaternization of 23.1%. The SEM image of SeNPs@TMC showed the same spherical shape as SeNPs@CS; however, the SeNPs@TMC were smaller than SeNPs@CS, with an average of 130 nm. Furthermore, an additional functionalizing molecule, folic acid, was introduced into the TMC structure. The degree of substitution of folic acid was 5.3%. The morphology of SeNPs@TMC-FA is uniformly spherical, with an average size of 261 nm, as shown in Figure 24D. The order of the sizes of the SeNPs from small to large is SeNPs@TMC, SeNPs@CS and SeNPs@TMC-FA. We assumed that the main effect of the stabilizer on particle size is due to the steric effect and chemical bonding (Daniel & Astruc, 2004). A possible explanation may be that TMC is more

positively charged than chitosan and therefore exhibited a stronger electrostatic interaction with the SeNP surface, resulting in the decrease in nanoparticle size. By contrast, using TMC-FA as a stabilizer instead of TMC or CS resulted in greater steric hindrance because of the bulky folic acid group present in TMC-FA. This steric effect resulted in weaker interaction between the positive charge of TMC-FA and the SeNP surface, which, in turn, resulted in a larger particle size. Interestingly, when SeNPs were synthesized in TMC-GA-FA ($\%DS_{GA} = 6.0$ and $\%DS_{FA} = 5.3$), the SeNPs@TMC-GA-FA exhibited a cubic-like structure. The average particle size in the sample was 322 nm, as shown in Figure 24E. Collectively, these results suggest that the formation and morphology of SeNPs can be influenced by the structure of the stabilizer through the self-assembly process.

In the case of the cubic-like structure, we note that the self-assembly process usually involves more than one driving force [44]. We hypothesized that the aromatic substituents (gallic acid and folic acid), which create π - π aromatic stacking, and the hydroxyl and amino groups, which govern hydrogen bonding, exposed more active functional groups on the surface of the SeNPs in comparison with CS, TMC and TMC-FA. That is, SeNPs@TMC-GA-FA exhibited more extensive intermolecular interactions between neighboring particles, leading to different assemblies of the final structure.

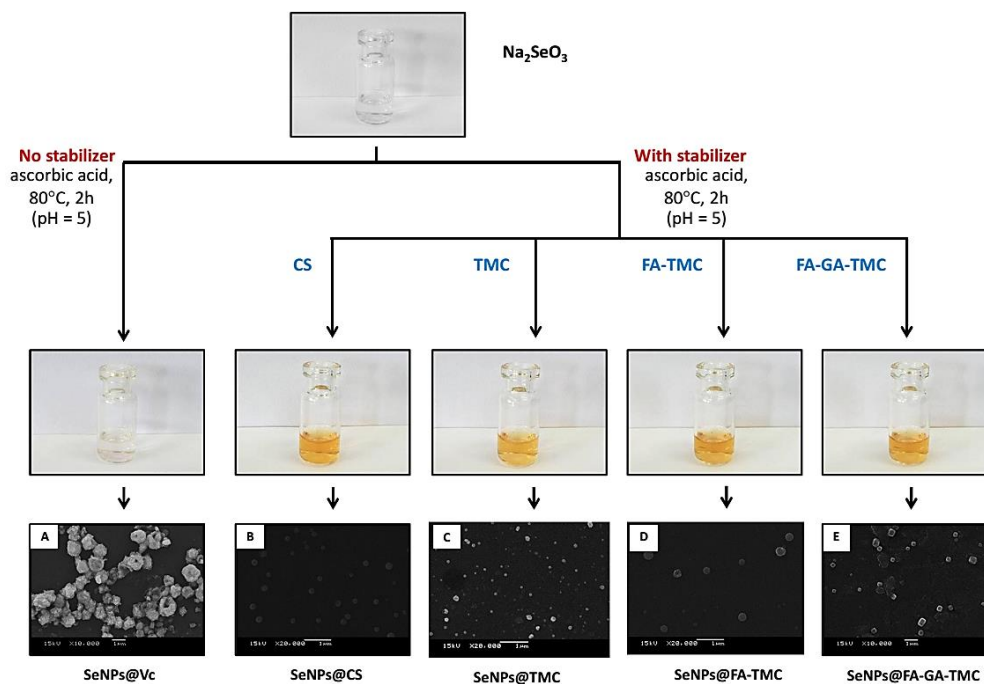


Figure 24 SEM images of (A) SeNPs@Vc, (B) SeNPs@CS, (C) SeNPs@TMC, (D) SeNPs@FA-TMC, and (E) SeNPs@FA-GA-TMC

4.3.2 TEM and EDX

The TEM images of SeNPs@TMC-GA-FA revealed the self-assembled conversion from spherical SeNPs to cubic-like structures; that is, the cubic-like SeNPs were secondary structures formed from numerous individual primary nanoparticles. We observed that adjacent particles attached to each other to form dimers and trimers and observed cubic-like SeNPs as the final structure (Figure 25A). These observations suggest that the cubic-like SeNPs form via a self-assembly mechanism. In addition, energy dispersive X-ray (EDX) analysis indicated the presence of Se atoms, as shown in Figure 25B.

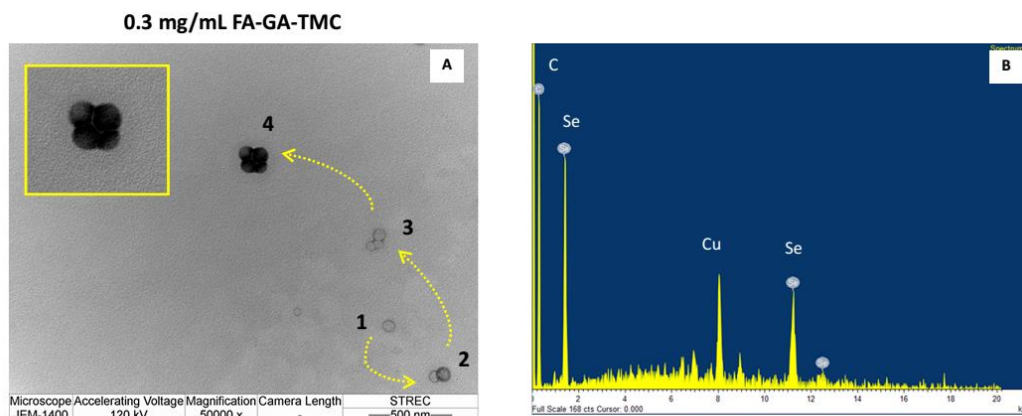


Figure 25 (A) TEM image and (B) EDX spectrum of SeNPs@FA-GA-TMC

Proposed mechanism of cubic-like SeNPs

In previous work, it was found that when chitosan was used as the template, SeNPs were conjugated with the hydroxyl group of chitosan and the positive charge of the amino group on the outer surface of the nanoparticles provided electrostatic repulsion between particles; as a result, the particles retained their spherical shape [50]. Compared with unmodified chitosan, the structure of TMC-GA-FA contains three key structural features: the positive charge from the $-N^+(CH_3)_3$ of quaternized chitosan, the hydrophobic parts of the phenyl rings of both gallic acid and folic acid, and the hydrogen bonds from the hydrogen bonding groups of gallic acid, folic acid and the chitosan backbone.

On the basis of the aforementioned results, we propose a possible mechanism for the formation of cubic-like SeNPs as follows (Figure 26). First, primary spherical SeNPs form via the reduction of sodium selenite by ascorbic acid with FA-GA-TMC surface decoration, where the $N^+(CH_3)_3$ groups of the chitosan backbone surround the SeNP core by electrostatic interaction and the phenyl rings of the gallic acid and folic acid substituents are directed toward the outside of the structure. Second, the particles move independently in their surrounding space, performing a random walk and resulting in the oriented attachment of pairs. Third, other nearest-neighbor particles

move to stack above and below these pairs via π - π stacking of the phenyl ring of gallic acid and folic acid and also via the hydrogen bonding between both substituents that bond on the surfaces of particles. Finally, these four particles assemble to form cubic-like nanoparticles as a final structure. Therefore, we expected that the formation of the cubic-like SeNPs should be favored by π - π stacking of the rigid phenyl ring of gallic acid.

To test this hypothesis, SeNPs were fabricated using TMC-FA as a stabilizer instead of TMC-GA-FA. As shown in Figure 24D, in the absence of gallic acid, the SEM image showed spherical shape of nanoparticles. This could be contributed to the folic acid is flexible and provides more intermolecular interactions, such as π - π stacking, hydrogen bonding, electrostatic interaction and van der Waals interaction, leading to promote the close packing of nanoparticles [69]. Thereby the spherical shape, instead of cubic-like structure, became the main products. Although the more in-depth mechanism of cubic nanoparticle formation is not entirely clear and is currently under investigation, this work demonstrates the critical role of the stabilizer or template that provides the different intermolecular interactions for the shape-controlled synthesis of SeNPs through a self-assembly process.

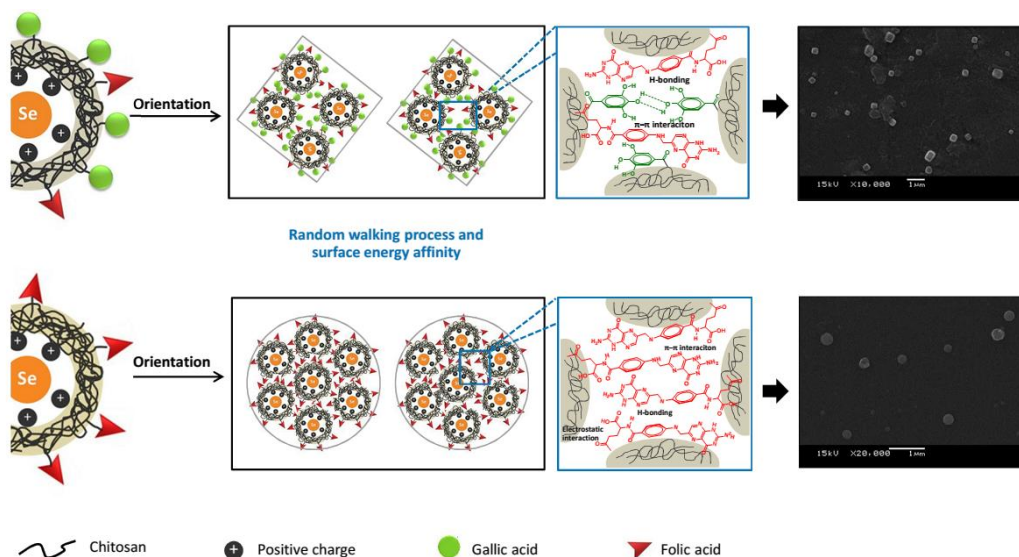


Figure 26 Scheme of the proposed mechanism for the formation

4.3.3 UV/VIS

All types of SeNPs were further characterized by UV/VIS spectroscopy, due to color change from colorless sodium selenite to orange color (SeNPs). As shown in appendix (Figure A2), there was no absorption peak in spectra of CS and TMC, while TMC-FA and TMC-GA-FA exhibited two characteristic peaks of folic acid at 289 and 365 nm and similar peaks was found in SeNP@FA-TMC. According to Figure 27, UV/Vis spectra of SeNPs@Vc, SeNPs@CS, SeNPs@TMC, SeNPs@TMC-FA and SeNPs@TMC-GA-FA showed maximum absorption peak at 295, 264, 262, 257 and 257 nm, respectively. This could be attributed to the formation of nanoparticles. The phenomena of the position shift of absorption peaks might relate to the variation of the particle size, as the red-shift of absorption peak with increasing size of nanoparticles [54].

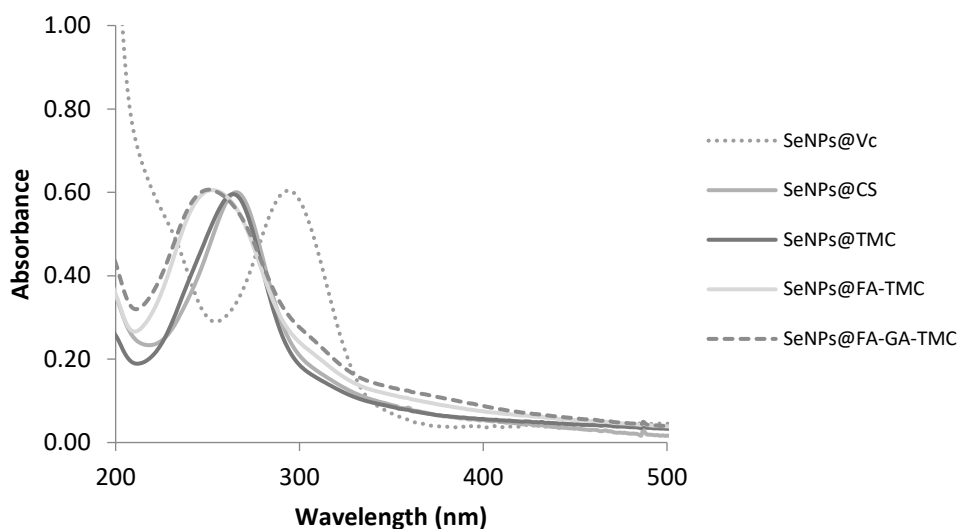


Figure 27 UV/VIS spectrum of SeNPs stabilized with different types of stabilizer

4.3.4 DLS

The control of the average particle size and narrow size distribution is essential to use NPs in many applications. Therefore, the size distribution of SeNPs with or without stabilizer was evaluated through dynamic light scattering (DLS). In the absence of stabilizer, SeNPs showed the two main peaks centered around 400 nm and over 1000 nm, while SeNPs@CS, SeNPs@TMC, SeNPs@TMC-FA and SeNPs@TMC-GA-FA exhibited comparatively smaller dimensions and narrow size distribution as shown in Table 2.

4.3.5 Zetasizer Analysis

In addition, according to Table 2, zeta potential of SeNPs@Vc was 14.1 mV, while attachment of CS elevated the zeta potential to 26.6 mV. These probably due to the positive charge of NH_3^+ group. The zeta potential showed that the zeta potential value of SeNPs@TMC was 31.1 mV, which suggested that the highly positive charged of chitosan we exposed on the surface of SeNPs. With using TMC-FA as stabilizer, it was found that the zeta potential of SeNPs@TMC-FA and SeNPs@TMC-GA-FA decreased to 28.4 and 30.1, respectively. These may due to negative charged OH and COO^- group of both gallic acid and folic acid decorated on the surface for nanoparticles. The zeta potential values at higher than +30mV or lower than -30mV of nanoparticles indicate the greater stability of stabilizer.

Table 2 Characterization of SeNPs stabilized with all types of stabilizers

Types of SeNPs	Size (nm)		Shape	Zeta potential
	SEM	DLS		
SeNPs@VC	>500	>500	Sphere	14.1
SeNPs@CS	198	115	Sphere	26.6
SeNPs@TMC	130	182	Sphere	31.1
SeNPs@TMC-FA	261	125	Sphere	28.4
SeNPs@TMC-GA-FA	322	180	Cubic-like	30.1

*ND = not detect

4.4 Preliminary cytotoxic study of selenium nanocarriers using modified chitosan as a stabilizer

4.4.1 The effect of functionalized molecules on the surface of SeNPs

Besides size and shape, surface functionalization of NPs is one of the important factor influencing the properties of NPs, especially in medical applications. Since, we have modified the positively charged chitosan, TMC to improve its solubility and enhance cellular uptake. Furthermore, folic acid and its conjugates have been well investigated in recent years to specifically target the folate receptor, which is overexpressed human tumor cells, as well as enhance cellular uptake through endocytosis in resistant cells. We, therefore, modified folic acid conjugated-N-trimethyl chitosan (TMC-FA) and folic acid-gallic acid-N-trimethyl chitosan (TMC-GA-FA) and further used these compounds as stabilizers for the fabrication SeNPs

To explore the influence of a functionalized molecule on the surface of SeNPs, SeNPs stabilized with different types of stabilizers, SeNPs@CS, SeNPs@TMC, SeNPs@TMC-FA and SeNPs@TMC-GA-FA were subjected to preliminary screening for their cytotoxicity at a concentration of 3 μM against resistant, NCI/ADR-RES cancer cells by the MTT assay. Among them, SeNPs@TMC-FA exhibited the highest cytotoxicity against NCI/ADR-RES with 46% inhibition at a concentration of 3 μM and showed the lowest cytotoxicity toward normal human WI-38 cells as shown in Figure 28. These results suggest that SeNPs@TMC-FA possess great selectivity between cancer and normal cells. This selectivity is due to the targeting molecule, FA, which targets the folate receptor that is overexpressed in cancer cells and results in stronger cytotoxic effects. Therefore, we will focus on SeNPs@TMC-FA as the nanocarriers for delivery of DOX.

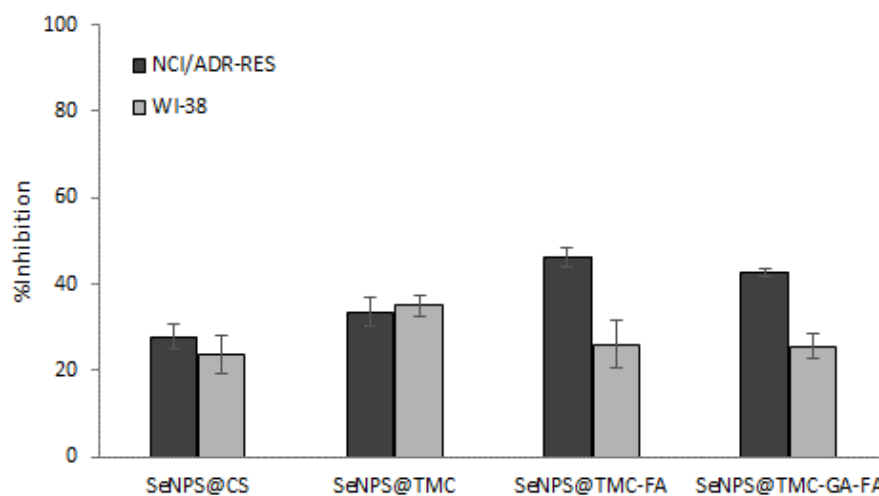


Figure 28 Growth inhibition by SeNPs with different types of stabilizers at a concentration of 3 μM against resistant NCI/ADR-RES cancer and WI-38 normal cells

4.4.2 The effect of folic acid content in SeNPs@TMC-FA on their cytotoxic activity

Folic acid is a ligand that is useful for enhancing nanoparticle cellular uptake via the folate-receptor endocytosis leading to overcoming MDR [70]. We assumed that the reason the SeNPs@TMC-FA exhibited the highest cytotoxicity against resistant cancer cells over others types of stabilizers is directly related to the amount of folic acid decorated on SeNPs surface. Therefore, SeNPs stabilized at different concentrations of TMC-FA, including SeNPs@TMC-FA1 (0.3 mg/mL), SeNPs@TMC-FA2 (0.6 mg/mL), and SeNPs@TMC-FA3 (0.9 mg/mL) were prepared. The amount of folic acid on the surface of nanoparticles was quantified by UV/VIS spectroscopy as shown in Fig 5. The UV absorption spectra of SeNPs@TMC-FA showed a strong peak at wavelength of 286 nm $\pi \rightarrow \pi^*$ transition of the C=C bond and a weak absorption peak at 365 nm, corresponding to the $n \rightarrow \pi^*$ transition of the C=O bond of folic acid. The amount of folic acid evaluated by absorbance at 365 nm in UV-VIS spectra.

These indicated that folic acid content in SeNPs@TMC-FA at 0.3, 0.6 and 0.9 mg/mL was 14.4, 34.7 and 50.5 ppm, respectively.

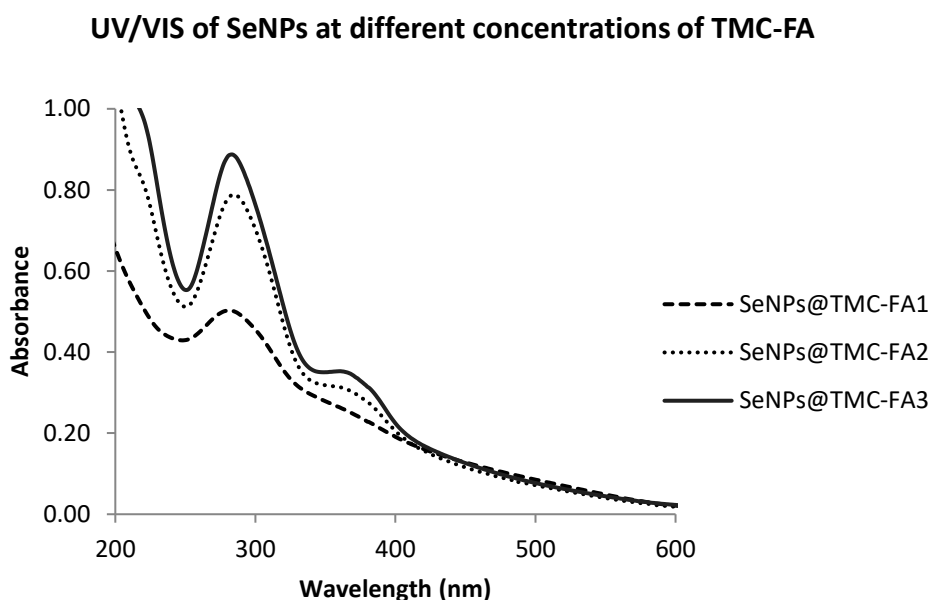


Figure 29 UV/VIS of SeNPs at different concentrations of TMC-FA

Three different amounts of folic acid-decorated SeNPs were subjected to preliminary screening for their cytotoxicity against resistant, NCI/ADR-RES cancer cells by the MTT assay. According to Table 3, with the lowest amount of Folic acid (SeNPs@TMC-FA1), as expected, it showed the lowest activity with IC_{50} value of 8.5 μ M, while SeNPs@TMC-FA2 and SeNPs@TMC-FA3 had higher cytotoxic activity with IC_{50} value of 2.9 and 3.4, respectively. Since, there was no significant difference between the IC_{50} of those SeNPs@TMC-FA2 and SeNPs@TMC-FA3. This might be because high degree of FA creating high binding affinity between nanoparticles and receptor located on cell membrane, therefore, it might not be able to allow cargo be released into the cells. However, according to TEM images, SeNPs@TMC-FA2 showed slightly smaller in size. Therefore, SeNPs@TMC-FA2 were chosen as the nanocarriers for delivery of DOX.

Table 3 Characterization of SeNPs@TMC-FA at different concentrations

Types of SeNPs	FA content (ppm)	Size (nm)	Shape	IC ₅₀ (μ M)
SeNPs@TMC-FA1	14.4	78.1	Sphere	8.5
SeNPs@TMC-FA2	34.7	71.2	Sphere	2.9
SeNPs@TMC-FA3	50.5	68.4	Sphere	3.4



Part III Fabrication of doxorubicin drug-loaded SeNPs and evaluation of their biological activity

4.5 Preparation and Characterization of DOX-SeNPs@TMC-FA

Drug-loaded SeNPs (DOX-SeNPs@TMC-FA) were successfully prepared by the reduction of sodium selenite with ascorbic acid in the presence of TMC-FA as illustrated in Figure 30. We stirred nanoparticles in a saturated aqueous drug solution for the drug to be absorbed or adsorbed onto the particles. The entrapment of the drug onto the nanoparticles may be because of diffusion, surface charges, or encapsulation of the drug into the space between coating and the particle. The binding of DOX to the SeNPs@TMC-FA was predominantly through electrostatic interactions between the positively charged ammonium of TMC-FA and the negatively charged hydroxyl group of DOX.

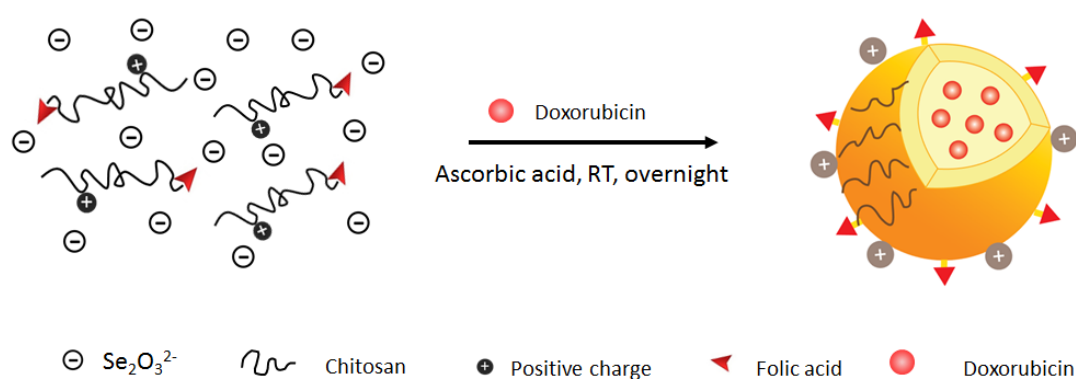


Figure 30 Preparation and proposed structure of DOX-SeNPs@TMC-FA

Since chitosan outer coating of SeNPs provides pH-sensitive swelling property and is a controlled drug release polymer, providing selective drug release in acidic intracellular vesicles in targeted tumor cells [13]. Therefore, the morphology of DOX-SeNPs@TMC-FA was characterized at pH 7.4 and 5.3. pH 7.4 represents the pH of the

bloodstream and normal tissue, whereas pH 5.3 represents the average acidity of intracellular endosomes and lysosomes (pH range = 4.5–6.5).

DOX-SeNPs@TMC-FA were small particles with an average diameter of 50 nm at pH 7.4. When the pH value of the DOX-SeNPs@TMC-FA dispersed solution changed from 7.4 to 5.3, a larger size of nanoparticles was observed, at approximately 110 nm (Figure 31A). The constituent selenium formed a compact core (size = 100 nm) and polymer surrounded the surface of nanoparticle (size = 136 nm), as shown in inserted of Figure 31B [52]. The corresponding EDX showed the presence of a strong signal from Se atoms, confirming that the nanoparticles were comprised of selenium, as shown in Figure 32.

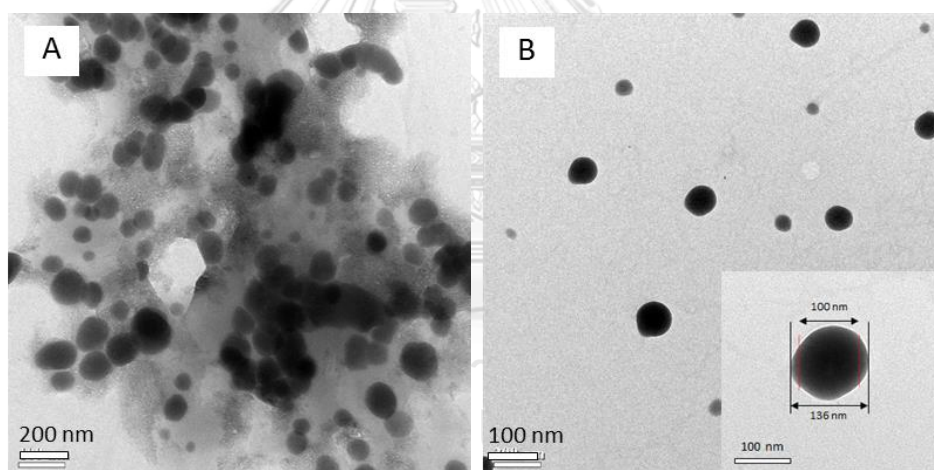


Figure 31 Characterization of DOX-SeNPs@TMC-FA: (A) TEM image of DOX-SeNPs@TMC-FA dispersed in PBS (pH 7.4) and in (B) acidic PBS solution, pH 5.3, and the inset shows an enlarged image

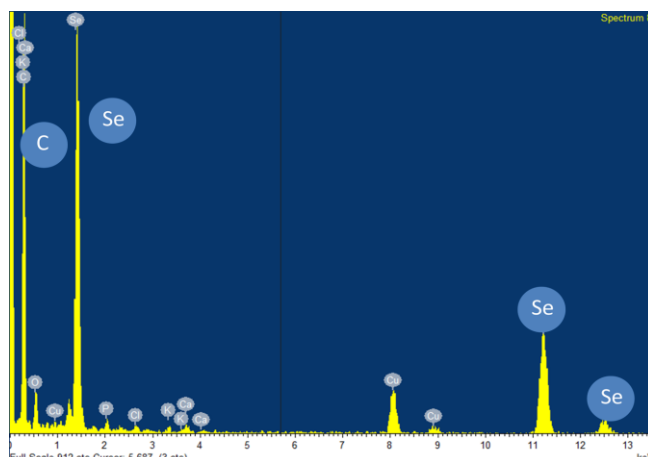


Figure 32 EDX analysis of DOX-SeNPs@TMC-FA

Diameters of DOX-SeNPs@TMC-FA, dispersed in PBS solution (5.3), were also determined by DLS (Figure 33A). It was observed that the average size of the nanoparticles was 146.4 nm, which is higher than the value obtained by TEM. The difference can be explained by the fact that the DLS technique provides the hydrodynamic radius of the nanoparticles, whereas TEM is only sensitive to electron-rich particles [71].

To examine the effects of DOX on the surface properties and stability of SeNPs, we measured the zeta potential. As shown in Figure 33B, the zeta potential of the SeNPs@TMC-FA was 49.0 mV, while the DOX-loaded SeNPs@TMC-FA had a zeta potential of 46.7 mV. This decrease of zeta potential value is probably due to the negative charge of the OH⁻ group of DOX and suggests that DOX can be loaded onto SeNPs@TMC-FA. In addition, fluorescence spectroscopy with excitation and emission wavelength of 485 and 590 nm, respectively, was used to quantify the loading amount of DOX into the nanocarriers. The efficiency of SeNPs@TMC-FA to load DOX after 24 h was 49.0%.

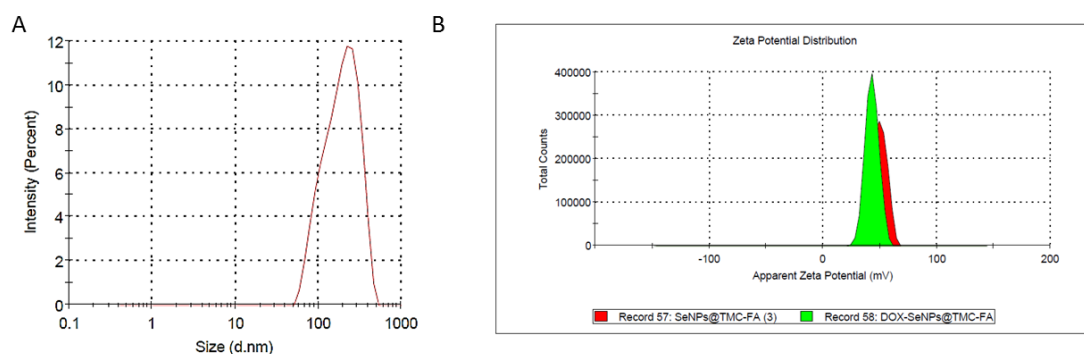


Figure 33 Characterization of DOX-SeNPs@TMC-FA: (A) size distribution from DLS analysis and (B) zeta potential of DOX-SeNPs@TMC-FA

To confirm the presence of DOX in the SeNPs@TMC-FA, DOX-SeNPs@TMC-FA were further characterized by FTIR. The FTIR spectrum of DOX showed multiple peaks at 3335 (O-H), 1729 (C=O), 1612 and 1581 (N-H) and 1411 (C-C) cm^{-1} (Figure 34) [13]. These peaks are also present in the FTIR spectrum of the DOX-loaded SeNPs@TMC-FA, indicating that DOX was successfully loaded onto the SeNPs@TMC-FA.

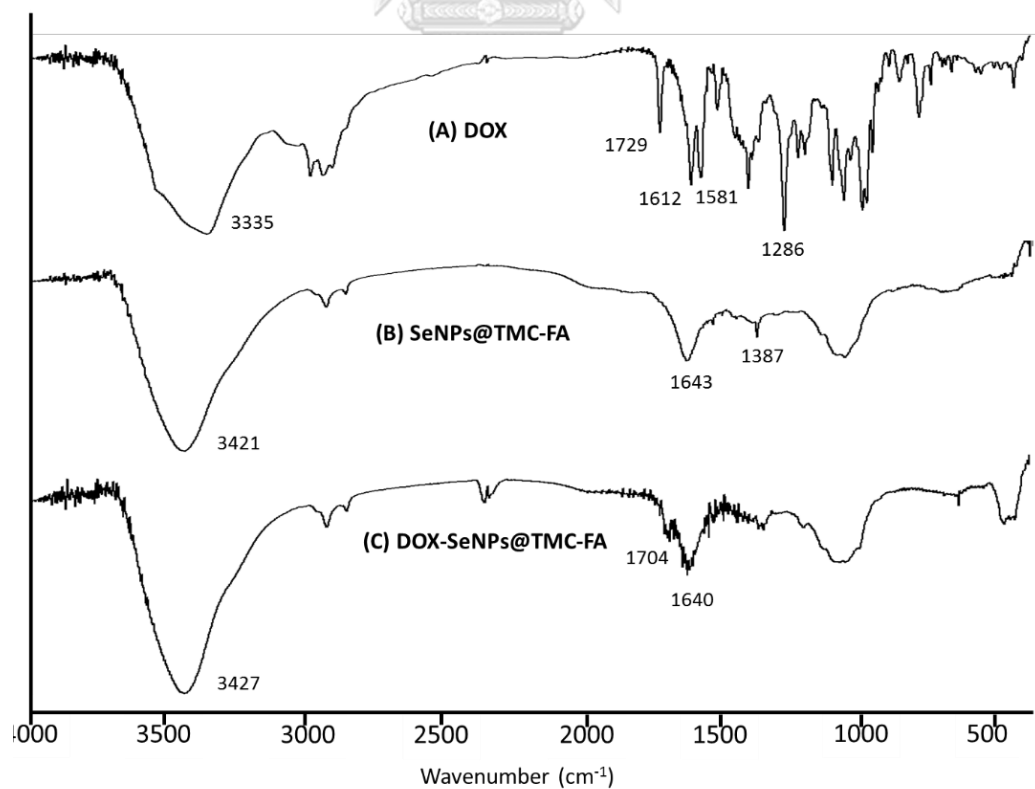


Figure 34 IR spectra of DOX, SeNPs@TMC-FA and DOX-loaded SeNPs@TMC-FA

4.6 Cytotoxic activities against sensitive (OVCAR8) and resistant (NCI/ADR-RES) ovarian cancer cells

4.6.1 MTT assay

The cytotoxicity of free drug, the nanocarriers and the drug-loaded nanocarriers was evaluated against resistant NCI/ADR-RES cells compared with sensitive OVCAR8 by the MTT assay. It is important to note that the NCI/ADR-RES cell line shares a large number of karyotypic abnormalities with OVCAR-8 cells but expresses high levels of the MDR1 (multidrug resistance protein 1)/P-glycoprotein, resulting in resistance to multiple anticancer drugs in clinical use, including paclitaxel and doxorubicin [72]

According to Table 4, we found that free DOX showed significantly lower activities in resistant cells compared with sensitive cells. The IC_{50} for the treatment of resistant cells, NCI/ADR-RES, was $8.54 \pm 2.27 \mu\text{M}$, while that of sensitive OVCAR8 cells, was $0.69 \pm 0.29 \mu\text{M}$, indicating that NCI/ADR-RES cells were resistance to DOX with a resistance index (RI) of 12.38. The RI value suggests a level of drug-resistance of the NCI/ADR-RES cells in comparison to its parental sensitive cells OVCAR8. Drug resistance is classified into three categories: drug sensitive with an RI ranging from 0 to 2, moderately drug resistant with an RI from 2 to 10, and highly drug-resistant with an RI higher than 10 [2, 73]. Once it was verified that NPs were able to effectively deliver drugs into resistant cancer cells, the ability of nanocarriers to deliver of DOX was then studied [74, 75].

Table 4 Cytotoxicity of DOX-SeNPs@TMC-FA, SeNPs@TMC-FA and DOX

Material	IC ₅₀ (μM)			
	OVCAR8	NCI/ADR-RES	RI*	Normal cells (WI-38)
DOX	0.69±0.29	8.54±2.27	12.38	1.12±0.13
SeNPs@TMC-FA	2.51±0.65	2.94±0.78	1.17	9.83±0.09
DOX-SeNPs@TMC-FA	1.00±0.16	0.89±0.45	0.89	2.60±0.17

*RI (resistance index): the ratio of IC₅₀ (NCI/ADR-RES) against IC₅₀ (OVCAR8)

DOX-loaded nanoparticles, DOX-SeNPs@TMC-FA were prepared and were further evaluated their cytotoxic activity, compared with free DOX and the nanocarriers, SeNPs@TMC-FA, against both sensitive and resistant cells. As listed in Table 4, the IC₅₀ values of free DOX against sensitive OVCAR8 cells and resistant NCI/ADR-RES cancer cells were obtained as 0.69 and 8.54 μM, respectively. After loading DOX onto the nanocarriers, the IC₅₀ value of DOX-SeNPs@TMC-FA was identified as 1.00 μM against the sensitive OVCAR8 cells, while the IC₅₀ value against the resistant NCI/ADR-RES cells was 0.89 μM. More importantly, the activity of DOX increased in resistant cells when loaded on SeNPs@TMC-FA by approximately 10-fold, decreasing the IC₅₀ values. The greater difference of IC₅₀ values between free DOX and DOX-SeNPs@TMC-FA found for the resistant NCI/ADR-RES cancer cells, indicated that TMC-FA modified SeNPs could enhance the antiproliferative activity of DOX and were able to efficiently overcome the drug resistance. In addition, we also evaluated the cytotoxicity of the nanocarriers without the drug, SeNPs@TMC-FA. The results indicated that they had toxicity to OVCAR8 and NCI/ADR-RES cells, with IC₅₀ values of 2.51 and 2.94 μM, respectively. Hence, the activity of nanocarriers themselves contributed to the lower IC₅₀ value of DOX-SeNPs@TMC-FA and was enhanced by cellular internalization of DOX.

In the toxicity test against normal cells (WI-38), DOX-SeNPs@TMC-FA showed a relatively low toxicity with an IC_{50} value of 2.60 μM , while the IC_{50} values of free DOX and nanocarriers were 1.12 and 9.83 μM , respectively, as shown in Table 4. Overall, the results suggest that DOX-SeNPs@TMC-FA effectively overcomes drug resistance and exhibits more potent activity in cancer cells, while it showed less toxicity towards normal cells. These might be improved by the surface functionalized target ligand FA of the SeNPs, which is expected to be taken up by endocytosis into the cells, and then, the drug is released away from P-gp located on the cell membrane. Additionally, the pH difference between normal and cancer cells may contribute as the pH of the tumor microenvironment is lower than that of normal cells due to the anaerobic glucose metabolism of cancer cells [13]. The higher cytotoxic activity observed in cancer cells than that in normal cells proved the pH-responsive swelling properties of DOX-SeNPs@TMC-FA and controlled release of DOX in the acidic environment of tumor cells.

4.6.2 Colony assay

To confirm the cytotoxic activity, we further studied the potency of DOX-SeNPs@TMC-FA on colony formation of NCI/ADR-RES cells compared with free DOX and SeNPs@TMC-FA. As shown in Figure 35, DOX-SeNPs@TMC-FA suppressed colony formation in a dose-dependent manner in NCI/ADR-RES cells, especially at a concentration of 1 μM of DOX-SeNPs@TMC-FA, which showed the strongest inhibitory activity over SeNPs@TMC-FA and free DOX, which was consistent with the MTT results.

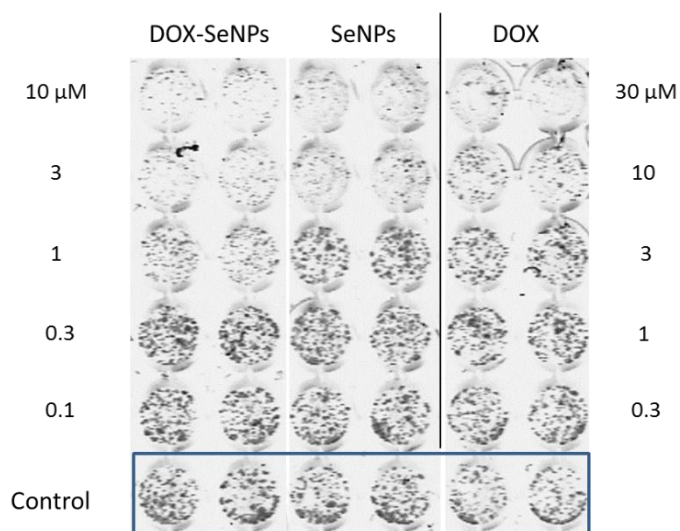


Figure 35 Colony formation assay of DOX, SeNPs@TMC-FA and DOX-SeNPs@TMC-FA

4.7 Cellular uptake

As we know, multidrug resistance remains an obstacle for cancer therapy. Normally, drugs do not effectively accumulate in the cytoplasm of the drug-resistant cells due to the high expression of P-gp on the cell membrane [13], leading to insufficient drug concentration to kill cancer cells. Previous studies suggested that the internalization mechanisms of free drug and drug-loaded nanocarriers are different. While free drug diffuses through the cell membrane, drug-loaded nanocarriers are taken up by endocytosis into cells. Thus, P-gp cannot pump out the drug, and the drug can accumulate in the cells. Therefore, the use of nanoparticle drug delivery to transport drugs to a targeted site may be a feasible strategy to solve this problem.

Cellular uptake is also the main factor for the bioactivity of nanoparticles. It was reported that the folate receptor is overexpressed in various types of human cancers. Therefore, a folate-modified polymeric carrier is utilized to achieve tumor-specific targeting and increase cellular uptake via a receptor-mediated effect. According to previous studies, it was found that FA surface conjugation significantly enhanced the cellular uptake of SeNPs by FA receptor-mediated endocytosis, and overcame the

multidrug resistance in R-HepG2 cells through the inhibition of ABC family protein expression [19].

The cytotoxicity result verified that the activity of DOX increased by approximately 10-fold and the IC_{50} values decreased, compared to free DOX in resistant cells when loaded on SeNPs@TMC-FA. We hypothesized that FA on the surface might be able to enhance the cellular uptake of nanoparticles. To confirm the role of folic acid in the uptake by cells, we evaluated the cellular uptake of coumarin-6 loaded SeNPs@TMC compared with coumarin-6 loaded SeNPs@TMC-FA in NCI/ADR-RES cells and treated with 1 μ M of the compounds for 24, 48 and 72 h. The cellular uptake was quantified by measuring the fluorescence intensity of coumarin-6 (Figure 36). We found that the uptake amounts of coumarin-6 loaded SeNPs@TMC were 1.72, 8.40 and 5.03 μ g per 5000 cells after 24, 48 and 72 h incubation at 1 μ M. Noticeably, the intracellular concentration increased to 2.79, 15.07 and 11.96 μ g per 5,000 cells, respectively after 24, 48 and 72 h incubation with coumarin-6 loaded SeNPs@TMC-FA, at the same concentration. The cellular uptake of coumarin-6 loaded SeNPs@TMC-FA was much higher than that of coumarin-6 loaded SeNPs@TMC. For instance, after 48 h of incubation, the cellular concentration of coumarin-6 loaded SeNPs@TMC-FA reached 15.07 μ g per 5,000 cells, which was 1.8-fold higher than the value for coumarin-6 loaded SeNPs@TMC. However, at 72 h, the concentration decreased from 8.40 to 5.03 μ g per 5,000 cells for coumarin-6 loaded SeNPs@TMC and from 15.07 to 11.96 μ g per 5,000 cells for coumarin-6 loaded SeNPs@TMC-FA. This might be due to the instability of the fluorescence dye for a long period of time. These results revealed that FA embellishment efficiently enhanced the cellular uptake of SeNPs and was tested since the folate receptor is overexpressed in a broad spectrum of human cancers, especially in ovarian cancers [11]. Against NCI/ADR-RES cells, FA targets the folate receptor and is then taken up by folate receptor-mediated endocytosis, which

consequently enhances cellular uptake and increased cytotoxicity as measured by the MTT assay.

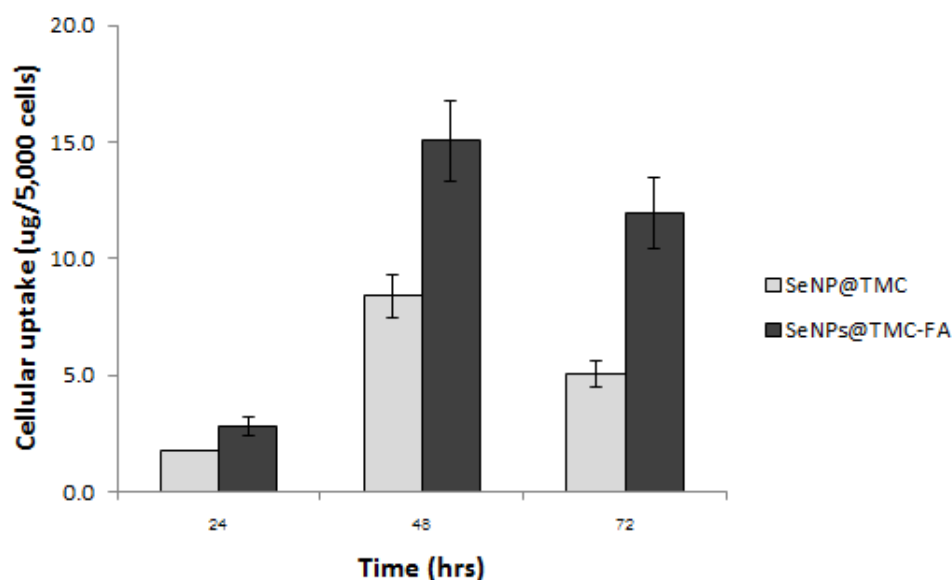


Figure 36 Quantitative analysis of cellular uptake efficacy of coumarin-6-loaded SeNPs at concentrations of 1 μ M for 24, 48 and 72 h in NCI/ADR-RES cells

4.8 Intracellular localization of DOX-SeNPs@TMC-FA

A fluorescence imaging technique was also employed to gain more insight into the intracellular trafficking of coumarin-6 loaded SeNPs@TMC-FA in NCI/ADR-RES cells. The nuclei of the cells are specifically visualized with Hoechst staining (blue color). According to Figure 37, the results reveal that SeNPs moved across the cell membrane and dispersed in the cytoplasm. Meanwhile, merged images revealed that the green fluorescence of coumarin-6 loaded SeNPs@TMC-FA was also observed in the cell nucleus, suggesting that SeNPs was taken up and further localized in the nucleus of NCI/ADR-RES cells, which might be the cellular target of SeNPs. The cellular uptake of the nanoparticles is facilitated by the targeting molecule, folic acid, and positive charge on the surface of the SeNPs.

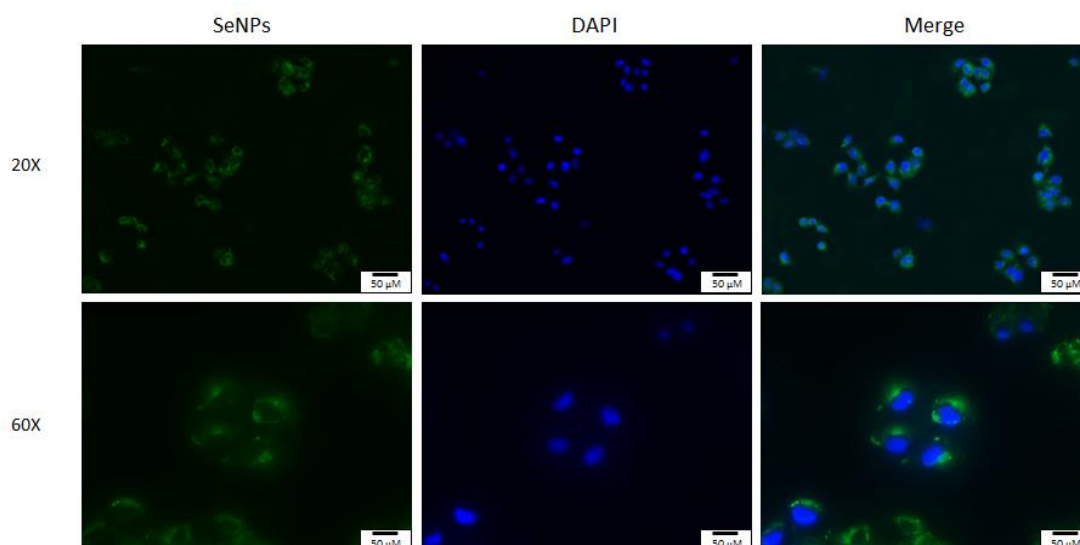


Figure 37 Intracellular localization of SeNPs in NCI/ADR-RES cells labeled with Hoechst (nucleus) and treated with SeNPs at 37°C for 6 h and visualized by fluorescence microscopy

4.9 Release profile of DOX-SeNPs@TMC-FA

Subsequently, to assess the applicability of SeNPs@TMC-FA in the delivery of anticancer drugs into resistant cells, the drug release behavior from nanoparticles was investigated in PBS solution at pH 7.4, which represents the pH value of typical blood and normal tissue, and at pH 5.3 to intimate the intracellular endosome and lysosome environments [59]. The quantity of DOX released by the SeNPs@TMC-FA was calculated by the fluorescence spectra. As expected, these DOX-SeNPs@TMC-FA exhibited a significantly enhanced DOX release rate at pH 5.3 compared to that at pH 7.4. As shown in Figure 38, the cumulative release amount of DOX from the nanoparticles at pH 5.3 was 54.1% within 2 h and reached 95.5% at 6 h, whereas the release rate at pH 7.4 was 12.3% at 2 h and 42.2% at 6 h, and complete release was observed by the end of the study at 72 h. As we know, chitosan is known to exhibit pH-dependent swelling and controlled drug release properties [13]. This release amount of DOX under two different pH solutions could be attributed to the existing

amino groups in chitosan backbone. At pH 7.4, chitosan was orderly aggregated due to the deprotonation of its amino groups, which was demonstrated in the TEM image by the shrinkage shape of the nanoparticles, and prevented the release of DOX from the nanoparticles [13, 59]. At pH 5.3, the protonized behavior of the amino groups led to chitosan dissolution and swelling, and the larger size of the nanoparticles facilitates the release of DOX from SeNPs@TMC-FA.

Taken together, pH-responsive nanocarriers provide selective drug release at acidic intracellular vesicles such as endosomes and lysosomes in targeted cancer cells. In addition, the use of FA as a targeting ligand may be a feasible strategy to enhance the cellular uptake of SeNPs by resistant cells through folate-receptor-mediated endocytosis, as well as minimize toxicity against normal cells. After SeNPs are taken up, they will be responsive to acidic pH for selective release and accumulation of the drug load in cells away from P-gp located on the cell membrane, resulting in enhanced antitumor efficacy in drug-resistant cancer cells. In addition, it could be concluded that the more acidic environment in cancer cells is helpful for the swelling of SeNPs@TMC-FA and controlled release of DOX. This gives an explanation to why DOX-SeNPs@TMC-FA showed less toxicity in normal cells than cancer cells in the MTT assay.

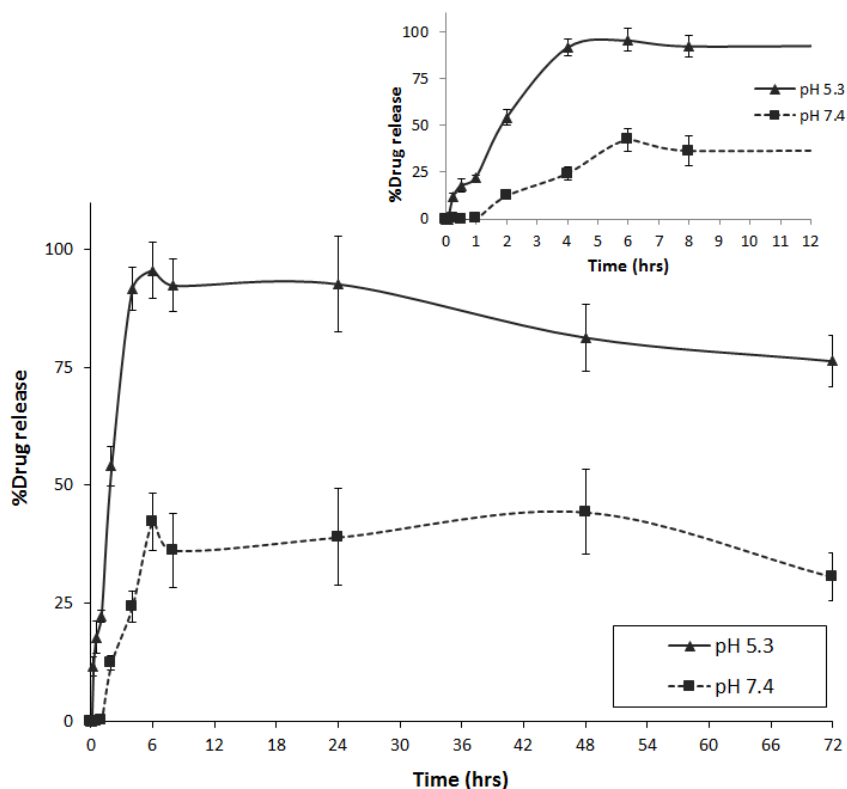


Figure 38 In vitro release profiles of DOX-SeNPs@TMC-FA in PBS solution at pH 7.4 and in acetic acid solution at pH 5.3

4.10 Cell morphology of NCI/ADR-RES after treatment with DOX-SeNPs@TMC-FA

To study the effect of DOX-SeNPs@TMC-FA on the cell morphology, cells were treated with SeNPs at a concentration of 1 μM for 24, 48 and 72 h compared with untreated cells. The morphological changes of the NCI/ADR-RES cells were examined using a fluorescence microscope (bright field). Untreated cells demonstrated a spindle shape. The time-dependent effect of DOX-SeNPs@TMC-FA is observed in Figure 39. As the time increased, the formation of membrane blebbing occurred; NCI/ADR-RES cells shrunk and changed from a spindle shape to a circular shape, and the number of adherent cells decreased. The results suggest that DOX-SeNPs@TMC-FA induces time-dependent morphologic damage of NCI/ADR-RES cells.

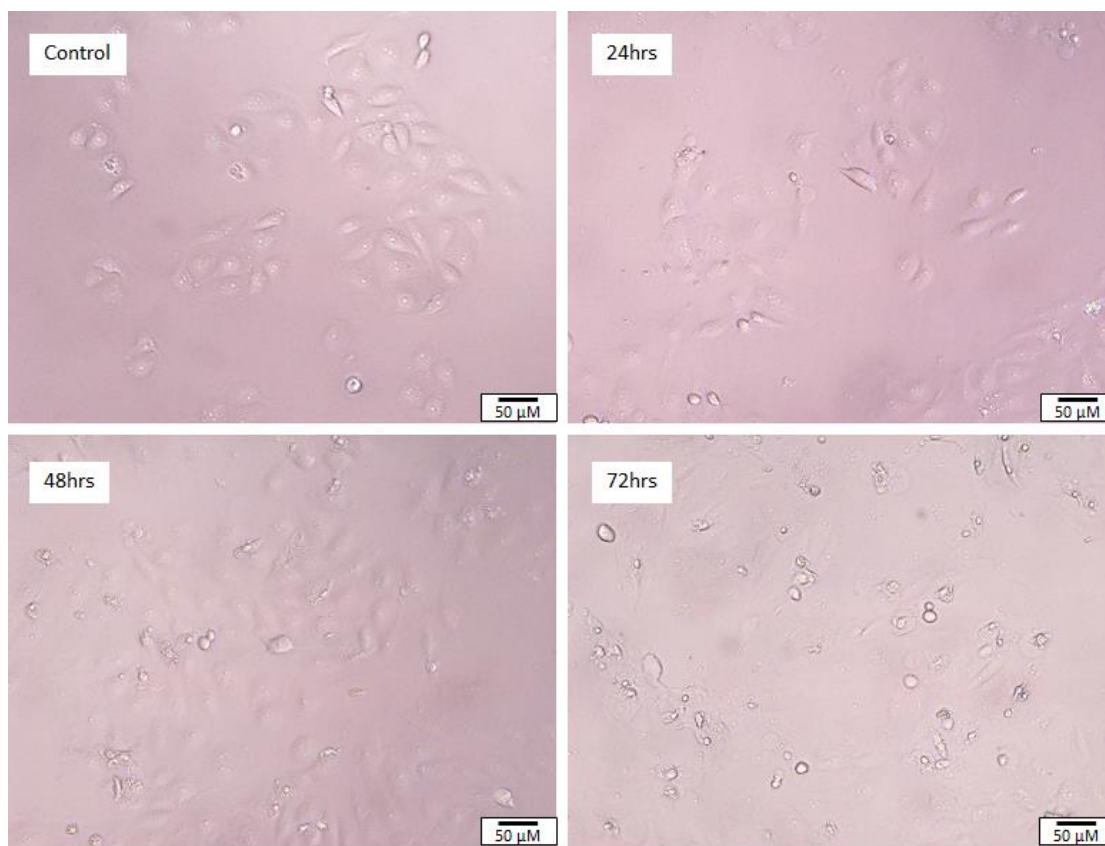


Figure 39 Morphology of NCI/ADR-RES cells treated with DOX-SeNPs@TMC-FA at 37°C for different periods of time and visualized under a fluorescence microscope

4.11 Mechanism of action of DOX-SeNPs@TMC-FA

4.11.1 Combination assay

The previous studies have demonstrated that apoptosis is the main mechanism accounting for the anticancer action of Se [59]. Therefore, to explore the mechanisms of cell death, cells were pretreated with four types of inhibitors before the addition of DOX-SeNPs@TMC-FA: (i) caspase inhibitor in the apoptosis pathway, (N-Benzyloxycarbonyl-Val-Ala-Asp(O-Me) fluoromethyl ketone; Z-VAD-FMK), (ii) ROS scavenger in the apoptosis pathway (n-acety-cysteine; NAC), (iii) ferroptosis inhibitor, (deferrioxamine; DFO) and (iv) necroptosis inhibitor (necrostatin; Necro).

According to Figure 40, the results demonstrated that SeNPs (3 μ M) are capable of killing the cells with a %inhibition of 66% (or 34% cell viability). As expected, the combination with Z-VAD-FMK rescued the cells with cell viability of 52%, and the IC_{50} was slightly increased from 1.00 ± 0.16 to 1.72 ± 0.42 μ M. However, treatment with NAC, DFO and Necro, which are a ROS scavenger, ferroptosis inhibitor, and necroptosis inhibitor, respectively, did not rescue the cell death. These results imply that DOX-SeNPs@TMC-FA might kill the cells via inducing the caspase apoptotic pathway.

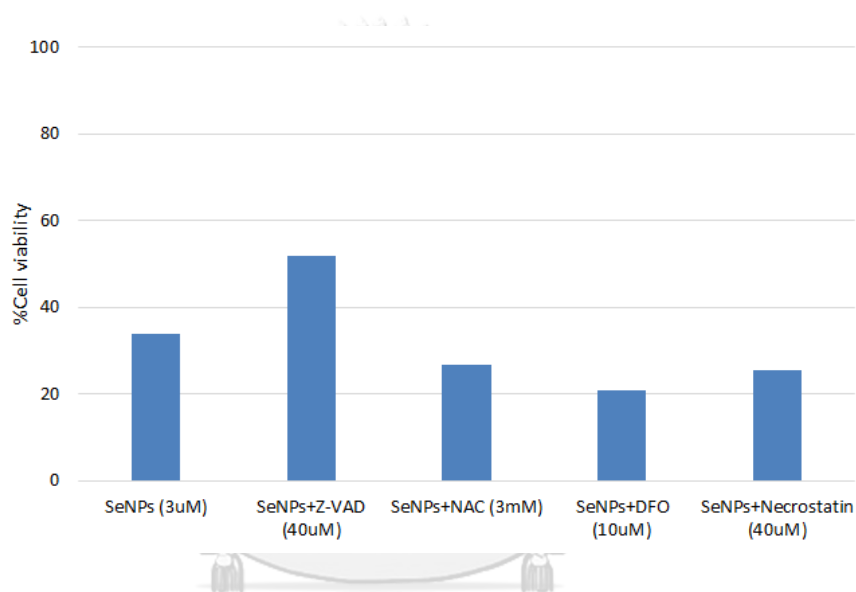


Figure 40 Cell viability of DOX-SeNPs@TMC-FA after pretreatment with Z-VAD (40 μ M), NAC (3 mM), DFO (10 μ M), Necrostatin (40 μ M) and Necro (10 μ M) in NCI/ADR-RES cells

4.11.2 Western blotting

To confirm the mechanisms involved in DOX-SeNPs@TMC-FA-induced apoptosis, the activities of apoptosis-associated proteins, caspase-3 and PARP, were determined by Western blot analysis. The results of the Western blot analysis showed that DOX-SeNPs@TMC-FA significantly increased caspase-3 and PARP activities, and the activation levels increased in time- and dose-dependent manners (Figure 41) that could contribute to apoptosis in NCI/ADR-RES cells. DOX and SeNPs were reported to induce apoptotic-cell death via the activation of caspase-3 and PARP in many cancer cells, [59, 76-78]. Taken together, apoptosis in these cells might be induced by both the drug, DOX, and the selenium nanocarriers, SeNPs@TMC-FA.

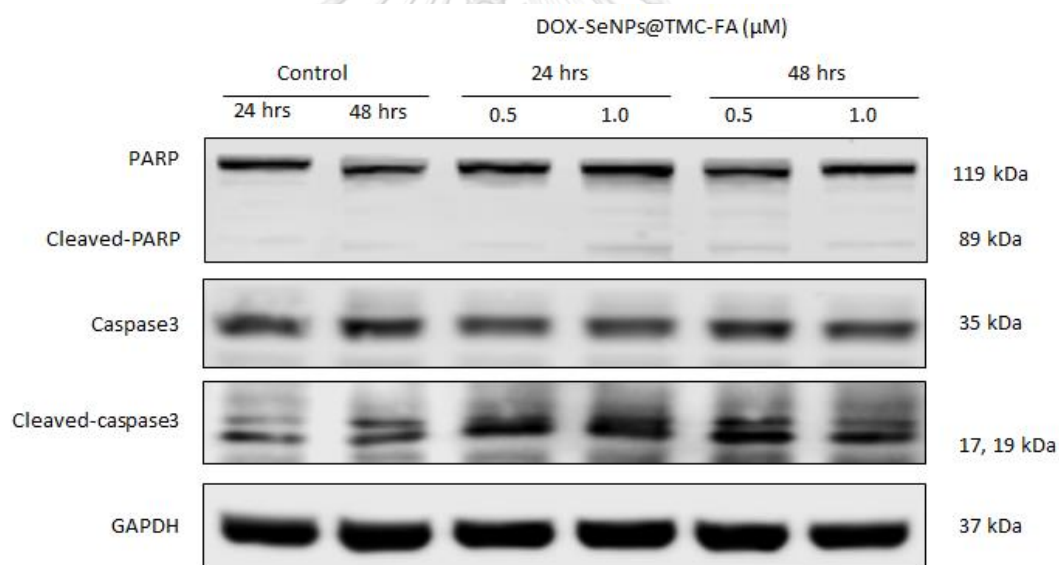


Figure 41 Effects of DOX-SeNPs@TMC-FA on the expression levels of apoptosis-associated proteins, PARP and Caspase-3, was analyzed by Western blotting.

NCI/ADR-RES cells were treated with DOX-SeNPs@TMC-FA at different concentrations (0.5 and 1.0 μM) for 24 h

CHAPTER V

Conclusion

In conclusion, we demonstrated that pH-sensitive SeNPs@TMC-FA as nanocarriers deliver DOX into resistant NCI/ADR-RES cells. The cytotoxicity of the DOX-SeNPs@TMC-FA was evaluated and found to enhance the activity of DOX by approximately 10-fold, resulting in decreased IC_{50} values compared to free DOX. SeNPs@TMC-FA were taken up by cells, with cellular uptake increased further by folate receptor-mediated endocytosis, to overcome multidrug resistance. Fluorescence microscopy images revealed that nanoparticles were dispersed in the cytoplasm and located around the nucleus. In addition, the DOX release profiles showed a pH dependence, which exhibited a faster release of DOX at pH 5.3 than at pH 7.4. The Western blot results suggested that SeNPs@TMC-FA induce cell apoptosis, which could contribute to regulation of caspase-3 and PARP. According to these results, it is inferred that SeNPs@TMC-FA has the potential to be used as a pH-responsive drug delivery system, which could target tumor cells and overcome resistance in NCI/ADR-RES cells.

REFERENCES

1. Luesakul, U., T. Palaga, K. Krusong, N. Ngamrojanavanich, T. Vilaivan, S. Puthong, and N. Muangsin, *Synthesis, cytotoxicity, DNA binding and topoisomerase II inhibition of cassiarin A derivatives*. *Bioorg Med Chem Lett*, **2014**, 24(13), 2845-2850.
2. Wang, R.H., J. Bai, J. Deng, C.J. Fang, and X. Chen, *TAT-Modified Gold Nanoparticle Carrier with Enhanced Anticancer Activity and Size Effect on Overcoming Multidrug Resistance*. *ACS Appl Mater Interfaces*, **2017**, 9(7), 5828-5837.
3. Amin, M.L., *P-glycoprotein Inhibition for Optimal Drug Delivery*. *Drug Target Insights*, **2013**, 7, 27-34.
4. Zheng, W., T. Yin, Q. Chen, X. Qin, X. Huang, S. Zhao, T. Xu, L. Chen, and J. Liu, *Co-delivery of Se nanoparticles and pooled SiRNAs for overcoming drug resistance mediated by P-glycoprotein and class III β -tubulin in drug-resistant breast cancers*. *Acta Biomaterialia*, **2016**, 31, 197-210.
5. Abdallah, H.M., A.M. Al-Abd, R.S. El-Dine, and A.M. El-Halawany, *P-glycoprotein inhibitors of natural origin as potential tumor chemo-sensitizers: A review*. *Journal of Advanced Research*, **2015**, 6(1), 45-62.
6. Alexis, F., E.M. Pridgen, R. Langer, and O.C. Farokhzad, *Nanoparticle technologies for cancer therapy*. *Handb Exp Pharmacol*, **2010**(197), 55-86.
7. Black, K.C.L., Y. Wang, H.P. Luehmann, X. Cai, W. Xing, B. Pang, Y. Zhao, C.S. Cutler, L.V. Wang, Y. Liu, and Y. Xia, *Radioactive ^{198}Au -Doped Nanostructures with Different Shapes for In Vivo Analyses of Their Biodistribution, Tumor Uptake, and Intratumoral Distribution*. *ACS Nano*, **2014**, 8(5), 4385-4394.
8. Ren, Y., T. Zhao, G. Mao, M. Zhang, F. Li, Y. Zou, L. Yang, and X. Wu, *Antitumor activity of hyaluronic acid-selenium nanoparticles in Heps tumor*

- mice models*. International Journal of Biological Macromolecules, **2013**, 57, 57-62.
9. Sperling, R.A. and W.J. Parak, *Surface modification, functionalization and bioconjugation of colloidal inorganic nanoparticles*. Philosophical Transactions of the Royal Society A: Mathematical, Physical and Engineering Sciences, **2010**, 368(1915), 1333.
 10. Liu, J., X. Ma, S. Jin, X. Xue, C. Zhang, T. Wei, W. Guo, and X.-J. Liang, *Zinc Oxide Nanoparticles as Adjuvant To Facilitate Doxorubicin Intracellular Accumulation and Visualize pH-Responsive Release for Overcoming Drug Resistance*. Molecular Pharmaceutics, **2016**, 13(5), 1723-1730.
 11. Wang, Y., L. Dou, H. He, Y. Zhang, and Q. Shen, *Multifunctional Nanoparticles as Nanocarrier for Vincristine Sulfate Delivery To Overcome Tumor Multidrug Resistance*. Molecular Pharmaceutics, **2014**, 11(3), 885-894.
 12. Li, Y., Y. Deng, X. Tian, H. Ke, M. Guo, A. Zhu, T. Yang, Z. Guo, Z. Ge, X. Yang, and H. Chen, *Multipronged Design of Light-Triggered Nanoparticles To Overcome Cisplatin Resistance for Efficient Ablation of Resistant Tumor*. ACS Nano, **2015**, 9(10), 9626-9637.
 13. Unsoy, G., R. Khodadust, S. Yalcin, P. Mutlu, and U. Gunduz, *Synthesis of Doxorubicin loaded magnetic chitosan nanoparticles for pH responsive targeted drug delivery*. Eur J Pharm Sci, **2014**, 62, 243-250.
 14. Bai, Y., Y. Wang, Y. Zhou, W. Li, and W. Zheng, *Modification and modulation of saccharides on elemental selenium nanoparticles in liquid phase*. Materials Letters, **2008**, 62(15), 2311-2314.
 15. Hong, M., L. Wu, L. Tian, and J. Zhu, *Controlled assembly of Au, Ag, and Pt nanoparticles with chitosan*. Chemistry, **2009**, 15(24), 5935-5941.
 16. Sun, Y., H. Liu, L. Yang, B. Sun, and J. Liu, *Transformation of thiolated chitosan-templated gold nanoparticles to huge microcubes*. Materials Research Bulletin, **2014**, 53, 89-95.
 17. Saraswathy, M. and S. Gong, *Recent developments in the co-delivery of siRNA and small molecule anticancer drugs for cancer treatment*. Materials Today, **2014**, 17(6), 298-306.

18. Zheng, W., C. Cao, Y. Liu, Q. Yu, C. Zheng, D. Sun, X. Ren, and J. Liu, *Multifunctional polyamidoamine-modified selenium nanoparticles dual-delivering siRNA and cisplatin to A549/DDP cells for reversal multidrug resistance*. *Acta Biomaterialia*, **2015**, 11, 368-380.
19. Liu, T., L. Zeng, W. Jiang, Y. Fu, W. Zheng, and T. Chen, *Rational design of cancer-targeted selenium nanoparticles to antagonize multidrug resistance in cancer cells*. *Nanomedicine*, **2015**, 11(4), 947-958.
20. Chen, Q., Q. Yu, Y. Liu, D. Bhavsar, L. Yang, X. Ren, D. Sun, W. Zheng, J. Liu, and L.M. Chen, *Multifunctional selenium nanoparticles: Chiral selectivity of delivering MDR-siRNA for reversal of multidrug resistance and real-time biofluorescence imaging*. *Nanomedicine*, **2015**, 11(7), 1773-1784.
21. Parker, N., M.J. Turk, E. Westrick, J.D. Lewis, P.S. Low, and C.P. Leamon, *Folate receptor expression in carcinomas and normal tissues determined by a quantitative radioligand binding assay*. *Anal Biochem*, **2005**, 338(2), 284-293.
22. Wang, Y., L. Dou, H. He, Y. Zhang, and Q. Shen, *Multifunctional nanoparticles as nanocarrier for vincristine sulfate delivery to overcome tumor multidrug resistance*. *Mol Pharm*, **2014**, 11(3), 885-894.
23. Patel, N.R., B.S. Pattni, A.H. Abouzeid, and V.P. Torchilin, *Nanopreparations to overcome multidrug resistance in cancer*. *Adv Drug Deliv Rev*, **2013**, 65(13-14), 1748-1762.
24. Zheng, W., C. Cao, Y. Liu, Q. Yu, C. Zheng, D. Sun, X. Ren, and J. Liu, *Multifunctional polyamidoamine-modified selenium nanoparticles dual-delivering siRNA and cisplatin to A549/DDP cells for reversal multidrug resistance*. *Acta Biomater*, **2015**, 11, 368-380.
25. Chen, Y., H. Chen, and J. Shi, *Inorganic Nanoparticle-Based Drug Codelivery Nanosystems To Overcome the Multidrug Resistance of Cancer Cells*. *Molecular Pharmaceutics*, **2014**, 11(8), 2495-2510.
26. Gao, Z., L. Zhang, and Y. Sun, *Nanotechnology applied to overcome tumor drug resistance*. *J Control Release*, **2012**, 162(1), 45-55.

27. Nakamura, Y., A. Mochida, P.L. Choyke, and H. Kobayashi, *Nanodrug Delivery: Is the Enhanced Permeability and Retention Effect Sufficient for Curing Cancer?* *Bioconjugate Chemistry*, **2016**, 27(10), 2225-2238.
28. Stockhofe, K., J.M. Postema, H. Schieferstein, and T.L. Ross, *Radiolabeling of Nanoparticles and Polymers for PET Imaging*. Pharmaceuticals (Basel), **2014**, 7(4), 392-418.
29. Cho, E.C., C. Glaus, J. Chen, M.J. Welch, and Y. Xia, *Inorganic nanoparticle-based contrast agents for molecular imaging*. *Trends in molecular medicine*, **2010**, 16(12), 561-573.
30. Verma, J., S. Lal, and C.J. Van Noorden, *Nanoparticles for hyperthermic therapy: synthesis strategies and applications in glioblastoma*. *Int J Nanomedicine*, **2014**, 9, 2863-2877.
31. Abadeer, N.S. and C.J. Murphy, *Recent Progress in Cancer Thermal Therapy Using Gold Nanoparticles*. *The Journal of Physical Chemistry C*, **2016**, 120(9), 4691-4716.
32. Cheng, Y., R.A. Morshed, B. Auffinger, A.L. Tobias, and M.S. Lesniak, *Multifunctional nanoparticles for brain tumor imaging and therapy*. *Adv Drug Deliv Rev*, **2014**, 66, 42-57.
33. Bhamidipati, M. and L. Fabris, *Multiparametric Assessment of Gold Nanoparticle Cytotoxicity in Cancerous and Healthy Cells: The Role of Size, Shape, and Surface Chemistry*. *Bioconjugate Chemistry*, **2017**, 28(2), 449-460.
34. Cheng, Y., J.D. Meyers, R.S. Agnes, T.L. Doane, M.E. Kenney, A.M. Broome, C. Burda, and J.P. Basilion, *Addressing brain tumors with targeted gold nanoparticles: a new gold standard for hydrophobic drug delivery?* *Small*, **2011**, 7(16), 2301-2306.
35. Lockman, P.R., J.M. Koziara, R.J. Mumper, and D.D. Allen, *Nanoparticle surface charges alter blood-brain barrier integrity and permeability*. *J Drug Target*, **2004**, 12(9-10), 635-641.
36. Decuzzi, P., B. Godin, T. Tanaka, S.Y. Lee, C. Chiappini, X. Liu, and M. Ferrari, *Size and shape effects in the biodistribution of intravascularly injected particles*. *Journal of Controlled Release*, **2010**, 141(3), 320-327.

37. Petri, B., A. Bootz, A. Khalansky, T. Hekmatara, R. Müller, R. Uhl, J. Kreuter, and S. Gelperina, *Chemotherapy of brain tumour using doxorubicin bound to surfactant-coated poly(butyl cyanoacrylate) nanoparticles: Revisiting the role of surfactants*. *Journal of Controlled Release*, **2007**, 117(1), 51-58.
38. Gromnicova, R., H.A. Davies, P. Sreekanthreddy, I.A. Romero, T. Lund, I.M. Roitt, J.B. Phillips, and D.K. Male, *Glucose-Coated Gold Nanoparticles Transfer across Human Brain Endothelium and Enter Astrocytes In Vitro*. *PLOS ONE*, **2013**, 8(12), e81043.
39. Choi, C.H.J., C.A. Alabi, P. Webster, and M.E. Davis, *Mechanism of active targeting in solid tumors with transferrin-containing gold nanoparticles*. *Proceedings of the National Academy of Sciences*, **2010**, 107(3), 1235-1240.
40. Saraiva, C., C. Praça, R. Ferreira, T. Santos, L. Ferreira, and L. Bernardino, *Nanoparticle-mediated brain drug delivery: Overcoming blood–brain barrier to treat neurodegenerative diseases*. *Journal of Controlled Release*, **2016**, 235, 34-47.
41. Wang, L., *Synthetic methods of CuS nanoparticles and their applications for imaging and cancer therapy*. *RSC Advances*, **2016**, 6(86), 82596-82615.
42. Alexander, K.T., E.M., *Concepts of the stabilization of metal nanoparticles in ionic liquids*. *Applications of Ionic Liquids in Science and Technology*. 2011: InTech.
43. Abedini, A., A.A.A. Bakar, F. Larki, P.S. Menon, M.S. Islam, and S. Shaari, *Recent Advances in Shape-Controlled Synthesis of Noble Metal Nanoparticles by Radiolysis Route*. *Nanoscale Research Letters*, **2016**, 11, 287.
44. Yang, Y., S. Wang, Y. Wang, X. Wang, Q. Wang, and M. Chen, *Advances in self-assembled chitosan nanomaterials for drug delivery*. *Biotechnology Advances*, **2014**, 32(7), 1301-1316.
45. Tomizaki, K.Y., K. Kishioka, H. Kobayashi, A. Kobayashi, N. Yamada, S. Kataoka, T. Imai, and M. Kasuno, *Roles of aromatic side chains and template effects of the hydrophobic cavity of a self-assembled peptide nanoarchitecture for anisotropic growth of gold nanocrystals*. *Bioorg Med Chem*, **2015**, 23(22), 7282-7291.

46. Ding, Y., G. Gu, X.-H. Xia, and Q. Huo, *Cysteine-grafted chitosan-mediated gold nanoparticle assembly: from nanochains to microcubes*. *Journal of Materials Chemistry*, **2009**, 19(6), 795-799.
47. Oh, N. and J.H. Park, *Endocytosis and exocytosis of nanoparticles in mammalian cells*. *Int J Nanomedicine*, **2014**, 9 Suppl 1, 51-63.
48. Mout, R., D.F. Moyano, S. Rana, and V.M. Rotello, *Surface functionalization of nanoparticles for nanomedicine*. *Chem Soc Rev*, **2012**, 41(7), 2539-2544.
49. Liu, W., X. Li, Y.S. Wong, W. Zheng, Y. Zhang, W. Cao, and T. Chen, *Selenium nanoparticles as a carrier of 5-fluorouracil to achieve anticancer synergism*. *ACS Nano*, **2012**, 6(8), 6578-6591.
50. Yu, B., Y. Zhang, W. Zheng, C. Fan, and T. Chen, *Positive surface charge enhances selective cellular uptake and anticancer efficacy of selenium nanoparticles*. *Inorg Chem*, **2012**, 51(16), 8956-8963.
51. Cao, X.B., Y. Xie, S.Y. Zhang, and F.Q. Li, *Ultra-Thin Trigonal Selenium Nanoribbons Developed from Series-Wound Beads*. *Advanced Materials*, **2004**, 16(7), 649-653.
52. Kumar, A., I. Sevonkaev, and D.V. Goia, *Synthesis of selenium particles with various morphologies*. *Journal of Colloid and Interface Science*, **2014**, 416, 119-123.
53. Yin, H.Y., Z. Xu, H.H. Bao, J.Y. Bai, and Y.F. Zheng, *Single crystal trigonal selenium nanoplates converted from selenium nanoparticles*. *Chemistry Letters*, **2005**, 34(1), 122-123.
54. Chen, Z., Y. Shen, A. Xie, J. Zhu, Z. Wu, and F. Huang, *l-Cysteine-Assisted Controlled Synthesis of Selenium Nanospheres and Nanorods*. *Crystal Growth & Design*, **2009**, 9(3), 1327-1333.
55. Cai, X., Y. Luo, W. Zhang, D. Du, and Y. Lin, *pH-Sensitive ZnO Quantum Dots-Doxorubicin Nanoparticles for Lung Cancer Targeted Drug Delivery*. *ACS Applied Materials & Interfaces*, **2016**, 8(34), 22442-22450.
56. Zhou, L., H. Wang, and Y. Li, *Stimuli-Responsive Nanomedicines for Overcoming Cancer Multidrug Resistance*. *Theranostics*, **2018**, 8(4), 1059-1074.

57. Suvannasara, P., N. Praphairaksit, and N. Muangsin, *Self-assembly of mucoadhesive nanofibers*. RSC Advances, **2014**, 4(102), 58664-58673.
58. Komenek, S., U. Luesakul, S. Ekgasit, T. Vilaivan, N. Praphairaksit, S. Puthong, and N. Muangsin, *Nanogold-Gallate Chitosan-Targeted Pulmonary Delivery for Treatment of Lung Cancer*. AAPS PharmSciTech, **2017**, 18(4), 1104-1115.
59. Huang, Y., L. He, W. Liu, C. Fan, W. Zheng, Y.S. Wong, and T. Chen, *Selective cellular uptake and induction of apoptosis of cancer-targeted selenium nanoparticles*. Biomaterials, **2013**, 34(29), 7106-7116.
60. Lee, D.W., C. Lim, J.N. Israelachvili, and D.S. Hwang, *Strong adhesion and cohesion of chitosan in aqueous solutions*. Langmuir : the ACS journal of surfaces and colloids, **2013**, 29(46), 14222-14229.
61. Pettine, M., F. Gennari, and L. Campanella, *The reaction of selenium (IV) with ascorbic acid: Its relevance in aqueous and soil systems*. Chemosphere, **2013**, 90(2), 245-250.
62. Lin, Z.-H. and C.R. Chris Wang, *Evidence on the size-dependent absorption spectral evolution of selenium nanoparticles*. Materials Chemistry and Physics, **2005**, 92(2), 591-594.
63. Wu, S.J., T.M. Don, C.W. Lin, and F.L. Mi, *Delivery of berberine using chitosan/fucoidan-aurine conjugate nanoparticles for treatment of defective intestinal epithelial tight junction barrier*. Mar Drugs, **2014**, 12(11), 5677-5697.
64. Jiang, X.C., W.M. Chen, C.Y. Chen, S.X. Xiong, and A.B. Yu, *Role of Temperature in the Growth of Silver Nanoparticles Through a Synergetic Reduction Approach*. Nanoscale Research Letters, **2011**, 6(1), 32-32.
65. Zhang, J., E.W. Taylor, X. Wan, and D. Peng, *Impact of heat treatment on size, structure, and bioactivity of elemental selenium nanoparticles*. Int J Nanomedicine, **2012**, 7, 815-825.
66. Guo, L., F. Tong, H. Liu, H. Yang, and J. Li, *Shape-controlled synthesis of self-assembly cubic CuO nanostructures by microwave*. Materials Letters, **2012**, 71, 32-35.

67. Johnson, J.A., M.-L. Saboungi, P. Thiyagarajan, R. Csencsits, and D. Meisel, *Selenium Nanoparticles: A Small-Angle Neutron Scattering Study*. The Journal of Physical Chemistry B, **1999**, 103(1), 59-63.
68. Zhang, S.-Y., J. Zhang, H.-Y. Wang, and H.-Y. Chen, *Synthesis of selenium nanoparticles in the presence of polysaccharides*. Materials Letters, **2004**, 58(21), 2590-2594.
69. Park, Y., S.X.M. Boerrigter, J. Yeon, S.H. Lee, S.K. Kang, and E.H. Lee, *New Metastable Packing Polymorph of Donepezil Grown on Stable Polymorph Substrates*. Crystal Growth & Design, **2016**, 16(5), 2552-2560.
70. Yang, S.J., F.H. Lin, K.C. Tsai, M.F. Wei, H.M. Tsai, J.M. Wong, and M.J. Shieh, *Folic acid-conjugated chitosan nanoparticles enhanced protoporphyrin IX accumulation in colorectal cancer cells*. Bioconjug Chem, **2010**, 21(4), 679-689.
71. Kong, H., J. Yang, Y. Zhang, Y. Fang, K. Nishinari, and G.O. Phillips, *Synthesis and antioxidant properties of gum arabic-stabilized selenium nanoparticles*. International Journal of Biological Macromolecules, **2014**, 65, 155-162.
72. Xu, S., A.N. Butkevich, R. Yamada, Y. Zhou, B. Debnath, R. Duncan, E. Zandi, N.A. Petasis, and N. Neamati, *Discovery of an orally active small-molecule irreversible inhibitor of protein disulfide isomerase for ovarian cancer treatment*. Proceedings of the National Academy of Sciences of the United States of America, **2012**, 109(40), 16348-16353.
73. Zhang, X., M. Yashiro, H. Qiu, T. Nishii, T. Matsuzaki, and K. Hirakawa, *Establishment and characterization of multidrug-resistant gastric cancer cell lines*. Anticancer Res, **2010**, 30(3), 915-921.
74. Lee, S.-M., H.J. Kim, S.Y. Kim, M.-K. Kwon, S. Kim, A. Cho, M. Yun, J.-S. Shin, and K.-H. Yoo, *Drug-loaded gold plasmonic nanoparticles for treatment of multidrug resistance in cancer*. Biomaterials, **2014**, 35(7), 2272-2282.
75. Kievit, F.M., F.Y. Wang, C. Fang, H. Mok, K. Wang, J.R. Silber, R.G. Ellenbogen, and M. Zhang, *Doxorubicin loaded iron oxide nanoparticles overcome multidrug resistance in cancer in vitro*. Journal of Controlled Release, **2011**, 152(1), 76-83.

76. Park, B., D. Park, D.-K. Rhee, and S. Pyo, *Diosgenin protects doxorubicin-induced cell apoptosis in macrophages: involvement of MAPK and ATF-3 pathways*. The FASEB Journal, **2012**, 26(1 Supplement), 1119.1118.
77. Wang, S., E.A. Konorev, S. Kotamraju, J. Joseph, S. Kalivendi, and B. Kalyanaraman, *Doxorubicin Induces Apoptosis in Normal and Tumor Cells via Distinctly Different Mechanisms: INTERMEDIACY OF H₂O₂- AND p53-DEPENDENT PATHWAYS*. Journal of Biological Chemistry, **2004**, 279(24), 25535-25543.
78. Pi, J., H. Jin, R. Liu, B. Song, Q. Wu, L. Liu, J. Jiang, F. Yang, H. Cai, and J. Cai, *Pathway of cytotoxicity induced by folic acid modified selenium nanoparticles in MCF-7 cells*. Appl Microbiol Biotechnol, **2013**, 97(3), 1051-1062.





APPENDIX

จุฬาลงกรณ์มหาวิทยาลัย
CHULALONGKORN UNIVERSITY

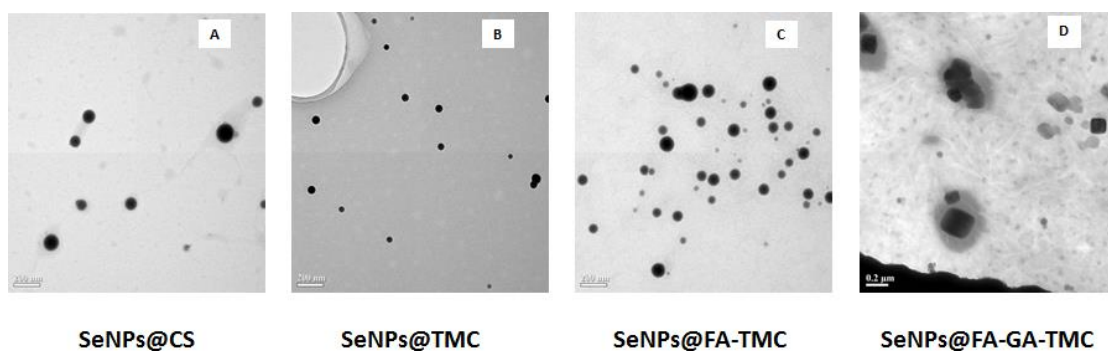


Figure A1 TEM images of SeNPs stabilized with different types of stabilizers



UV/VIS spectrum of stabilizers (CS, TMC, TMC-FA and TMC-GA-FA)

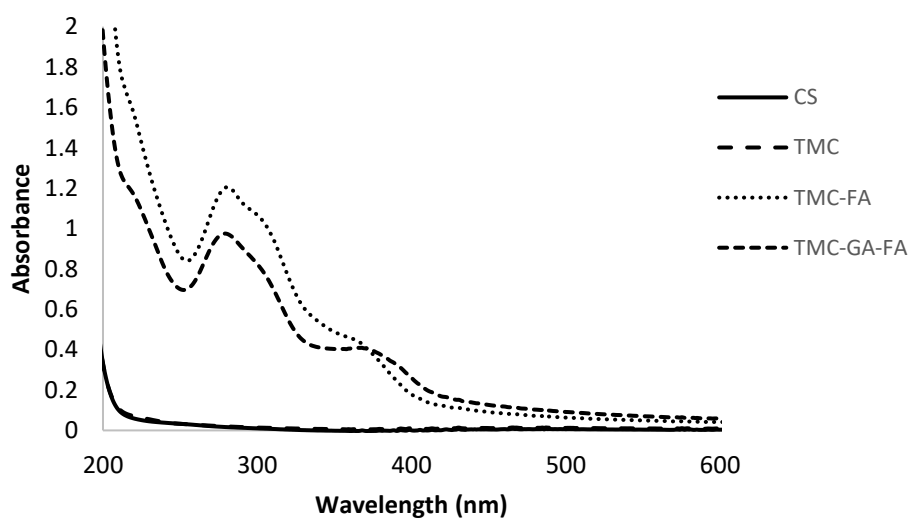


Figure A2 UV/VIS spectrum of stabilizing agents

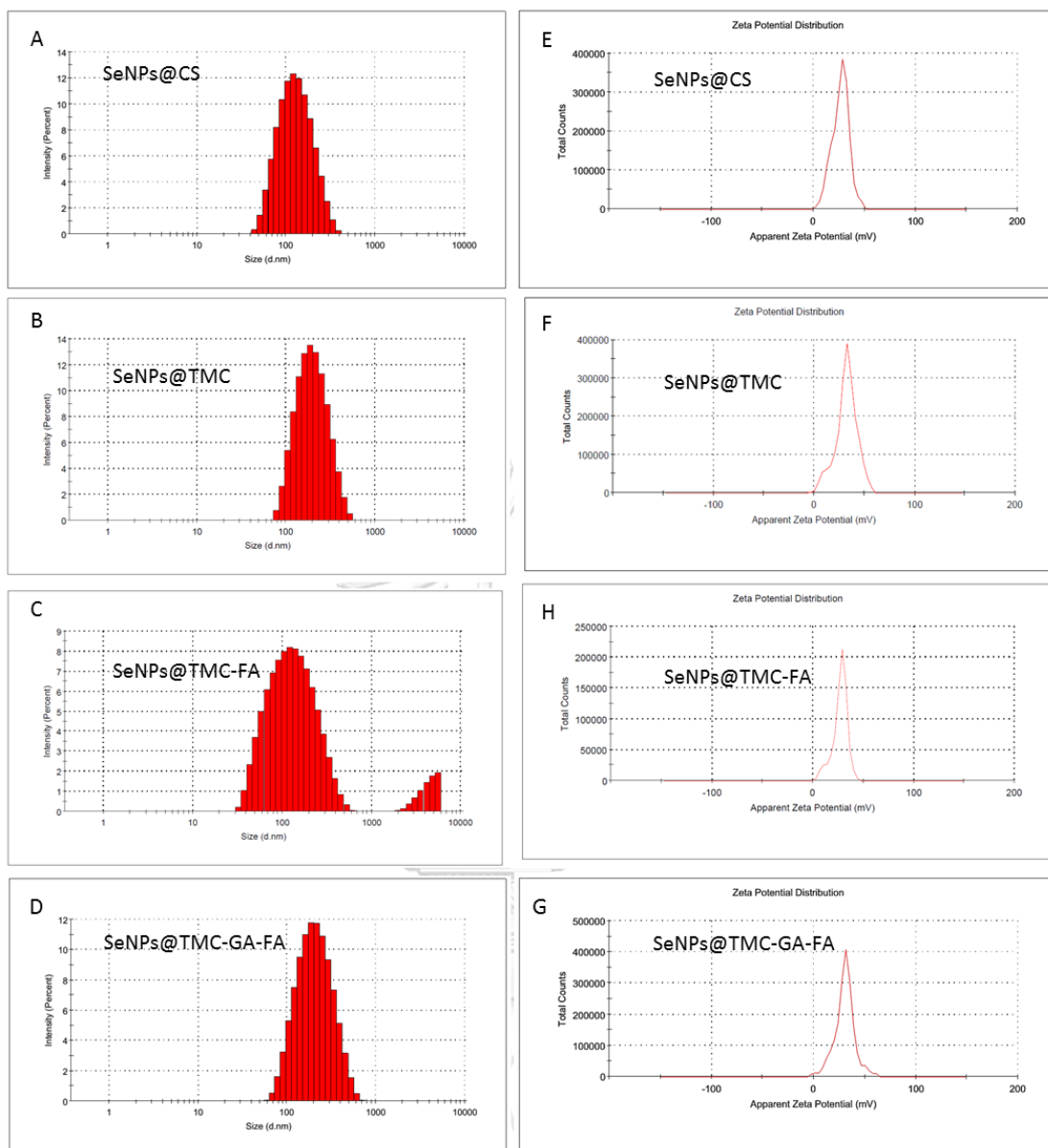


Figure A3 DLS and zeta potential of SeNPs stabilized with different types of stabilizers

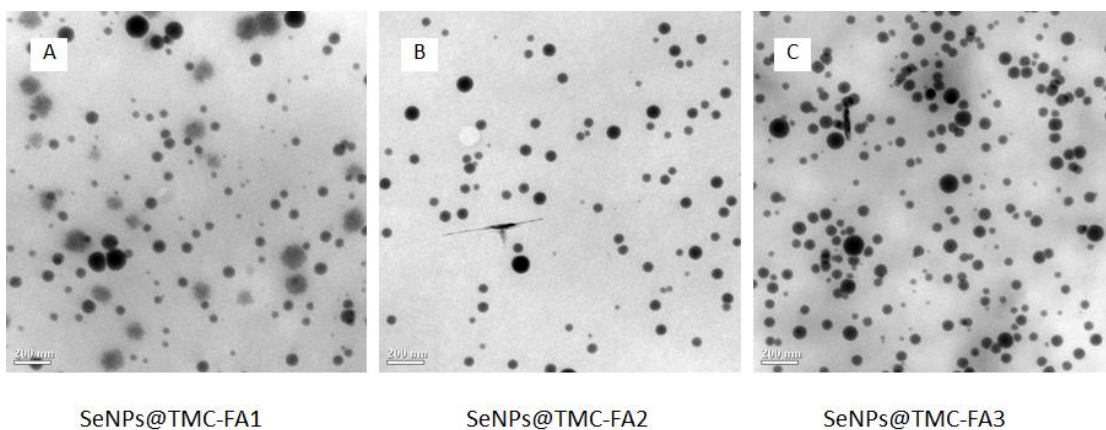


Figure A4 TEM images of (A) SeNPs@TMC-FA1, (B) SeNPs@TMC-FA2 and (C) SeNPs@TMC-FA3



VITA

Name: Miss Urarika Luesakul

Sex: Female

Date of birth: 18 May 1989

Place of birth: Phuket

Nationality: Thai

Religion: Buddhism

Address: 157 Phatthalung Road, Muang, Trang, 92000

University Education:

- Bachelor Degree in Chemistry from Chulalongkorn University, 2007- 2010
- Master degree of Chemistry, Faculty of Science, Chulalongkorn University, 2011-2013
- Ph.D in Chemistry, Faculty of Science, Chulalongkorn University, 2014-2018

Publications จุฬาลงกรณ์มหาวิทยาลัย

- Luesakul, U., Puthong, S., Neamati, N., & Muangsin, N., pH-responsive selenium nanoparticles stabilized by folate-chitosan delivering doxorubicin for overcoming drug-resistant cancer cells. Carbohydrate Polymers, 2018, 181(Supplement C), 841-850.
- Luesakul, U., Komenek, S., Puthong, S., & Muangsin, N., Shape-controlled synthesis of cubic-like selenium nanoparticles via the self-assembly method. Carbohydrate Polymers, 2016, 153(Supplement C), 435-444.



จุฬาลงกรณ์มหาวิทยาลัย
CHULALONGKORN UNIVERSITY